Helsinki Eye Lab
Department of Ophthalmology
Faculty of Medicine
University of Helsinki
Finland

# TEAR FILM LIPID LAYER ORGANIZATION AND EVAPORATION RESISTANCE

## BIOPHYSICAL STUDIES ON TEAR FILM LIPIDS

**Riku O. Paananen**

DOCTORAL DISSERTATION

To be presented for public examination with the permission of the Faculty of Medicine of the University of Helsinki, in Lecture Hall 2, Biomedicum Helsinki 1, on the 7th of May 2021 at 13:15 o'clock.

Helsinki 2021

**Supervisors**

Professor Juha Holopainen
Department of Ophthalmology
University of Helsinki
Helsinki, Finland

Adjunct Professor Jukka Moilanen
Department of Ophthalmology
University of Helsinki
Helsinki, Finland

Professor Ilpo Vattulainen
Department of Physics
University of Helsinki
Helsinki, Finland

**Reviewers**

Professor Emma Sparr
Division of Physical Chemistry
Lund University
Lund, Sweden

Professor Kari Laasonen
Department of Chemistry and Materials Science
Aalto University
Espoo, Finland

**Opponent**

Professor Kai Kaarniranta
Faculty of Health Sciences
University of Eastern Finland
Kuopio, Finland

The Faculty of Medicine uses the Urkund system (plagiarism recognition) to examine all doctoral dissertations.

ISBN 978-951-51-7175-7 (paperback)
ISBN 978-951-51-7176-4 (PDF)

Unigrafia 2021

# ABSTRACT

The ocular surface is covered by the tear film that provides a smooth optical surface required for clear vision, offers lubrication necessary for eye movement, and maintains a suitable microenvironment for the ocular surface cells. The tear film can be divided into two separate layers: the aqueous layer, which makes up the bulk of the tear film, and a thin tear film lipid layer (TFLL), which covers the aqueous layer. The TFLL is considered to stabilize the tear film by slowing down evaporation of water from the aqueous tear film. The loss of this stabilizing function of the TFLL is believed to play a central role in the development of most cases of dry eye disease. However, the structure of the TFLL remains poorly characterized, and currently no consensus exists on the molecular level organization within the TFLL. Due to this lack of understanding of TFLL organization on a molecular level, the basis underlying the stabilizing mechanism has remained unclear.

In this thesis, the aim was to gain insight into the molecular level structure of the TFLL by dissecting how different lipids in the TFLL organize at the aqueous interface. Further, the effects of interfacial organization of different lipid classes on the evaporation resistance was studied to understand how these structural characteristics are related to the evaporation resistance of the TFLL.

The lipids studied in this work cover most of the lipid classes that are found in the TFLL, namely wax esters (WEs), cholesteryl esters (CEs), Type II diesters (DiE), and O-acyl-ω-hydroxy fatty acids (OAHFAs). For each lipid class, model compounds representing the most abundant lipids in the TFLL were used. The organization and evaporation resistance of each lipid class was studied experimentally using a Langmuir trough model system, and this work was complemented by molecular dynamics simulations.

This thesis project identified OAHFAs and WEs as the most important lipid classes related to TFLL evaporation resistance. The evaporation resistance of both OAHFAs and WEs was related to the formation of solid monomolecular structures at the aqueous interface. WEs formed solid crystals of monomolecular thickness at the aqueous surface, which spread to cover the surface at a narrow temperature range below the melting point of the WE facilitated by coexistence with a disordered WE monolayer. Long-chained OAHFAs formed a solid monolayer phase on the aqueous interface that provided up to 5 s/cm of evaporation resistance, making OAHFAs even more effective in resisting evaporation than WEs.

However, such condensed monolayers inhibited the spreading of nonpolar CE multilayers, which challenges the role of polar lipids in spreading and stabilizing the TFLL. Instead, these results suggest that polar TFLL lipids, mainly OAHFAs, form a condensed monolayer that is directly responsible for the evaporation resistance of the TFLL.

# CONTENTS

# LIST OF ORIGINAL PUBLICATIONS

This thesis is based on the following publications, which will be referred to in the text by their roman numerals:

I Paananen RO, Rantamäki AH, Holopainen JM. Antievaporative Mechanism of Wax Esters: Implications for the Function of Tear Fluid. *Langmuir* 2014; 30(20):5897–5902.

II Paananen RO, Rantamäki AH, Parshintsev J, Holopainen JM. The Effect of Ambient Ozone on Unsaturated Tear Film Wax Esters. *Invest Ophthalmol Vis Sci* 2015; 56(13):8054–8062.

III Paananen RO, Javanainen M, Holopainen JM, Vattulainen I. Crystalline Wax Esters Regulate the Evaporation Resistance of Tear Film Lipid Layers Associated with Dry Eye Syndrome. *J Phys Chem Lett* 2019; 10(14):3893–3898.

IV Bland HC, Moilanen JA, Ekholm FS, Paananen RO. Investigating the Role of Specific Tear Film Lipids Connected to Dry Eye Syndrome: A Study on O-Acyl-ω-hydroxy Fatty Acids and Diesters. *Langmuir* 2019; 35(9): 3545–3552.

V Paananen RO, Viitaja T, Olżyńska, A, Ekholm FS, Moilanen J, Cwiklik L. Interactions of Polar Lipids with Cholesteryl Ester Multilayers Elucidate Tear Film Lipid Layer Structure. *Ocul Surf* 2020; 18(4): 545–553.



In addition, some unpublished material is presented.

# SYMBOLS AND ABBREVIATIONS

| | |
|---|---|
| ADDE | aqueous-deficient dry eye |
| AO | arachidyl oleate |
| AWAT | acyl-CoA wax alcohol acyltransferase |
| BAM | Brewster angle microscopy |
| BO | behenyl oleate |
| BP | behenyl palmitoleate |
| CE | cholesteryl ester |
| CI | Criegee intermediate |
| CN | cholesteryl nervonate |
| CYP | cytochrome P450 |
| DBT | dihydrolipoamide branched chain transacylase E2 |
| DED | dry eye disease |
| DiE | diester |
| EDE | evaporative dry eye |
| Ed-HSQC | edited heteronuclear single quantum coherence |
| ELOVL | elongation of very long fatty acid protein |
| FAR | fatty acyl-CoA reductase |
| FM | fluorescence microscopy |
| HHP | hydroxyhydroperoxide |
| HMBC | heteronuclear multiple-bond correlation spectroscopy |
| IL | interleukin |
| LC-MS | liquid chromatography-mass spectrometry |
| MAPK | mitogen-activated protein kinase |
| MGD | Meibomian gland dysfunction |
| MMP | matrix metalloproteinase |
| NFκB | nuclear factor kappa-light-chain-enhancer of activated B cells |
| NMR | nuclear magnetic resonance |
| OAHFA | O-acyl-ω-hydroxy fatty acid |
| OAHFAL | O-acyl-ω-hydroxy fatty alcohol |
| PBS | phosphate-buffered saline |
| PL | phospholipid |
| PMF | potential of mean force |
| POPC | 1-palmitoyl-2-oleoyl-sn-glycero-3-phosphocholine |
| PTFE | poly(tetrafluoroethylene) |
| sIgA | secretory Immunoglobulin A |
| SOAT | sterol O-acyltransferase |
| TFLL | tear film lipid layer |
| TG | triglyceride |
| TNF | tumor necrosis factor |
| WE | wax ester |

| | |
|---|---|
| $\pi$ | surface pressure |
| $\sigma$ | surface tension |
| $J$ | evaporative flux |
| $T$ | temperature |
| $C(T)$ | concentration of water vapor at temperature $T$ |
| $R$ | evaporation resistance |
| $C_s$ | isothermal compressibility |
| $a$ | mean molecular area |
| $\mu_\perp$ | effective molecular dipole moment normal to subphase surface |
| $\varepsilon_0$ | permittivity of free space |
| $\Delta V$ | surface potential |
| $r$ | reflectance |
| $d$ | thickness of lipid film |
| $M$ | mass of water absorbed by desiccant |
| $A$ | area of the desiccant box surface |
| $t$ | time of absorption |
| $\boldsymbol{a}$ | acceleration |
| $\boldsymbol{F}$ | force |
| $z$ | position |
| $\Delta A(z)$ | Helmholtz free energy difference between positions $z_1$ and $z$ |
| $N_A$ | Avogadro's constant |
| $k$ | Boltzmann constant |
| $D(z)$ | local diffusion coefficient at position $z$ |

# 1 INTRODUCTION

The tear film is a thin aqueous layer that covers the ocular surface (see Figure 1). It provides lubrication for the movement of the eyes and eyelids, protects the ocular surface epithelia from the surrounding environment, and forms a smooth refractive interface necessary for clear vision. Since the tear film is directly exposed to the surrounding air, it undergoes thinning mainly due to evaporation of water,[1-5] which limits how long the eye can be kept open. In a healthy condition the tear film remains stable between blinks, and it is stabilized by the presence of the tear film lipid layer (TFLL) that resides on the surface of the aqueous tear film.[6-9]

The TFLL is a thin oily film with a thickness ranging in tens of nanometres,[1] and historically it has been considered to act as a barrier to evaporation of water from the ocular surface.[6-9] The TFLL is composed of a wide array of special lipids with very long hydrocarbon chains, including wax esters (WE), cholesteryl esters (CE), O-acyl-ω-hydroxy fatty acids (OAHFA) and diesters (DiE).[10] The physical properties of these exotic lipids have remained relatively poorly known, and many conflicting models of TFLL structure have been proposed.[11-14] Recently even the anti-evaporative function of the TFLL has been disputed and the basis of the stabilizing mechanism of the TFLL is not clear.[8,15] This controversy has important implications for clinical practice, since excessive evaporation is considered to be a central factor in most cases of dry eye disease (DED),[16] which affects hundreds of millions of people worldwide.[17] In order to better understand the pathology of DED and provide improved treatments that improve tear film stability, current models of TFLL structure and function need to be revised.

The aim of this thesis was to address this issue by studying the connection between molecular level organization of various TFLL lipid classes and their evaporation resistance. This was achieved by studying pure model lipids representing different TFLL lipid classes with experimental and computational models at the aqueous interface. The molecular organization and surface properties and of these films were connected to their evaporation resistance to find out their role in TFLL function.

This thesis starts with an overview of the physiology of the ocular surface and the tear film in Chapter 2, followed by description of the current understanding regarding TFLL composition, structure, and function with brief discussion of the related theoretical concepts. The involvement of the TFLL in DED is discussed in detail at the end of Chapter 2. Chapter 3 details the specific aims of this thesis, and Chapter 4 provides an overview of the experimental and computational methods employed in this work. The main results of the attached Publications I–V are presented and discussed in Chapter 5, followed by a summary and a state-of-the-art description of TFLL structure and function based on this work in Chapter 6.

# 2 REVIEW OF THE LITERATURE

## 2.1 OCULAR SURFACE

This section provides the biological context for the results presented in this thesis by describing the different components of the ocular surface system. In addition to the tear film, which is the focus of this thesis, the ocular surface system at the anterior surface of the eye consists of the cornea, conjunctiva, main and accessory lacrimal glands, eyelids, eyelashes and the meibomian glands (Figure 1).[16] All the components of the ocular surface are connected by a continuous epithelium, and act in synergy to maintain a transparent and smooth refractive surface for light to enter the eye, which is central for maintaining clear vision. Light enters the eye through the cornea, which is a transparent tissue that forms the anterior surface of the eye. Cornea is also the main refractive structure of the eye, making up approximately 40 D of the total 60 D refractive power of the eye.[18] Most of the cornea is composed of the corneal stroma, which consists of highly organized lamellae of collagen fibrils that are embedded in a proteoglycan-rich matrix. The collagen fibrils are composed of collagen type I and type V and have a uniform 30 nm diameter and regular 65 nm spacing, which results in cornea being transparent, while simultaneously having considerable tensile strength.[19]

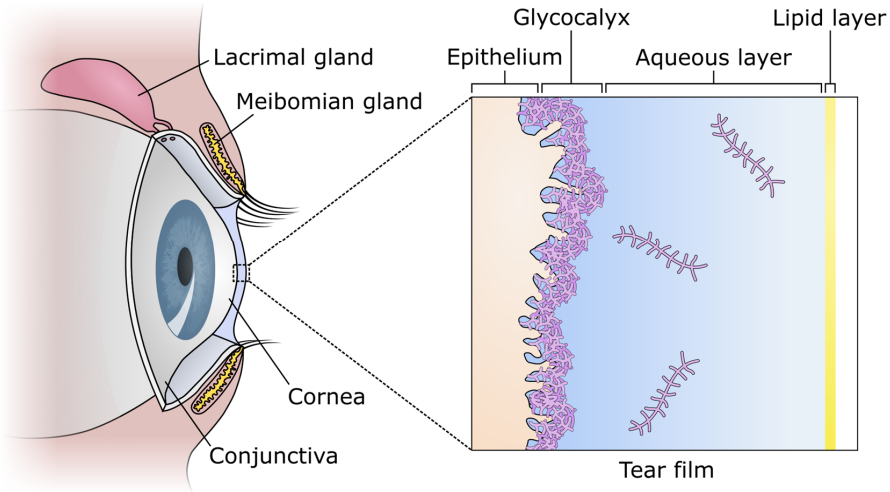


**Figure 1** A schematic representation of the ocular surface and the structure of the tear film. Ocular mucins are depicted in purple.

The anterior surface of the cornea is covered by the corneal epithelium, which consists of five to six layers of squamous, non-keratinized, non-secretory epithelial cells. The transparent cornea is connected to the surrounding white sclera in a region called the limbus, where the corneal epithelium continuously transitions into conjunctival epithelium. Conjunctival epithelium lines the surface of the globe from the limbus to the conjunctival sac and continues along the inner surfaces of the eyelids, connecting to the epidermis of the eyelid skin (Figure 1).

The superficial epithelial cells of the corneal and conjunctival epithelia form the outermost cell layer of the ocular surface. They have an irregular surface covered by microvilli and microplicae,[20] which is coated with a glycocalyx that contains membrane-associated mucin glycoproteins (Figure 1), mainly MUC1, MUC4 and, MUC16.[21,22] The membrane-associated mucins reduce the friction between the eyelids and the globe by providing boundary lubrication and by forming a barrier against allergens or pathogens. The high density of hydrophilic glycans in the glycocalyx also makes the epithelial surface highly wettable, allowing the aqueous tear fluid to spread on its surface.

The tear film covers the cornea and conjunctiva, extending to the eyelid margin, where it forms a meniscus that wets the mucocutaneous junction. At the mucocutaneous junction, the wettable conjunctival epithelium transitions to a less hydrophilic skin surface (Figure 1). Aqueous tear fluid is produced by the main and accessory lacrimal glands, which are located within the bony orbit of the eye and open into the conjunctival sac between the eyelids and the eye (Figure 1). Lacrimal glands are mostly comprised of acinar cells that secrete tear fluid by using a variety of ion transporters and channels to secrete $K^+$ and $Cl^-$ ions into the lacrimal gland ducts, followed by flow of water and $Na^+$ into the ducts through the paracellular pathway.[23] The acinar cells of the lacrimal glands also secrete most of the proteins found in tear fluid, mainly by exocytosis, but also by transcytosis and ectodomain shedding.[23]

The aqueous tear film is covered by a layer of lipids produced by the Meibomian glands, which are located within the tarsal plates in the eyelids (Figure 1). Meibomian glands are composed of clusters of acini that are arranged around long central ducts that run in parallel over the whole eyelid and open at the eyelid margin. The acini are filled with secretory cells called meibocytes that synthesize meibomian lipids. The synthesized lipids gradually accumulate into lipid droplets inside the meibocytes as they move towards the entrance of the Meibomian gland acinus during their maturation.[24,25] Eventually the meibocytes lose their nucleus and also their cell membrane as all the cell contents are released into the central Meibomian gland ductule.[26] The whole cell contents form the oily secretory product of the glands termed meibum.[27] The ductules open at the eyelid margin and meibum spreads as a separate layer on the surface of the aqueous tear film.

## 2.2 TEAR FILM

The tear film is a complex film formed by the aqueous tear fluid secreted from the lacrimal glands, the meibum secreted from the Meibomian glands, and mucins originating from the corneal and conjunctival epithelia that cover the ocular surface. The tear film is very thin, with a total thickness of only around 3 μm,[28,29] and most of the aqueous tear fluid volume actually resides in the upper and lower menisci at the eyelid margins, as well as under the eyelids in the conjunctival sac. The tear film can be divided into two parts: the aqueous layer, which makes up most of the tear film thickness, and the thin lipid layer, which covers the aqueous tear film (Figure 1).[15] The tear film lipid layer is very thin compared to the aqueous layer, with recent estimates indicating a mean thickness value of approximately 40 nm.[1] In addition to the two tear film layers, the corneal and conjunctival epithelia underlying the tear film are coated by membrane-associated mucins as discussed in the previous section. They extend up to 500 nm into the tear film,[20,30] forming the boundary between the epithelium and the tear film (Figure 1). This layer of mucins, as well as some of the secreted mucins are sometimes considered to form a third layer of the tear film.[15]

The functions of the tear film are to smooth out the irregular surface of the corneal epithelium, providing a refractive interface with minimal scattering for the light to enter the eye, to provide lubrication that allows movement of the eye and eyelids, and to protect the ocular surface tissues that are exposed to the environment. In this section, the composition, structure and dynamics of the aqueous tear film are discussed, whereas the tear film lipid layer will be discussed in detail in the following section.

### 2.2.1 AQUEOUS TEAR FILM

The aqueous layer of the tear film consists of water with dissolved electrolytes, metabolites, and proteins, including secreted mucin glycoproteins. The aqueous tear fluid is isotonic with plasma and has a similar electrolyte composition, although with a lower [$Ca^{2+}$] concentration and a higher [$K^{+}$] concentration.[31]

Almost 1800 proteins have been identified in human tears to date,[15] and the typical protein concentration of tear fluid is 6–10 mg/mL.[32,33] However, a large fraction of the identified proteins may originate from the epithelia of ocular tissues, since commonly used tear collection methods such as Schirmer's strip and polyester wick cause some abrasion of the epithelia during tear collection.[34] In fact, only a handful of proteins secreted by the lacrimal glands, namely lysozyme, lactoferrin, secretory Immunoglobulin A (sIgA), and tear lipocalin occur in the tear fluid at high concentrations and make up approximately 80% of total tear fluid proteins.[33,35] The main functions of these abundant proteins appear to be antimicrobial and anti-inflammatory. Lysozyme catalyses hydrolysis of β-1,4 glycosidic bonds in

bacterial cell wall carbohydrates,[36] lactoferrin chelates iron required for bacterial growth and binds to bacterial lipopolysaccharides,[37,38] and sIgA blocks micro-organisms and toxins by immune exclusion.[39] Tear lipocalin may also have antimicrobial or antiviral activity, but due to its lipid-binding properties, it has also been suggested to scavenge lipids from the ocular surface.[40]

In contrast to the major proteins in the tear film, secreted mucins in the tear film are mainly produced by goblet cells, which are interspersed within the conjunctival epithelium.[41] Most of the secreted mucins consist of MUC5AC, whereas MUC2 and MUC19 appear to be present in minor quantities.[42-45] Secreted mucins provide lubrication likely via the "sacrificial layer mechanism",[46] where mucins are sheared off due to the movement of the eyelids. In addition, they aid in clearance of contaminants such as desquamated cells, foreign bodies, allergens, and pathogens.[47]

### 2.2.2 TEAR FILM DYNAMICS

In addition to the static tear film structure described above, there are important dynamical aspects to tear film function. There is a balance of tear fluid secretion and drainage, where the secreted tear fluid flows to the menisci at the eyelid margins, then towards the nasal canthus and eventually drains into the nasal cavity through the lacrimal puncta.[48] The tear film over the cornea and conjunctiva is regularly replenished by the blinking action of the eyelids, during which tear fluid from under the eyelid and the menisci is distributed onto the ocular surface.[49] During the interblink period, a significant fraction of the aqueous tear film evaporates to the surrounding environment, resulting in thinning of the tear film.[1-5] The thinning rates show large variability, but a typical rate is approximately 4 μm/min.[3-5]

Evaporation of water from the ocular surface results in reduction in the temperature of the cornea and increased tear osmolarity. These events activate a population of cold receptors in nerve endings located in the superficial epithelial layers of the cornea.[50] The afferent signal generated by these receptors travels through the ophthalmic branch of the trigeminal nerve to the mid-brain, where it is integrated and an efferent signal is sent to the lacrimal glands.[23,50] The activation of these cold receptors increases tear secretion without the sensation of ocular pain, likely maintaining the adequate level of tear production in normal conditions.[50]

If the eye is kept open without blinking, the tear film eventually dewets as a result of thinning and dry spots form on the ocular surface, exposing the underlying epithelium. This event is called tear film breakup and causes acute discomfort and irritation, caused by the activation of other sensory nerve endings located within the cornea and conjunctiva that respond to a wide variety of mechanical, chemical and thermal stimuli.[23,50] Activation of most of these sensory nerves results in a sensation of pain, as well as increased tear production in attempt to rehydrate the ocular surface and

flush out the source of the harmful stimulus.[23,50] In healthy subjects, tear film breakup occurs approximately 10 seconds after a blink,[51,52] but since the typical blink interval is around 4 seconds,[53] blinking is frequent enough to prevent breakup from occurring in normal conditions.

The tear film lipid layer displays distinct dynamics compared to the aqueous layer. Meibum is secreted from the Meibomian glands to the surface of the tear film at a slow steady rate between blinks,[54] and an additional small aliquot of meibum is secreted with each blink.[7] Secreted meibum collects at the eyelid margin to form a reservoir of lipid on the surface of the tear film.[26] Following the upstroke of a blink, the TFLL rapidly spreads upwards on the surface of the aqueous tear film from the marginal reservoir, presumably driven by a surface tension gradient and covers the aqueous layer within approximately 1 second.[55,56] The lipid layer is not drained through the lacrimal puncta like the aqueous tear fluid, but instead gradually flows over onto the eyelid skin and eyelashes as new meibum is secreted from the Meibomian glands.[57] As a result of the different dynamics, the turnover of the TFLL (1%/min) is much slower than the turnover of the aqueous tear fluid (10–20%/min).[58,59]

## 2.3 TEAR FILM LIPID LAYER

The tear film lipid layer has been proposed to have several different functions, such as forming a hydrophobic barrier on the eyelids to prevent overspill of tears, providing a barrier for foreign particles, or anti-microbial activity, but the main function is most commonly considered to be the stabilization of the underlying aqueous tear film.[6-9] As described in the previous section, a thin aqueous film such as the tear film is not inherently stable when exposed to the surrounding environment, but undergoes thinning and eventually breaks up if the eye is kept open. The TFLL is widely considered to delay tear film breakup from occurring, allowing the eye to be kept open for a longer time between blinks. To give a state-of-the-art view of the TFLL function, this section will review the current knowledge regarding the composition and physical properties of tear films lipids, as well as the experimental data and the proposed models regarding TFLL structure and function.

### 2.3.1 TEAR FILM LIPID LAYER COMPOSITION

It is difficult to determine the composition of the TFLL *in situ*, but lipidomic analyses of tear fluid and meibum samples can be used to infer the composition of the TFLL. Meibum has a distinctly unique composition (Table 1), mostly consisting of wax esters and cholesteryl esters, with smaller amounts of special lipids such as O-acyl-ω-hydroxy fatty acids and diesters.[10,27,60-63]

**Table 1** *Lipidomic studies on the composition of Meibomian gland secretions.*

| **Reference** | Kunnen 2016[63] | Brown 2013[60] | Chen 2013[62] | Lam 2014[61] | Nicolaides 1981[27] | Saville 2011[64] |
|---|---|---|---|---|---|---|
| **Sample type** | Patient | Patient | Patient | Patient | Cadaver | Patient |
| **Lipid** | mol% | mol% | mass% | mol% | mass% | mass% |
| **WE** | **42** | **52** | **48** | **43** | **35** | |
| **CE** | **46** | **44** | **40** | **49** | **29.5** | |
| **OAHFA** | **3.8** | **3.1** | | **2.9** | | |
| **DiE** | | | **7.7** | | **8.4** | |
| Type I-St | | | 4.3 | | | |
| Type II | | | 3.4 | | | |
| **Other lipids** | **7.6** | **1.5** | **4.3** | **4.6** | **27.1** | |
| Cholesterol | 4.2 | | | 1.6 | 1.8 | |
| TG | 3.3 | 1.5 | | 2.4 | 4 | |
| Diacyl PL | 0.08 | 0.0077 | | 0.5 | | 0.0018 |
| Lyso PL | 0.08 | 0.0006 | | 0.1 | | |

In addition, small amounts of other lipids such as cholesterol, triglycerides (TG), and phospholipids (PL) have been detected in meibum.[10,27,60-64] Meibum also contains some proteins,[65] mainly keratins, likely originating from the keratinized epithelial cells lining the Meibomian gland ducts.[66,67]

The main Meibomian lipid classes also display special structural characteristics, such as atypically long hydrocarbon chains (20–36 carbons),[10,60-62] and a high degree of methyl branching.[27] The most abundant species from each lipid class are depicted in Figure 2, and the chain lengths as well as the degree of saturation and methyl branching in each lipid class are shown in Table 2. Most wax esters are composed of an unsaturated fatty acid chain and a long, branched saturated fatty alcohol chain.[27,60,62,68] Cholesteryl ester acyl chains are similar to WE alcohol chains, with very long chain lengths and mostly saturated, branched chains.[12,13,15] OAHFAs have an even more unusual structure, with the hydroxy fatty acid chains consisting almost exclusively of ultra-long chains with a single double bond in the n-9 or n-7 position.[60,69,70] The acyl chains of OAHFAs are predominantly oleate and palmitoleate as in WEs.[60,69,70] Type I-St and II diesters share the same distribution of chain lengths with OAHFAs, reflecting shared synthetic pathways between these ultra-long-chain lipid classes.[71]

The unique composition of meibomian lipids is reflected in the expression profile of lipid-synthesis enzymes in the eyelids, which express high levels of elongation of very long chain fatty acids proteins (ELOVL1–7), fatty acyl-CoA reductases (FAR1–2), acyl-CoA wax alcohol acyltransferases (AWAT1–2), sterol O-acyltransferases (SOAT1–2), cytochrome oxidases (CYP4F22 and others), and dihydrolipoamide branched chain transacylase E2 (DBT).[72]

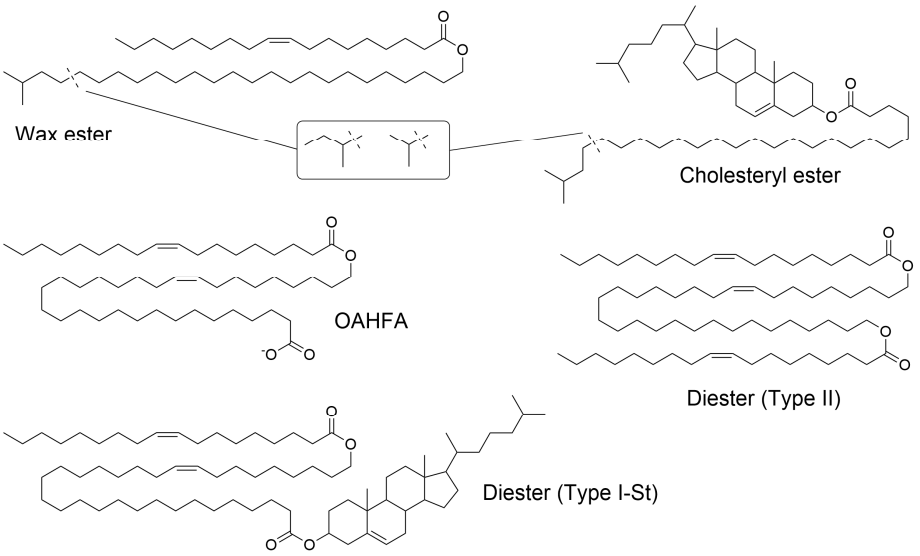


**Figure 2** Main lipid components of the Meibomian gland secretions. The most abundant compound is shown from each lipid class. For wax and cholesteryl esters, also two other abundant compounds are shown.

ELOVLs are involved in the synthesis of the long-chained fatty acids found in meibomian lipids, and FARs convert the long-chained fatty acids to fatty alcohols.[71-73] These fatty acids and alcohols as well as cholesterol are then used as substrates by AWATs and SOATs to produce WEs and CEs.[71,72] CYPs are involved in producing the ω-hydroxy fatty acids required for producing OAHFAs and diesters,[71,72,74] whereas DBT may be involved in synthesizing the branched chain fatty acids found in meibomian lipids.[71,72]

Although most of the TFLL originates from the Meibomian glands, it is possible that some lipids originate from other sources. However, the lipids detected in tear fluid (Table 3) and meibum samples (Table 1) are mostly the same, the main lipid components being WEs and CEs, whereas smaller amounts of OAHFAs have also been detected in both sample types.[27,60-64,75,76] Type I-St and type II diesters have been detected in meibum, but due to the unavailability of suitable standards, they have not been included in the analyses of most studies and therefore have not been specifically identified in tear fluid samples. However, it is likely that diesters occur in the tear fluid in similar abundance as in meibum. The largest difference between meibum and tear fluid samples is observed in phospholipids, which have only been detected in very low amounts in meibum samples (Table 1), whereas much higher fractions (up to 15 mol%) have been detected in tear samples (Table 3). This has led to controversy regarding the role of phospholipids in the TFLL, and some authors have argued that phospholipids are an important part of the TFLL,[14] while others have disputed this view.[10]

**Table 2** *Hydrocarbon chain characteristics of the lipid classes in Meibomian gland secretions. Typical length includes the most abundant lipid species that make up at least 50 mol% of the total lipids. Iso and Anteiso refer to methyl-branched hydrocarbon chains, with the methyl substitution at the ω-2 and ω-3 positions, respectively.*

| Lipid | Typical length (carbons) | Saturated (%) | | | Unsaturated (%) |
|---|---|---|---|---|---|
| | | Normal | Iso | Anteiso | |
| **WE**[27,60,62,68] | | | | | |
| Fatty acid | 16–18 | 3 | 8 | 12 | 77 |
| Fatty alcohol | 24–26 | 7 | 47 | 23 | 22 |
| **CE**[27,60,62] | | | | | |
| Fatty acid | 23–27 | 3 | 45 | 29 | 22 |
| **OAHFA/DiE**[60,62,69,70,77] | | | | | |
| Hydroxy fatty acid | 30–34 | 0-9 | 0 | 0 | 91–100 |
| Fatty acid | 16–18 | 2-8 | - | - | 92–98 |

Several details of the recent lipidomic studies suggest that the quantity of phospholipids in the TFLL is likely small. First, all the recent lipidomic studies found only negligible amounts of phospholipids in meibum.[60,61,63,64,78,79] The lack of phospholipids in meibum, despite the holocrine secretion method of the Meibomian glands, suggests that there may be some mechanisms to remove meibocyte cell membrane phospholipids from meibum. However, it seems counter-intuitive that phospholipids would be removed from meibum but produced from other sources into the TFLL.

Second, it is likely that some, possibly even most of the phospholipids detected in tear samples (Table 3) may be contamination from ocular surface cells. This can be estimated by comparing the results obtained with different tear collection methods. When tears are collected using Schirmer's strips, the strips are placed between the conjunctiva and the eyelid and rub against the epithelial surfaces, which almost certainly leads to collection of lipid material from the epithelial cells in the samples. In fact, Lam et al. found that tears collected using Schirmer's strips contained 5–10 times more phospholipids compared to tears collected with glass capillaries.[61] Large variation in tear phospholipid levels was also observed between different days in the same subjects, as well as between subjects, which also suggests that they are affected by contamination.[80,81] In addition, collection of tears with poly(tetrafluoroethylene) (PTFE) capillaries results in similar levels of phospholipids as detected in meibum, whereas tears collected with glass capillaries contain significantly higher levels of phospholipids.[82,83] Even using different methods to collect meibum result in significant differences in levels of the most abundant phospholipids, suggesting that they are especially sensitive to contamination.[63]

**Table 3** *Lipidomic studies on tear fluid samples collected using either Schirmer's strips or glass capillaries.*

| **Reference** | Lam et al. (2014a)[61] | Lam et al. (2014b)[76] | Lam et al. (2014c)[75] | Rohit et al. (2014)[84] | Brown et al. (2013)[60] |
|---|---|---|---|---|---|
| **Sample type** | Schirmer | Schirmer | Schirmer | Glass capillary | Glass capillary |
| **Lipid** | mol% | mol% | mol% | mol% | mol% |
| **WE** | **35.2** | **44** | **46** | **29** | **43** |
| **CE** | **44.8** | **30** | **33** | **54.8** | **39** |
| **OAHFA** | **2.5** | **1.3** | **1.1** | **1.8** | **4.4** |
| **Other lipids** | **17** | **25.4** | **20** | **14.3** | **14.1** |
| Cholesterol | 5.9 | 7.7 | 7 | 8.2 | |
| TG | 2.8 | 3 | 1.4 | 0.8 | 2.1 |
| Diacyl PL | 5.9 | 9.8 | 6.4 | 1.5 | 4 |
| Lyso PL | 2.4 | 4.6 | 4.6 | 3.8 | 8 |

Third, studies using glass capillaries to collect tears, likely resulting in less contamination than Schirmer's strips, have found that most of the phospholipids detected in the tear fluid are lysophospholipids,[60,84-86] which are relatively soluble in water. In fact, the water solubility of the most predominant lysophospholipid, 1-palmitoyl-sn-glycero-3-phosphocholine (critical micelle concentration 4–8 μM)[87] is of the same order of magnitude as the detected phospholipid concentrations (0–20 μM).[85] Therefore, the lysophospholipids will likely be largely dissolved in the aqueous layer of the tear film. In addition, a large fraction of the tear fluid diacyl phospholipids that would likely partition to the TFLL due to their low water solubility, appear to be bound to tear lipocalin in the aqueous layer.[85]

In addition to phospholipids, small amounts of free cholesterol and TGs have also been detected in the tear fluid and in meibum.[60,61,63,75,76,84] However, some studies may have overestimated the abundance of cholesterol and TGs, since a large fraction of the cholesterol detected using direct-infusion mass spectroscopy can actually originate from disassociation of CEs and diesters, and low-molecular-weight TG standards have been used in many studies, leading in overestimation of the higher molecular weight TGs.[10] In addition, any cellular contamination in the samples would be expected to result in increased levels of cholesterol and TGs in addition to phospholipids. Taking all the above considerations into account, it appears likely that only small amounts of phospholipids, cholesterol, or triglycerides exist in the TFLL, despite being detected in some studies. Therefore, the normal lipid composition of the human TFLL is likely close to meibum composition, namely containing approximately 45 mol% of WEs and CEs each, 3 mol% of Type I-St DiEs, Type II DiEs, and OAHFAs each, and 0–2 mol% of cholesterol and triglycerides each.

### 2.3.2 PHYSICAL PROPERTIES OF TEAR FILM LIPIDS

Since many of the lipids that make up the TFLL are specific to the tear film and are not found in other tissues, the research literature on their physical properties is limited. Most of the relevant data available concerns WEs and CEs and it is reviewed in this subsection to give a general overview of their phase behaviour and structure of different phases.

As shown in Table 2, most of the tear film WEs are composed of a saturated alkoxy chain and an unsaturated acyl chain. Unfortunately, no information is available on the crystal structure of such wax esters, but some insight into their solid-state properties can be obtained by considering the studies on completely saturated WEs and jojoba-like WEs with unsaturated alkoxy and acyl chains. Pioneering X-ray and electron diffraction studies on saturated WEs have discovered that they organize into crystals with chains extended and packed in lamellae, similar to linear hydrocarbons.[88-91] In contrast to linear hydrocarbons of corresponding length, which pack in lamellae where the chains are oriented perpendicular to the interlamellar surface,[92] most saturated WEs have been found to adopt a lamellar structure with tilted chains (Figure 3A),[88-91] likely to accommodate the crowding of ester groups next to each other. Jojoba-like WEs with two double bonds have also been identified to pack in a similar lamellar crystal structure,[93] although the detailed structure is not known. Asymmetric saturated WEs, where the ester group is offset from the centre of the molecule, can also organize in a rectangular crystal polymorph without tilt (Figure 3B),[90,91] likely since the neighbouring WEs can adopt an antiparallel orientation, which avoids the crowding of the ester groups.[94]

The presence of the ester group also alters the thermotropic behaviour of wax esters compared to hydrocarbons. Upon heating, linear alkanes undergo a transition a rotator phase before melting,[92,95] where the molecules have long range positional order in all dimensions but have rotational freedom around their long axis.[95] Such a rotator phase is not observed in wax esters, which melt directly from the crystal phase to an isotropic liquid phase.[93,96] Therefore, the ester group appears to restrict the rotation of wax ester molecules around their long axis when they are ordered in lamellae. Saturated WEs generally melt at higher than physiological temperatures,[97] whereas jojoba-like WEs are in liquid phase at physiological temperatures.[93] However, tear-film-like WEs with a saturated alkoxy chain and an unsaturated acyl chain melt close to physiological temperatures.[96,98,99]

Cholesteryl esters display a variety of crystal structures and relatively complicated thermotropic behaviour depending on the chain length.[100,101] Here the discussion will focus on CEs with acyl chain lengths over 20 carbons, corresponding to the most abundant tear film CEs. Cholesteryl esters with long, saturated linear acyl chains have melting points of over 80 °C. They pack in a bilayer crystal structure with antiparallel orientation, where the acyl chains interdigitate to form high-density layers (Figure 3C).[100,101]

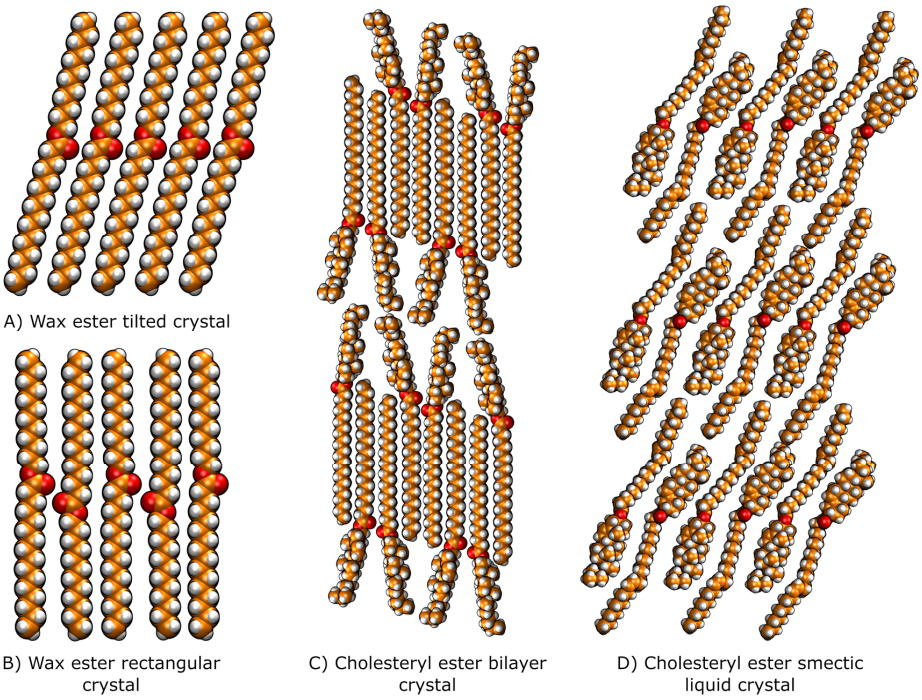


**Figure 3** Schematic representation of molecular organization in selected wax ester and cholesteryl ester phases. Carbon atoms are shown in orange, oxygen atoms in red, and hydrogens in white. Note that the atom positions do not reflect the exact crystal structure but rather a visualization of the general organization is provided.

These crystals melt directly to the isotropic phase and no complex phase behaviour in observed.[100] Unsaturated CEs pack in more complicated crystal structures termed monolayer I or monolayer II and undergo a transition to a smectic liquid crystal phase at relatively low temperatures (43 °C for cholesteryl nervonate) before melting to the isotropic liquid phase.[100] In the smectic liquid crystal phase, the molecules have antiparallel orientation and are tilted by about 54° with respect to the smectic plane, whereas the acyl chains are disordered and protrude to the interfacial region (Figure 3D).[100] It is clear that the presence of a double bond in the long acyl chain drastically alters both the thermotropic and crystal properties of CEs, but currently no studies have examined how iso- or anteiso-branching present in most abundant tear film CEs affects their properties.

Although the bulk properties of tear film lipids described here give an overall view of their organization, they do not completely describe how these lipids behave when introduced to an aqueous interface on the surface of the tear film. This will be discussed in the following subsection.

### 2.3.3 TEAR FILM LIPIDS AT AQUEOUS INTERFACES

At the surface of the aqueous tear film, the self-assembly of different lipids is highly influenced by the polarity of the lipids in question. The polarity of a lipid generally depends on the number of polar functional groups, such as ester, carboxylic acid, or phosphate groups in the molecule. However, also the number and length of nonpolar hydrocarbons in the molecule is important. When lipids are in contact with an aqueous interface, the polar groups in the lipid molecules will tend to orient towards water due to the favourable interactions with the polar water molecules, whereas the nonpolar hydrocarbon parts of the molecule are not strongly attracted to water. In addition, the hydrophobic effect makes it unfavourable for the nonpolar parts of the molecule to enter the water phase, and they are therefore generally oriented away from the water surface. As a result of these effects, polar lipids form an ordered monomolecular layer at the air-water interface (Figure 4A). Such a film is called a Langmuir monolayer, when it is formed by lipids that are insoluble in water. When the surface concentration of lipids in the monolayer is sufficiently high, the neighbouring lipid molecules begin to repulse each other due to entropic repulsion of the hydrocarbon chains and complex repulsive interactions between polar groups including steric, hydration force, and electrostatic contributions.[102] These forces act in the opposite direction than the surface tension of water (Figure 4A), resulting in a decrease of surface tension, defined as surface pressure

$$\pi = \sigma_{\mathrm{w}} - \sigma, \tag{1}$$

where $\sigma_{\mathrm{w}}$ is the surface tension of a pure water interface and $\sigma$ is the surface tension in the presence of the lipid monolayer.

This description is valid for polar lipids, where the interactions between the polar groups and water molecules are strong compared to other forces in the system. However, in the case of increasingly nonpolar molecules, such as many of the tear film lipids, the intra-molecular van der Waals interactions between the hydrocarbon sections of the lipid molecules start to dominate over the polar groups.[103] As a result, very nonpolar molecules do not spread to form a monolayer at the water surface, but dewet to form droplets or solid aggregates instead (Figure 4B).[103]

When polar lipids are mixed with nonpolar lipids, the polar lipids can act as spreaders and cause the spreading of the lipids as a uniform layer on the aqueous surface (Figure 4C). When the thickness of such films is less than 100 μm, they are called duplex films.[104] Duplex films are thick enough that they can be considered to exhibit bulk lipid properties with two distinct (water-lipid and lipid-air) interfaces, but thin enough that the effects of gravity are negligible.[103,104] Polar lipids promote the initial formation of duplex films, since they form a monolayer at the lipid-water interface, lowering its surface tension ($\sigma_{\mathrm{lw}}$).[103,104]

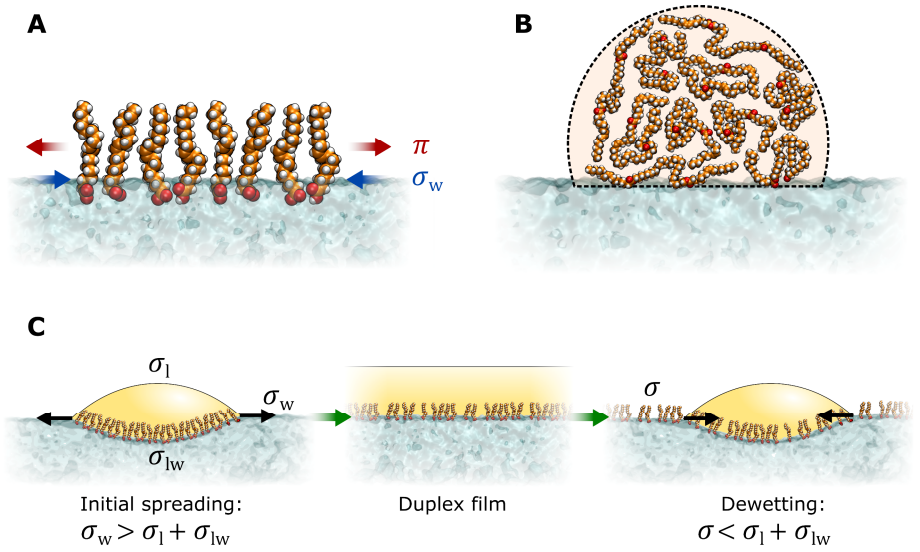


**Figure 4** General organization of polar and nonpolar lipids at the air-water interface. Oxygen atoms are depicted in red, carbons in orange, and hydrogens in white. **A)** Polar lipids form a monolayer with the polar groups facing the water phase and hydrocarbons facing the air phase. Surface tension of the water interface ($\sigma_w$), and surface pressure excerted by the lipid monolayer ($\pi$) are depicted by arrows. **B)** Highly nonpolar lipids collect to form liquid lenses or solid aggregates on the water surface. **C)** Mixtures of polar and nonpolar lipids may initially spread to form a duplex film due to the low lipid-water surface tension ($\sigma_{lw}$). However, lowering of water surface tension from $\sigma_w$ to $\sigma$ by polar lipids eventually leads to dewetting of the duplex film. Only polar lipids are explicitly shown.

However, with time, the polar lipids spread from the interface between the nonpolar lipids and water to the air-water interface and lower its surface tension also, causing the nonpolar lipids to dewet into aggregates again.[103] Therefore, duplex films are inherently unstable. However, the dewetting process may be slow enough to allow for a duplex layer to be maintained for extended periods of time in case of some lipids.

Most of the tear film lipids (Figure 2), such as WEs, CEs, and diesters are highly nonpolar, with typically only one polar ester group per 35–55 carbon atoms. They are much more nonpolar than triglycerides (20 or less carbons per ester group), for example, which are considered to be nonpolar lipids in most contexts. As a result, nonpolar tear film lipids have been suggested not to spread as monolayers but rather aggregate on the aqueous interface.[105] Unfortunately, the most abundant tear film lipids have not been directly studied on the aqueous interface, but some aspects of their interfacial organization can be inferred based on results on analogous model lipids.

Wax esters have been found to form condensed raft-like aggregates at temperatures below the melting point of the WE.[99,106-109] In this state, the molecules at the aqueous surface have been suggested to adopt a “hairpin” configuration, with the ester group facing the aqueous interface and the

hydrocarbon chains oriented vertically and closely packed together.[106,110] However, it is clear that in this state WEs do not effectively spread on the aqueous interface, but form multi-layered aggregates that are unstable and do not re-spread on the aqueous surface after compression.[99,109] When the temperature is increased above the melting point of the wax ester, the films have been shown to expand and form a more uniform film, indicating formation of a monolayer by wax esters.[99,106,109,111] This expanded monolayer state has been characterized as having a V-shaped molecular conformation, where the ester group is facing the water and hydrocarbons are pointing towards the air, but the hydrocarbon chains are highly disordered.[99,106,111,112]

Saturated cholesteryl esters with at least 14 carbons in the acyl chain do not spread on the air-water interface but form crystalline aggregates with structure corresponding to the bulk bilayer arrangement of saturated CEs.[109,113] In contrast, unsaturated CEs with acyl chain lengths of 14–18 carbons spread on the aqueous interface to form a "double layer".[114,115] This structure has been suggested to consist of a monolayer at the aqueous interface and an overlying second monomolecular layer of CEs.[114] The molecules in the underlying monolayer have been proposed to orient their ester groups towards water and hydrocarbon regions towards air,[114] similar to the WE monolayer organization described above. The overlying CE layer has been suggested to consist of CEs packed in parallel with their steroid nuclei adjacent to each other, although an antiparallel organization resembling the smectic liquid crystal state (Figure 3D) could not be ruled out.[114] However, unsaturated cholesteryl nervonate with a 24-carbon acyl chain, corresponding to typical CE chain lengths in meibum (Table 2), did not spread to form a monolayer or a double layer, but instead formed large multilamellar liquid crystalline aggregates.[109,116]

Although WEs and CEs can spread to form a monolayer or a double layer, they are still only weakly surface-active, and generate only low surface pressures (< 10 mN/m).[99,109,111,112,115] In general, increasing the hydrocarbon chain lengths in WEs and CEs decreases the surface pressure that they can generate,[99,115] since increasing the size of the hydrocarbon moieties makes the molecules less polar, promoting aggregation. Considering that the WE and CE analogues used in the studies described above are mostly shorter than the very long CEs and WEs that are most abundant in the TFLL (Table 2), it is likely that the WEs and CEs in the TFLL would not readily spread on the tear film surface, but rather be prone to forming aggregates.

The organization of OAHFAs at the aqueous surface has been studied using a short-chain analogue, (O-oleyl) ω-hydroxy palmitic acid (16:0/18:1), which readily formed a monolayer that could reach surface pressures of at least 15 mN/m.[112] A molecular orientation with both the carboxylic acid and the ester group lying on the water surface at low surface concentrations was suggested, whereas at high surface concentrations OAHFAs were suggested to adopt an extended conformation where the ester groups detach from the water surface.[112] These results highlight the more polar character of OAHFAs

compared to other TFLL lipid classes. Due to the presence of the polar carboxylic acid group, TFLL OAHFAs are expected to readily spread on the aqueous tear film surface and potentially aid the spreading of non-polar TFLL lipids as a duplex layer as described above. The organization of such complex films will be discussed in the following subsection.

### 2.3.4 STRUCTURE OF THE TEAR FILM LIPID LAYER

Although experimental studies concerning the organization of individual TFLL lipid classes have provided important clues concerning their organization at the aqueous interface, the overall structure of the TFLL is still largely unknown. Over the years, several models of TFLL structure have been proposed in attempts to describe its molecular level organization. These models will be discussed briefly in this subsection, together with most recent experimental evidence regarding TFLL structure.

The thickness of the TFLL has been estimated to be approximately 40 nm,[1] suggesting that it is at least 10 molecules thick on average. Therefore, the TFLL has been characterized as a duplex film mostly consisting of nonpolar lipids with a monolayer of more polar lipids at the interface between the nonpolar lipids and the aqueous tear film.[117] The pioneering model by McCulley and Shine described the polar lipid monolayer as an ordered hexagonal lattice,[11] resembling ordered phases in Langmuir monolayers.[118] The nonpolar lipids were considered to form ordered lamellae on top of the polar layer, with some intercalation of lipids between the layers.[11] King-Smith et al. later proposed a similar model that maintains the ordered structure of the nonpolar layer, but additionally suggests that the CEs and WEs are organized into stacked lamellae with alternating layers of high and low degree of order.[12] Each lamella would consist of interdigitated WEs and/or CEs, and contain a tightly packed central layer composed of long, saturated hydrocarbon chains of the WE alkoxy chains and/or CE acyl chains, whereas the unsaturated WE acyl chains and CE cholesteryl moieties would be oriented towards the outside of each lamella.[12] In contrast to these lamellar models, Rosenfeld et al. suggested that only the polar monolayer and the nonpolar lipids directly adjacent to the polar monolayer are ordered.[13] Instead, most of the film should be considered as an isotropic liquid, which contains suspended lamellar lipid crystallites that are randomly distributed throughout the liquid layer.[13] Svitova et al. suggested a similar isotropic duplex film model but emphasized the role of phospholipids in the TFLL organization.[14] Instead of suspended crystallites of nonpolar lipids within the duplex layer, they suggested that an inverted bilayer of phospholipids and ceramides would be present at the lipid-air interface.[14] Cwiklik highlighted the dynamical aspect of the TFLL during blinking of the eyelids, suggesting that three-dimensional assemblies of lipids are formed during blinking, both in the aqueous tear film and inside the nonpolar sublayer.[119]

Currently there is not enough experimental evidence to confirm which of the models described above most accurately reflects the structure of the TFLL. The molecular level structure of the TFLL is highly challenging to study directly, but studies using different model systems have provided important clues in this respect. The simplest model system is to study molecular order in Meibomian gland secretions. In healthy subjects, meibum is in a liquid state inside the Meibomian glands. However, meibum starts to crystallize at 35–36 °C,[13,66,96] and since the temperature of the ocular surface is a few degrees lower than body temperature (32–36 °C),[120-123] meibum becomes partially crystalline as it is spreads on the surface of the tear film. Infrared spectroscopy studies have found that approximately 30–50% of the hydrocarbon chains in meibum are in the *trans*-conformation at physiological temperatures.[124] Small angle X-ray scattering has revealed three lamellar phases in meibum with d-spacings of 111 Å, 49 Å, and 43 Å.[125] The phases with shorter lamellar spacing melted at around 34 °C, whereas the phase with longer spacing persisted to higher temperatures.[125] The nature of these lamellar phases remains currently unknown, but the short periodicity phases with the highest intensity could reasonably be formed by lamellae of wax esters or cholesteryl esters in an extended conformation. The long periodicity phase could originate from the longer OAHFAs or diesters. These results have confirmed that TFLL lipids form lamellar ordered structures at the conditions present on the ocular surface but cannot answer how these structures are organized with respect to the aqueous tear film surface.

Another model system, which can be used to study TFLL organization on the aqueous tear film surface, consists of spreading meibomian lipids on the surface of an aqueous layer, typically in a Langmuir trough. When a small amount of meibum is spread over an aqueous interface, a non-uniform layer consisting of thin and thick regions is formed.[125-129] The thin regions likely only contain a monolayer of polar lipids, whereas the thicker regions have a solid appearance and have been suggested to consist of some form of a multilayer of polar and nonpolar lipids.[127,129,130] When more meibomian lipids are added to the aqueous surface, the whole water surface becomes covered by a thick lipid film,[125-129] and eventually even thicker (tens of nanometers) droplets of lipids form on the film surface.[116] Similar thick droplets and other types of local thickness patterns have also been observed directly in the TFLL *in vivo* using high-resolution microscopy,[131,132] but currently the origin of these different patterns is poorly understood. Some of the patterns may be related to dewetting processes, where the lipid layer breaks into lenses on the surface of the aqueous layer, while others may be due to local variation in the lipid composition.[131] However, it is clear that the thickness of the TFLL is not uniform as it is typically presented in TFLL models, but regions of lower and higher thickness exist over the ocular surface.

Grazing incidence X-ray diffraction studies have shown that meibomian lipid films spread on an aqueous surface form a monolayer with an ordered structure.[133,134] In human meibum, the monolayer structure resembles the *Ov* phase identified in fatty acid monolayers, suggesting that the ordered lattice at the aqueous interface is formed by OAHFAs and/or wax esters, and likely not cholesteryl esters.[134] X-ray reflectivity of meibum films on water surface at room temperature also suggested the formation of multilayers,[134] with spacing corresponding to the lamellar phases observed in bulk meibum.[125] These results confirmed the ordered structure of the polar monolayer at the interface, and the presence of some multilamellar ordering by the nonpolar lipids, at least in room temperature. However, it is currently unclear to what extent this ordering persists at physiological temperatures.

To summarize, all the TFLL models presented agree that polar TFLL lipids form a thin ordered layer at the aqueous tear film surface. As described in subsection 2.3.1, most recent lipidomic studies suggest that this polar sublayer mostly consists of OAHFAs. Nonpolar CEs, WEs, and diesters reside over the polar sublayer, and experimental evidence has indicated that at least part of the nonpolar lipids form some type of crystalline or liquid-crystalline structures. However, currently no consensus exists on how these ordered regions of nonpolar lipids are organized. Some models consider that the ordering effect of the water interface extends all across the nonpolar layer, ordering it into lamellae parallel to the water surface, whereas others consider that it only extends up to a few layers of molecules from the interface, beyond which the nonpolar lipids act identical to bulk lipids. Moreover, the importance of local variations in TFLL thickness and structure remain poorly understood.

Recent TFLL models also suggest that proteins from the aqueous layer of the tear film adsorb to the polar sublayer of TFLL.[13,14,119] However, the function of these adsorbed proteins remains largely unknown. Model systems have been used to study the interaction of various tear fluid proteins with the TFLL lipids, but the nature of these interactions remains elusive. Studies using bovine submaxillary gland mucin as a model of secreted ocular mucins have suggested that mucins facilitate the spreading of the TFLL lipids.[14,117,135,136] However, this effect is still unclear, since bovine submaxillary gland mucin is more surface active than pure bovine or rabbit ocular mucins, which are not surface active even at much higher concentrations than those occurring in the tear fluid.[136,137] Tear lipocalin has been shown to adsorb to meibomian lipid films,[138,139] but its effect on the TFLL is not well understood. Tear lipocalin is a lipid-binding protein that binds a wide array of ligands,[40] but interestingly, none of the main TFLL lipids.[140] Therefore, it might have a role in transferring unwanted lipids away from the TFLL.[140] Also other tear film proteins, such as lysozyme or lactoferrin may adsorb to the TFLL,[14,141,142] and might stabilize it or alter its rheological properties, but these effects remain poorly characterized. Also, it has been argued that although protein adsorption occurs in model systems

with loosely packed meibomian lipids, adsorption would be blocked by the densely packed TFLL in physiological conditions.[9,14]

As described in this subsection, there are still many aspects of TFLL structure that remain poorly understood. These uncertainties have led to controversy regarding how the TFLL achieves its stabilizing function, which will be discussed in the following subsection.

### 2.3.5 STABILIZING MECHANISM OF THE TEAR FILM LIPID LAYER

As described in the beginning of this section, the TFLL is considered to stabilize the aqueous tear film while the eye is open and prevent formation of dry spots on the ocular surface. However, the underlying physical mechanism behind the stabilizing effect remains unclear. There are at least three different stabilization mechanisms by which the TFLL has been proposed to act: 1) by reducing the surface tension of the aqueous tear fluid, 2) by stabilizing the aqueous tear film against dewetting due to the viscoelasticity of the lipid film, and 3) by slowing down evaporation of water from the aqueous tear fluid.

The first mechanism, which proposes that the TFLL decreases the surface tension of the aqueous tear fluid to allow the formation of a stable thin aqueous film on the ocular surface, instead of dewetting into droplets, is often presented even in recent literature.[7,15] However, there are several factors that make it very unlikely to be a major stabilization mechanism. First, experimental studies have shown that the corneal epithelium is highly wettable by water due to the presence of the hydrophilic glycocalyx.[143,144] Therefore, no lowering of surface tension is needed to form a thin aqueous film on the surface of the eye. Second, theoretical considerations have shown that high surface tension would actually stabilize the aqueous tear film against rupture.[145,146] Third, if decreasing the surface tension would be a major function of the TFLL, it would be expected to contain larger amounts of polar lipids that effectively reduce surface tension, as is the case with lung surfactant,[105] rather than mostly nonpolar lipids with very low surface activity.

The second mechanism proposes that the TFLL stabilizes the aqueous tear film against rupture by forming a viscoelastic shell on the surface of the tear film. In theory, a viscoelastic lipid layer on the surface of the aqueous tear film could resist the deformation of the tear film surface that occurs during break-up, and hence stabilize the tear film against breakup. This mechanism has only been explored by a few studies using aqueous films on either silicon wafers or silicone hydrogel contact lenses as models of the tear film.[147,148] They found that a viscoelastic layer formed by meibum can slow down the onset of dewetting instability of aqueous films and lower the critical thickness at which dewetting occurs.[147,148] However, the substrates used were less wettable than the ocular surface epithelium, and therefore it remains to be seen whether such an effect is relevant for the TFLL.

The third mechanism, which proposes that the TFLL slows down the evaporation rate of water from the aqueous tear film, is the most widely proposed and studied stabilizing mechanism of the TFLL. This kind of function would be plausible, since evaporation has been shown to be the main factor contributing to tear film thinning,[2,3] and thin lipid films have long been known to be capable of resisting evaporation.[149] There is wide body of evidence on the evaporation resistant function of the TFLL,[1,146,150-156] although some contradictory findings have also been presented.[157-162] These issues are discussed in detail in the following subsections, starting with the theoretical aspects of evaporation resistance, followed by a discussion of the evaporation resistance of tear film lipids.

### 2.3.6 THEORY OF EVAPORATION RESISTANCE

Evaporation resistance of lipid films can be measured in a highly controlled way by first spreading a lipid film on the surface of a container filled with water and then either measuring the loss of water from the container, or the absorption of water in some desiccant material outside the container. However, performing these studies in practice is not as simple as they might seem, since the evaporation process depends both on the rate at which water molecules escape from the water surface, and the rate at which they move into the surrounding air via diffusion and convection. The evaporation process in the presence of a lipid film has been recently reviewed by Cerretani et al.[162] and can be briefly summarized as follows:

When a pure water surface is exposed to air, evaporation occurs if the water vapor concentration in the air, $C_\infty$, is lower than the saturated water vapor concentration in equilibrium with liquid water, $C_\mathrm{w}^\mathrm{sat}$, at the temperature of the water surface $T_\mathrm{w}$. The evaporation process can be divided into two steps (Figure 5). First, the water molecules escape from the liquid water to a thin vapor layer above the water surface. This molecular-kinetic evaporative flux is associated with interfacial resistance to evaporation $R_\mathrm{I}$. Second, after escaping from the liquid water, the water molecules encounter the gas molecules in the surrounding air and move away from the surface via diffusion and convection, characterized by the mass-transfer resistance $R_\mathrm{M}$. Therefore, the evaporative flux $J_\mathrm{w}$ from the pure water surface can be stated as

$$J_\mathrm{w} = \frac{C_\mathrm{w}^\mathrm{sat}(T_\mathrm{w}) - C_\infty}{R_\mathrm{I} + R_\mathrm{M}}. \qquad (2)$$

The molecular-kinetic resistance to evaporation $R_\mathrm{I}$ can be described by the gas-kinetic theory using the Hertz-Knudsen equation[163,164] and has a value of approximately $10^{-4}$ s/cm at temperatures relevant to the ocular surface. The mass-transfer resistance $R_\mathrm{M}$ can vary by several orders of magnitude, depending on the conditions.

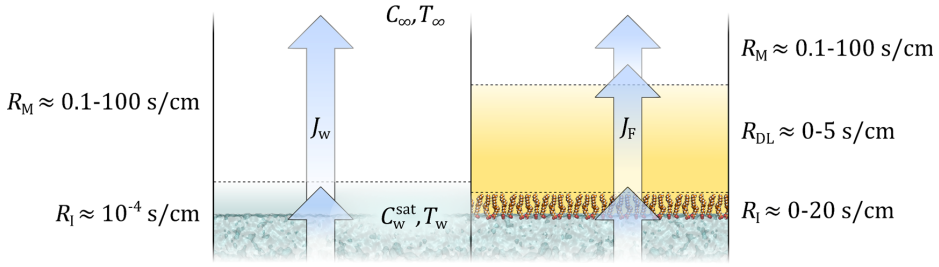


**Figure 5** Evaporative flux from pure a water surface ($J_w$, left) and a water surface covered by a lipid film ($J_F$, right). Evaporation is driven by the difference in water vapor concentration in equilibrium with the water surface ($C_w^{sat}$) at temperature $T_w$ and the water vapor concentration in the surrounding environment ($C_\infty$) at temperature $T_\infty$. Different sources of evaporation resistance and typical values are shown, including interfacial resistance to evaporation ($R_I$), mass-transfer resistance ($R_M$), and duplex layer evaporation resistance ($R_{DL}$).

Typical values range from 0.1 s/cm (10 m/s airflow over the surface) to 100 s/cm (30 cm stagnant air layer over the surface).[162] By comparing the relative magnitudes of $R_I$ and $R_M$, it is clear that in conditions relevant to the ocular surface, evaporation rate from a pure water surface is mainly determined by the convective flow in the surrounding air. However, the presence of an ordered lipid monolayer on the water surface can drastically increase the interfacial resistance to escape from the water surface, $R_I$. The evaporation resistance of monolayers formed by many classes of polar lipids have been described in detail using either desiccant-based methods in a Langmuir trough,[165,166] or experimental setups utilizing high airflow.[167,168] Monolayers of saturated linear polar lipids, such as fatty acids or alcohols, for example, readily form evaporation resistant monolayers.[168-170] The evaporation resistance appears to depend on the formation of a tightly packed condensed monolayer phase, and monolayers of lipids that do not form such a structure, such as cholesterol or unsaturated fatty acids, do not resist evaporation.[167] In the case of saturated polar lipids, evaporation resistance increases exponentially with increasing chain length.[171] The highest evaporation resistances (up to 20 s/cm) have therefore been obtained with long-chained fatty alcohol and oxyethanol monolayers at high surface pressures.[172]

Several theories have been proposed in attempts to describe the basis of evaporation resistance by lipid monolayers, such as the energy barrier theory,[165,169] the density fluctuation theory,[173] and the accessible area theory.[174] Although these theories predict some of the results obtained with saturated polar lipids and their mixtures reasonably well, none of them is widely applicable over a range of different lipids or lipid mixtures.[171] Especially the marked effects that impurities or molecules like cholesterol have on evaporation resistance cannot be described by these models.[171] These considerations have led to the suggestion that evaporation through monolayers proceeds mostly through domain boundaries present between

the condensed monolayer domains.[171] This suggestion has been supported by oxygen permeation studies,[175] which have indicated that the permeation through monolayer domain boundaries could be characterized by combining accessible area and energy barrier theories.[175]

If a thicker duplex film is also present on the water surface, it can cause an additional evaporation resistance component, $R_{\mathrm{DL}}$ (Figure 5). In this case, the evaporative flux through the film becomes

$$J_{\mathrm{F}} = \frac{C_{\mathrm{w}}^{\mathrm{sat}}(T_{\mathrm{w}}) - C_{\infty}}{R_{\mathrm{I}} + R_{\mathrm{DL}} + R_{\mathrm{M}}}. \tag{3}$$

Since the duplex film is considered to exhibit bulk lipid properties, the double layer resistance can be characterized as $R_{\mathrm{DL}} = L/Dk$, where $L$ is the thickness of the duplex layer, $D$ is the diffusion coefficient of water in the lipid and $k$ is the partition coefficient of water in the lipid phase. Using the air-oil partition coefficients reported for hydrocarbons (1.7),[176] the lowest estimated diffusion coefficient for water in oil ($1 \times 10^{-6}$ cm²/s),[162] and considering that the thickness of the TFLL is typically no more than 100 nm, such a disordered duplex layer of lipid can be estimated to cause up to 5 s/cm evaporation resistance.

The mass-transfer resistance from the ocular surface in ventilated room air or during walking is expected to be in the range of 1–5 s/cm, as estimated by Cerretani et al.[162] In these conditions, an ordered lipid monolayer could potentially reduce the evaporation rate by as much as 80–95%, whereas a duplex film could cause a reduction of approximately 50–80%. From the theoretical perspective, it is clear that a lipid film can cause a clinically significant reduction in evaporation rate from the ocular surface. However, it seems likely that TFLL evaporation resistance results mostly from an ordered lipid layer at the aqueous interface, especially since the nonpolar sublayer has a non-uniform structure and does not cover the whole tear film surface, as described in subsection 2.3.4.

### 2.3.7 EVAPORATION RESISTANCE OF TEAR FILM LIPIDS

Several attempts have been made to determine the evaporation reduction caused by Meibomian lipids using model systems. Reduction of evaporation by lipid films is commonly determined by measuring the evaporation rate in the presence and absence of a lipid film, while maintaining other experimental parameters constant. Typically, the ratio of evaporation rates in the presence and absence of a film, defined as

$$\frac{J_{\mathrm{F}}}{J_{\mathrm{w}}} = \frac{R_{\mathrm{M}}}{R_{\mathrm{I}} + R_{\mathrm{DL}} + R_{\mathrm{M}}} \tag{4}$$

is reported. Here the molecular-kinetic resistance to evaporation from a pure water surface has been neglected, since it is insignificantly small in most

experimental setups. As seen from equation (4), simply reporting the ratio of evaporation rates has a significant downside, namely that the ratio depends on the mass-transfer resistance $R_M$, which will be specific to the measurement system used. Therefore, results obtained with different measurement setups are not readily comparable. Further, the ratio of evaporation rates only provides relative information about the evaporation resistance of the lipid films studied, unless the mass transfer resistance is quantified or standard lipids with known evaporation resistance are used as controls. These factors must be considered when interpreting results from *in vitro* studies with Meibomian lipids, which have reported mostly negative results.

Brown & Dervichian[157] studied the evaporation reduction caused by spreading human meibum on the surface of saline-filled beakers and comparing that to pure saline at 37 °C but detected no reduction in evaporation. Miano et al.[177] used a pendant drop method to study the effect of bovine meibum on evaporation and found a 30% reduction at 25 °C and 36 °C. However, one of the co-authors has later claimed to have repeated the measurements and found no evaporation resistance, although the data have not been published.[8] Herok et al.[158] measured the evaporation reduction caused by human, rabbit, and bovine meibum using a thermo-microbalance at 37 °C and detected a less than 10% reduction with lipid film thicknesses in the micrometer-range. Borchman et al.[159,160] have measured evaporation reduction caused by various model lipids mimicking meibum, such as wax esters and cholesteryl esters. They measured water loss gravimetrically from plastic containers and found modest evaporation reductions when lipid layer was at least 10 μm thick. Sledge et al.[161] used the same system to measure the evaporation resistance of thick films of human meibum at 34 °C and found no evaporation reduction. Interestingly, they also measured evaporation reduction caused by fatty alcohols, which have been well established to form evaporation resistant films in the previous literature.[168,170] However, they found no reduction in evaporation by fatty alcohols using their method.[161] This is a strong sign that the methodology in the studies of Borchman et al.[159,160] and Sledge et al.[161] is not able to detect evaporation resistance of lipid monolayers properly. In fact, none of the studies listed here have included a positive control using evaporation resistant lipids to ensure that their methods can detect evaporation resistance by lipid monolayers. One of the reasons for the inability to detect evaporation resistance may be that these studies have been generally performed under stagnant air conditions. As discussed in the previous subchapter, this results in a large mass-transfer resistance in the surrounding air. As seen from equation (4), if the mass-transfer resistance is large compared to other resistances in the system, no evaporation reduction by the lipid film will be detected. Since the mass-transfer resistance was not quantified, the studies listed above have limited value when considering the evaporation resistance of tear film lipids.

Cerretani et al.[162] considered the issue of mass-transfer resistance in detail and used a custom system to measure the evaporation resistance of human and bovine meibum at 36 °C. Surprisingly, they also found that a 100 nm thick film of meibum had an evaporation resistance in the range of only 0.1 s/cm.[162] Rantamäki et al.[99,108] used a Langmuir trough-based system to measure evaporation reduction caused by model tear film lipids and found that wax esters reduced evaporation with similar efficiency as behenyl alcohol, which has one of the highest evaporation resistances reported (~20 s/cm).[170] However, this effect was only detected at a narrow temperature range below the melting point of each wax ester.[99] Therefore, previous measurements conducted at temperatures higher than meibum melting point at 36–37 °C may have missed this effect. In fact, Cerretani et al.[162] reported that in a few measurements performed at room temperature, the evaporation resistance of bovine meibum was an order of magnitude higher than at 36 °C but did not investigate this further. In conclusion, the failed attempts to detect evaporation resistance by TFLL lipids *in vitro* can largely be attributed to poor experimental methodology or unsuitable experimental conditions rather than proof that the TFLL is unable to resist evaporation.

The evaporation resistance of the TFLL has also been estimated *in vivo* by pioneering studies using rabbits and rhesus macaques.[150,151] These studies found that evaporation rate increased 4–17 folds after the ocular surface was flushed with saline to remove the TFLL,[150,151] resulting in an estimate of 13 s/cm for the evaporation resistance of the TFLL.[151] Evaporation rate decreased back to baseline after the TFLL was restored by blinking.[150] Although such direct methods to remove the TFLL have not been used in later studies, they have indirectly indicated the evaporation resistance of the TFLL. A recent mouse study showed that loss of ELOVL1, an enzyme involved in synthesis of Meibomian lipids, increased the evaporation rate from the ocular surface two-fold.[152] Clinical studies have also demonstrated the evaporation resistance of the TFLL in humans. Craig & Tomlinson observed the interference fringes on the tear film surface resulting from the TFLL and found that evaporation rate was increased several-fold in subjects, who had an abnormal lipid layer with variable pattern or no detectable lipid layer.[153] King-Smith et al. studied the relationship between lipid layer thickness and tear film thinning and found that a large part of subjects with a very thin (< 30 nm) lipid layer displayed rapid thinning, whereas subjects with a thicker TFLL had a slow thinning rate.[1] Since tear film thinning is mostly caused by evaporation,[2,3] these results demonstrate the role of the TFLL in slowing down evaporation from the ocular surface.

In addition, simultaneous imaging of TFLL reflection and the aqueous tear film stained by fluorescein showed that the thinning and breakup of the aqueous layer correlated with structures observed in the TFLL.[154] On the other hand, studies employing simultaneous thermal imaging and fluorescein staining have shown that regions of the tear film, where rapid

thinning and breakup occur undergo rapid cooling, likely as a result of increased evaporation from these regions.[178,179] A recent study by Dursch et al. used this method to estimate the relative evaporation rate from lipid-deficient areas and areas with intact lipid and found that evaporation rate was 50–95% lower in the regions covered by an intact TFLL.[155] These results support the model by Peng et al., which described local tear film thinning and breakup as a result of local defects in the TFLL.[146] A small study by Peng et al.[156] compared the evaporation from the ocular surface of human subjects with a mannequin eye consisting of oversaturated agarose solution and was able to estimate an evaporation resistance of 9–13 s/cm for the TFLL *in vivo*, in good agreement with the earlier results from animal studies.

In conclusion, the fact that *in vitro* studies have struggled to demonstrate the evaporation resistant properties of tear film lipids can be largely attributed to shortcomings in the methods employed. In contrast, *in vivo* studies have provided compelling evidence that a healthy TFLL stabilizes the tear film by slowing down evaporation from the ocular surface. The loss of TFLL evaporation resistance would lead to drying of the ocular surface and is therefore a central factor in the pathogenesis of dry eye disease, as outlined in the following section.

## 2.4 DRY EYE DISEASE

Dry eye disease has been defined by the Tear Film & Ocular Surface Society Dry Eye Workshop II as "a multifactorial disease of the ocular surface characterized by a loss of homeostasis of the tear film, and accompanied by ocular symptoms, in which tear film instability and hyperosmolarity, ocular surface inflammation and damage, and neurosensory abnormalities play etiological roles".[16] Dry eye disease is a very common disease, with a prevalence of 10–30%,[17] and therefore it constitutes a significant health concern. Common symptoms include discomfort and visual disturbance, which are often perceived as dryness, grittiness, pain, blurring of vision, and difficulties performing tasks like reading or driving.[180]

Dry eye disease can be generally classified into two predominant subtypes: aqueous-deficient dry eye (ADDE) and evaporative dry eye (EDE).[16] Aqueous-deficient dry eye encompasses conditions affecting the lacrimal glands, which results in insufficient production of aqueous tears.[16] Evaporative dry eye occurs when the Meibomian glands, eyelids, or the ocular surface are affected, leading to instability of the tear film, often due to accelerated evaporation from the ocular surface.[16] Both the aqueous-deficient and evaporative components of dry eye result in reduction of aqueous tear volume and hyperosmolarity of the tear fluid, which initiates an inflammatory cycle in the epithelial cells of the ocular surface that involves activation of mitogen-activated protein kinase (MAPK) and nuclear factor kappa-light-chain-enhancer of activated B cells (NFκB). This results in

production of inflammatory cytokines (interleukins IL-1α, IL-1β, tumor necrosis factor TNF-α and matrix metalloproteinase MMP-9) and recruitment of inflammatory cells.[181] These inflammatory mediators and the hyperosmolar stress itself lead to the death of epithelial cells, including the mucin-producing goblet cells. The epithelial damage and loss of mucins reduce the wettability of the ocular surface, making the tear film unstable.[181] This instability of the tear film further exacerbates the hyperosmolarity that initiated the inflammatory response, forming the so-called vicious circle of DED (Figure 6).

The osmotic, inflammatory, and mechanical stress caused by the instability of the tear film will initially result in reflex stimulation of the lacrimal gland, which acts to compensate for the lack of aqueous tear fluid. However, DED progression may reduce corneal sensitivity,[182,183] decreasing the effectiveness of aqueous tear production.[181] On the other hand, DED initiated by aqueous tear insufficiency, for example due to Sjögren's syndrome, can be accompanied by impaired Meibomian gland function.[184] Therefore, as DED progresses, it is increasingly likely that signs of both ADDE and EDE will become evident, resulting in a mixed subtype of DED.[16] Based on the epidemiological data, most dry eye cases (up to 85–90%) are of the evaporative or mixed subtype, which are closely linked to Meibomian gland dysfunction (MGD).[185-188] MGD was defined by The International Workshop on Meibomian Gland Dysfunction as "a chronic, diffuse abnormality of the meibomian glands, commonly characterized by terminal duct obstruction and/or qualitative/quantitative changes in the glandular secretion. This may result in alteration of the tear film, symptoms of eye irritation, clinically apparent inflammation, and ocular surface disease".[189]

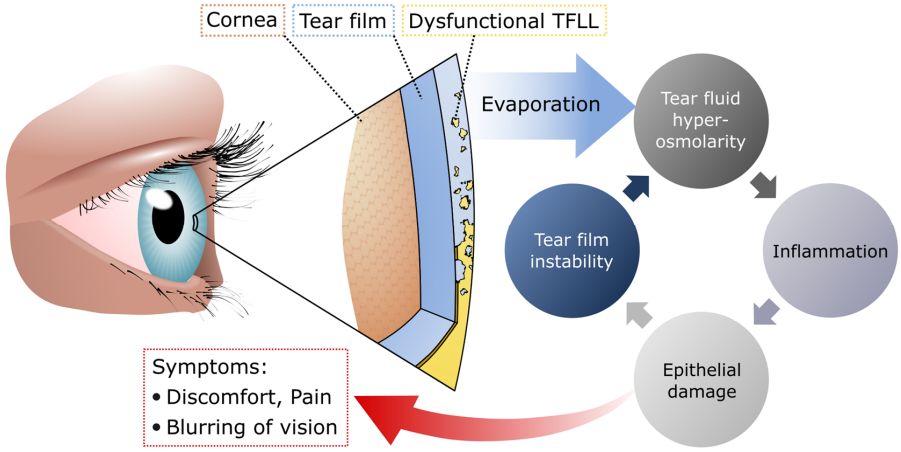


**Figure 6** The core mechanisms of evaporative dry eye disease (EDE). In EDE, the dysfunction of the tear film lipid layer (TFLL) leads to a hyper-evaporative state. This initiates a circle of hyperosmolarity, inflammation, epithelial damage, and tear film instability, which eventually leads to dry eye symptoms.

One of the hallmarks of Meibomian gland dysfunction is the change in meibum quality from a clear fluid, to a cloudy fluid, to a viscous fluid with particulate matter and eventually into an opaque, toothpaste-like material.[190] Since meibum is the main source of TFLL lipids, the changes in meibum quality and/or decrease in meibum secretion in MGD is considered to result in a deficiency in TFLL function and the loss of evaporation resistance. Excess evaporation initiates the vicious circle as described above leading to EDE (Figure 6). Therefore, mapping out TFLL function is central for understanding the pathogenesis of DED.

### 2.4.1 TEAR FILM LIPID LAYER IN DRY EYE DISEASE

Tear film lipid layer can be visually observed on the surface of the tear film as colorful interference fringes, and these patterns have been widely used as a tool to diagnose MGD and DED.[180] The interference patterns can be classified based on different classification schemes,[191,192] or used to estimate the thickness of the TFLL.[193,194] The intuitive hypothesis has been that a thicker lipid layer would improve the stability of the tear film. However, clinical studies have found only weak correlation between lipid layer thickness and dry eye symptoms or signs.[195-198] Therefore, the loss of tear film stability has been suggested to result from an abnormal lipid composition rather than decreased lipid layer thickness.[198] This would be in agreement with *in vivo* evaporation studies described in subsection 2.3.7, which have found increased evaporation through very thin or abnormal and thick lipid layers, but otherwise evaporation rate was unaffected by lipid layer thickness.[1,153] Therefore, lipid spreading pattern and kinetics[199] or lipid layer uniformity[200] may be better indicators of lipid layer function than thickness.

The importance of evaporation through the TFLL in DED can also be estimated by comparing evaporation rates from the ocular surface of patients with DED or MGD to normal subjects. These studies have been recently reviewed by Wong et al.[201], who found widely variable results due to the wide variation in experimental methods used and populations studied. However, 70% of the studies that compared normal subjects with DED, MGD, or blepharitis patients found an increased evaporation rate in the patients. In addition, two research groups that found either lower evaporation rates or no change in dry eye patients in early studies[202-207] have found increased evaporation rates in later studies,[208-212] possibly due to improvements in methodology. Up to four-fold increases in evaporation rate have been reported in DED patients,[153,213] but mostly the increases are modest (less than 2-fold). However, it is also possible that the increased evaporation in DED occurs only locally through defective areas of the TFLL, as described in subsection 2.3.7, which leads to formation of local dry spots. In this case, the overall rate of evaporation from the ocular surface may only slightly increase, although dry regions may rapidly form. Taken together these results from clinical studies support the hypothesis that loss of TFLL evaporation

resistance is an important pathological mechanism in the development of DED. However, many open questions still remain, such as how to effectively identify an abnormal TFLL structure, and what kind of changes in tear film lipid composition lead to compromised TFLL function in DED.

### 2.4.2 LIPID SPECIES ASSOCIATED WITH DRY EYE DISEASE

The lipid composition of the Meibomian gland secretions appears to be closely regulated in humans, since there is little variation in lipid composition between different subjects and between different days.[70,80,214] In fact, the lipid composition is very similar even across many mammals, such as humans, mice, dogs, cows, or tree shrews.[27,215,216] Interestingly, rabbits, which have been used quite extensively in ocular research, have a relatively distinct tear film lipid composition, although the structural features such as long hydrocarbon chains lengths are similar.[215] The closely controlled lipid composition is likely required to maintain the physical properties needed for the function of the TFLL.

The effects of changing the TFLL composition have been demonstrated in recent mouse studies by knocking out different enzymes involved in the synthesis of Meibomian lipids (ELOVL1, ELOVL3, and CYP4F39).[73,74,152] These knockouts caused alterations in the chain lengths of wax and cholesteryl esters, the balance between saturated and unsaturated hydrocarbon chains, or the amounts of OAHFAs and diesters, all of which resulted in a clear dry eye phenotype.[73,74,152] Therefore, maintaining the proper composition of the TFLL appears to be central for ocular surface health, and various changes in lipid composition can have deleterious effects on its function.

However, the changes in lipid composition associated with DED in humans are not well characterized. Pioneering studies investigated the lipid composition in blepharitis patients with eyelid inflammation and normal subjects and found small differences in various lipids.[217-223] However, these studies compared six different patient groups and the biggest differences often appeared within the normal subjects in these studies.[219,221] This pattern has not been replicated in later studies, making it difficult to make clear conclusions based on these early studies. Later studies have found differences in polar phospho- and sphingolipids in patients with blepharitis and dry eye,[224,225] but as these lipids only constitute a minute fraction of meibum lipids (Table 1), the significance of these findings is unclear.

A more recent study by Joffre et al. evaluated the fatty acids from all meibum lipid components together and found no changes in patients with ADDE, whereas patients with MGD had lower amounts of normal saturated fatty acids and increased amounts of branched and unsaturated fatty acids.[226] Lam et. al. found that levels of OAHFAs in tears decreased with increasing DED severity,[70] and eyelid-warming treatment for MGD increased OAHFA levels.[75] However, a similar trend was not detected in a larger study, although

OAHFA levels were negatively correlated with some dry eye signs.[76] In the larger study,[76] wax esters were also linked to DED. Specifically high molecular weight WEs with unsaturated fatty acid chains were increased in DED, whereas low molecular weight WEs and high molecular weight WEs with saturated fatty acid chains were decreased in DED.[76] Chen et al. analyzed the differences in nonpolar tear lipids in dry eye patients and found that CEs and triglycerides were increased in dry eye patients, whereas WEs and especially type I-St and type II diesters were decreased.[227] Interestingly, the decrease in diesters might also reflect a decrease in polar OAHFAs, since they share a synthetic pathway with diesters.[71] In conclusion, there is currently only limited information available from lipidomic studies to indicate what kind of changes in lipid composition are typically associated with DED or MGD. In addition, the results are variable, and no clear pattern has been identified.

An alternative approach to directly investigating the lipid composition as is done in lipidomic studies is to use methods such as infrared spectroscopy or nuclear magnetic resonance (NMR) spectroscopy to investigate the collective signals collected from meibum. These signals can be used to obtain information about the compositional changes in meibum related to ocular surface diseases. The advantage of these methods is that they can detect collective changes in composition, which may be significant even if the changes in the quantities of individual lipid species would be small.

Both infrared and NMR spectroscopy have showed that meibum from MGD patients contained less cholesteryl esters compared to normal subjects.[228,229] MGD patient meibum was also found to contain a lower number of methyl groups compared to normal subjects, which could be related to a lower amount of cholesteryl esters or a decrease in iso- or anteiso branching of the hydrocarbon chains.[230] MGD meibum has also been found to be more ordered compared to normal meibum,[231] which is reflected in a higher melting point and thickened appearance. However, it should be noted that some changes in the collective properties of meibum may be related to inclusion of proteins, such as keratin or other cell components in meibum, and may not directly reflect changes in lipid composition.

In conclusion, although meibum abnormality is a central feature of MGD and related DED, lipidomic and spectroscopic studies have not yet identified a clear pattern of associated changes in lipid composition. One possible reason for this may be the heterogeneity in the studied populations, and the fact that various different changes in composition can lead to altered TFLL function. When large numbers of samples are then compared, the different changes may be averaged out and may not be detected. Studies with more defined patient populations, based on meibum quality for example, might be able to provide clarity to this issue. In addition, the physical properties of many of the tear film lipids are poorly known. Improving the knowledge regarding the role of different lipid species in TFLL function can provide clues regarding the compositional requirements of a functioning TFLL.

# 3 AIMS OF THE STUDY

The aim of this thesis project was to gain insight into the organization and function of the tear film lipid layer and its role in maintaining ocular surface health. Since the organization of TFLL lipids at the aqueous tear film interface is likely crucial for evaporation resistance, as described in section 2.3, this work utilized Langmuir trough-based *in vitro* models combined with *in silico* simulations to provide detailed information about the properties of TFLL lipids at the aqueous surface. By using well-defined films comprised of model lipids, the work aimed to describe the structure of the TFLL at a molecular level and explain how the structure is related to the evaporation resistance of the TFLL film.

To pursue these aims, the focus of this thesis was on three specific objectives:

First, to elucidate the molecular level organization of the main tear film lipid classes including wax esters, cholesteryl esters, OAHFAs, and diesters on the surface of the aqueous tear film.

Second, to provide insight into the structures and mechanisms underlying the evaporation resistant properties of tear film lipids.

Third, to investigate the interplay of polar and nonpolar tear film lipids and to study the importance of polar lipids in TFLL organization.

# 4 METHODS

## 4.1 LIPID SYNTHESIS AND CHARACTERIZATION

Most lipids used in this thesis, including behenyl oleate (BO), behenyl palmitoleate (BP), arachidyl oleate (AO), cholesteryl nervonate (CN), and 1-palmitoyl-2-oleoyl-sn-glycero-3-phosphocholine (POPC) were obtained from commercial sources as described in the publications. However, some lipids specific to the TFLL, namely OAHFAs and diesters, were not commercially available. Therefore, to study the properties of these lipids, we synthesised a set of four diesters and three OAHFAs with varying chain lengths, using the synthetic pathways summarized in Figure 7. During the synthesis, also three O-acyl-ω-hydroxy fatty alcohols (OAHFAL) were formed as intermediate compounds. All the synthesized lipids contained oleate acyl chains, like the majority of TFLL OAHFAs and diesters.[60,62,69,77] The synthesis protocols are described in detail in Publication IV.

In short, the following reaction scheme was used: long-chained diols with 8, 12, 15, or 20 carbons were used as starting products. To synthesize the diesters, a diacylation reaction was performed using Fischer esterification with 2.4–3 equivalents of oleic acid at 100 °C under vacuum in the presence of 3.5 mol% of sodium bisulphate. To synthesize the OAHFALs, the Fischer esterification was modified to include 1.2 equivalents of oleic acid, which resulted in higher yields of monoacylated products. Finally, the alcohol group in the OAHFALs was oxidized using the Jones oxidation reaction in acetone with 2.2 equivalents of Jones reagent. After each reaction step, the products were extracted and purified using column chromatography. Reaction products were characterized by using the following methods: NMR spectra were recorded with a Bruker Avance III NMR spectrometer (Bruker BioSpin, Rheinstetten, Germany) operating at 500.13 MHz (1H: 500.13 MHz, 13C: 125.76 MHz), using the following 1D-techniques: $^{1}H$ and $^{13}C$ and 2D-techniques: edited heteronuclear single quantum coherence (Ed-HSQC) and heteronuclear multiple-bond correlation spectroscopy (HMBC). Product masses were recorded using high resolution mass spectrometry with Bruker Micro Q-TOF with electrospray ionization operated in positive mode. Melting points were determined using Büchi B-545 melting point instrument (Büchi Labortechnik, Flawil, Switzerland).

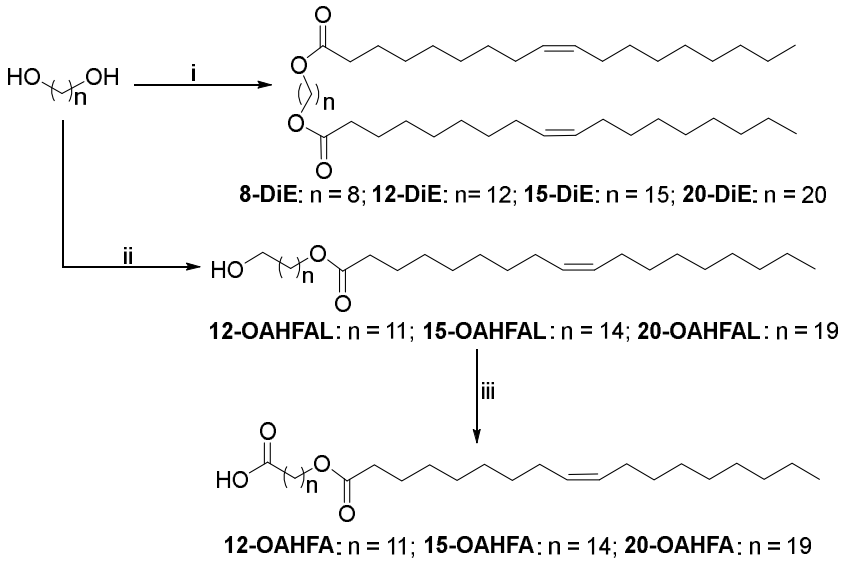


**Figure 7** Overview of reactions used to produce diesters, OAHFA, and OAHFAL analogues: i) Oleic acid (2.4-3 equiv.), the corresponding diol (n = 8, 12, 15 or 20), $NaHSO_4.H_2O$ (3.5 mol%), 100 ˚C, ~0.3 mbar, 2.5 hours. Yield: **8-DiE**: 82%; **12-DiE**: 63%; **15-DiE**: 67%; **20-DiE**: 57%. ii) Oleic acid (1.2 equiv.), the corresponding diol (n = 8, 12, 15 or 20), $NaHSO_4.H_2O$ (3.5 mol%), 100 ˚C, 0.3 mbar, 2.5 hours. Yield: **12-OAHFAL**: 46%; **15-OAHFAL**: 28%; **20-OAHFAL**: 48%. iii) Jones reagent (2.2 equiv.), acetone, 0 °C, 0.5 hours. Yield: **12-OAHFA**: quant.; **15-OAHFA**: 85%; **20-OAHFA**: 67%. Reprinted with permission from Bland et al.[232] (https://pubs.acs.org/doi/10.1021/acs.langmuir.8b04182). Copyright 2019 American Chemical Society.

## 4.2 LANGMUIR MONOLAYER EXPERIMENTS

Langmuir monolayer experiments were used to characterize the organization of different tear film lipids and lipid mixtures on the aqueous interface and evaluate their evaporation resistance. Two separate setups were used in Langmuir monolayer experiments. Most of the studies were performed using KSV Mini trough (Biolin Scientific, Stockholm, Sweden) equipped with a surface pressure balance with a platinum Wilhelmy plate, KSV SPOT surface potential meter, and KSV NIMA microBAM Brewster angle microscope (BAM). The trough temperature was monitored using a thermometer immersed into the subphase, and temperature was controlled by connecting the trough to a Lauda ECO E4 thermostat (Lauda, Germany). In order to utilize fluorescence microscopy in Publication V, some of the measurements were performed in a Kibron μTrough XS (Helsinki, Finland), equipped with a DyneProbe surface pressure sensor (KBN 315, Kibron), and a quartz-glass window for imaging using an inverted fluorescence microscope (Olympus, Hamburg, Germany). The trough temperature was controlled with a

temperature control plate connected to a Julabo F12-EC thermostat (Julabo, Seelbach, Germany).

Specific Langmuir trough experiments are described in detail in Publications I–V, but the general procedure of the measurements was as follows: The Langmuir trough was filled with either Milli-Q ultrapure water or phosphate-buffered saline (PBS), and the lipid was applied to the subphase surface in chloroform solution. After evaporation of the chloroform, the film was compressed and expanded using two barriers. During compression, either surface pressure or surface potential was measured, and the film was imaged using Brewster angle microscopy or fluorescence microscopy (FM). In Publication II, monolayers formed by unsaturated tear film lipids were discovered to be unstable in ambient laboratory conditions due to oxidation (see section 5.1). To avoid this in Publications II–V, the Langmuir trough was placed in a plastic enclosure, and dry air flowing through an ODS-3P ozone destruct unit (Ozone Solutions, Hull, Iowa) was passed into the enclosure to maintain a low ozone environment around the trough.

The compressibility of the films was further analysed by calculating the reciprocal of isothermal compressibility $C_s^{-1}$ from the surface pressure data using

$$C_s^{-1} = -a\frac{da}{d\pi}, \tag{5}$$

where $a$ is the mean molecular area and $\pi$ is the surface pressure. To investigate changes in orientation of electric dipoles in the lipids, the effective molecular dipole moment component normal to the subphase surface, $\mu_\perp$, was calculated from the measured surface potential values using the Helmholtz equation[233]

$$\mu_\perp = a\varepsilon_0(\Delta V), \tag{6}$$

where $\Delta V$ is the measured surface potential and $\varepsilon_0$ is the permittivity of the vacuum.

### 4.2.1 IMAGE ANALYSIS

Brewster angle microscopy and fluorescence microscopy were used to qualitatively evaluate the appearance of studied lipid films, and image analysis techniques were used to obtain quantitative variables from the captured images. In BAM, a black image is obtained when imaging a pure water surface, and the intensity of the images increases when a lipid film is introduced to the surface. In general, increase in the thickness and density of the lipid film increases the observed image intensity in BAM. Based on this principle, BAM images were used to estimate the thickness of condensed lipid monolayers using the following approach: As a first order

approximation, reflectance $r$ at the Brewster angle for a thin film residing on the water surface can be written

$$r \propto d^2, \tag{7}$$

where $d$ is the thickness of the film.[234] Using this relation, it is possible to compare the relative thicknesses of lipid films with similar optical properties, as was done in Publication V. In Publication I, we further used a set of fatty alcohols with varying chain lengths (1-Octadecanol, 1-Docosanol, 1-Hexacosanol and 1-Triacontanol) as standards to estimate the absolute thickness of wax ester films. Reflectance was determined from average intensity of BAM images captured from solid monolayers of each standard lipid, as well as a images of a pure PBS surface. The reflectance values measured from the different lipid films were then fitted to the theoretical thicknesses of the corresponding fatty alcohols in all-trans conformation using the equation

$$d = K\sqrt{r - r_{\mathrm{bg}}} \tag{8}$$

where $r$ is the reflectance of the lipid film, $r_{\mathrm{bg}}$ is background reflectance of the PBS subphase and $K$ is a constant. After the values of $K$ and $r_{\mathrm{bg}}$ were fitted using the theoretical thicknesses of the standard lipids, equation (8) could be used to estimate the thickness of any lipid film with similar optical properties to linear fatty alcohols in the solid monolayer phase.

In Publication V, multilayers formed on aqueous interface were investigated by calculating the multilayer volume and coverage based on BAM and FM images. Briefly, the images were first segmented into separate regions based on image intensity using multilevel thresholding with Otsu's method.[235] The number of multilayers in each region was determined based on the BAM intensity of the region. Based on the number of layers in each segment and the fraction of the interface covered by the segment, the total multilayer volume was then calculated. By using this method, the formation of multilayers during compression of lipid films can be followed quantitatively, and the mean area per lipid in the multilayer phase can be determined.

### 4.2.2 MONOLAYER COMPOSITION ANALYSIS

Analysis of lipid composition was performed in Publication II to assess the oxidation of wax esters during the Langmuir monolayer experiments. Further, the lipid composition of tear fluid samples from healthy subjects was analyzed to determine whether similar oxidation processes occurred in the tear film *in vivo*.

Lipids were collected at different time points during the Langmuir trough experiments by compressing the lipid films to a small (~ 5 cm$^2$) area using the barriers and an additional PTFE plate. The lipids were then collected

from the aqueous surface by sweeping the surface with a polyvinylidene fluoride (PVDF) filter. Both the PVDF filter and the PTFE plate were immersed into 2:1 chloroform:methanol to dissolve the collected lipids.

Tear sample collection was performed according to the Declaration of Helsinki and approved by the Ethical Committee of the Helsinki-Uusimaa Hospital District. Informed consent was obtained from each subject. Tear samples were collected from the lower conjunctival sac of 5 healthy volunteers (age 25–35 years) using 5 µl microcapillaries under a biomicroscope in three separate sessions. A total of 165 µl of tear fluid was pooled and lipids were extracted using a modified Folch extraction method.[86] All the lipid samples were stored in -80°C until analyzed.

The collected lipids were analyzed using thin-layer chromatography and liquid chromatography-mass spectrometry (LC-MS). Thin-layer chromatography was performed using TLC Silica gel 60 glass plates (Merck KGaA, Darmstadt, Germany), with 80:20:1 hexane/diethyl ether/acetic acid as the eluent. The lipids were charred using 3 wt% copper sulfate and 8 wt% phosphoric acid. The intensity of the spots was quantitated using imageJ,[236] and the values were scaled by the number of carbon atoms in each molecule to estimate the molar concentration of each detected compound.

LC-MS analysis was preformed using a Hewlett-Packard Series 1100 liquid chromatograph (Palo Alto, USA) in isocratic mode with methanol, modified with 5% chloroform and 2% ammonium acetate with Chromolith HighResolution RP-18 end-capped column (50 mm, 4.6 mm i.d., Merck, Darmstadt, Germany). The liquid chromatograph was coupled to an Esquire 3000 plus ion trap mass spectrometer (Bruker Daltonics, USA) using electrospray ionization. Automatic precursor ion selection from base peak chromatograms was used for tandem MS experiments. Standard samples containing behenyl oleate, stearyl oleate, myristyl oleate, cholesteryl oleate, tripalmitin, trimyristin, trilaurin, tricaprin, tricaprylin, and L-α-lysophosphatidylcholine from chicken egg were used to identify the major lipid classes in tear fluid samples.

### 4.2.3 EVAPORATION RESISTANCE

In Publication I, a custom system built around the Langmuir trough was used to measure the evaporation rates from the water surface. The trough was enclosed inside an acrylic box, and dry, filtered air was passed through the box. The airflow was monitored using Testo 410-1 airflow meter (Testo, Lenxkirch, Germany). Relative humidity inside the box was measured using a Testo 608-H1 digital hygrometer. The measurements were performed by first adding a known mass of PBS into the trough, applying the lipid on the PBS surface in chloroform solution, and allowing the chloroform to evaporate for 10 min. The door of the acrylic box was then closed, and after 90 minutes, the subphase was collected and weighed again to evaluate the water loss due to evaporation. The results were compared to evaporation rates obtained

without adding any lipid to the surface. Evaporation rates from a pure water surface as a function of the relative humidity in the surrounding air were used to obtain an estimate that the mass-transfer resistance in the system (1.9 ± 0.3 s/cm), which enabled calculating the evaporation resistance of the lipid films. However, this estimate is not very reliable due to the relatively low range of relative humidity (30-50%) available for the fit. In addition, this setup for measuring evaporation resistance had some other shortcomings. First, the film could not be readily compressed to a desired surface pressure for the measurement, since that would have affected the surface area available for evaporation. Second, the measurements required a lot of time to complete and many measurements from a pure water surface were required to estimate the mass-transfer resistance.

To overcome these shortcomings, we developed an improved method for Publications IV–V, based on the method described by Langmuir and Schaefer.[165] The idea behind this method is to minimize the mass-transfer resistance to evaporation by placing a desiccant-filled container very close to the water surface and determining the amount of water absorbed by the desiccant. This also enables measuring evaporation resistance locally, making it possible to perform measurements of compressed films.

The desiccant containers were prepared by filling a plastic box with either lithium chloride or silica gel and covering the opening of the box with two layers of Millipore Immobilon -P PVDF membrane with 450 nm pore size (Bedford, MA). The filter held the desiccant material inside the box but allowed water vapor to pass through into the desiccant. For this setup, the evaporation rate from the water surface under the desiccant container becomes

$$J_{\mathrm{F}} = \frac{M}{At} = \frac{C_{\mathrm{w}}^{\mathrm{sat}}(T_{\mathrm{w}}) - C_0(T_0)}{R_{\mathrm{I}} + R_{\mathrm{M}} + R_{\mathrm{memb}}}, \tag{9}$$

where $M$ is the mass absorbed by the desiccant during the experiment, $A$ is the area of the desiccant box, $t$ is the time elapsed during the measurement. $C_0$ is the the water vapor concentration in equilibrium with the dessicant at the temperature of the dessicant $T_0$. The additional evaporation resistance term $R_{\mathrm{memb}}$ denotes the diffusion of water through the membrane to the desiccant surface.

Now, since $R_{\mathrm{M}}$ and $R_{\mathrm{memb}}$ are not affected by the presence of a lipid film, the interfacial evaporation resistance caused by a lipid layer residing at the water surface can be calculated as

$$R_{\mathrm{I}} = At[C_{\mathrm{w}}^{\mathrm{sat}}(T_{\mathrm{w}}) - C_0(T_0)]\left(\frac{1}{M} - \frac{1}{M_{\mathrm{w}}}\right), \tag{10}$$

where $M$ and $M_w$ are the water masses absorbed by the desiccant during the experiments in the absence and presence of a lipid film, respectively. The term $[C_{\mathrm{w}}^{\mathrm{sat}}(T_{\mathrm{w}}) - C_0(T_0)]$ can be determined either based on literature values,

or by performing a set of control experiments from a pure water surface, where the distance between the desiccant box and the water surface is varied.

The mass of absorbed water was determined by first weighing the desiccant container and placing it a few millimetres above the subphase with the filter facing the subphase surface. The container was held in position for 5 minutes, removed and weighed again to determine the mass of absorbed water. The measurements were performed in sets as follows: First, PBS preheated to the desired temperature was added to the trough to form the subphase. Second, evaporation rate was measured from the pure PBS surface as a control. Third, a lipid monolayer was prepared as described in the beginning of this section. Fourth, the film was compressed to a set of mean molecular areas or surface pressures, and evaporation resistance was measured at each point. Additional measurements were performed by placing the desiccant container into the measurement enclosure, but away from the subphase surface to estimate the amount of water absorbed from the surrounding air instead of the subphase. This value was subtracted from all the other measurements of the same set. In addition, a correction was employed to account for the change in the distance between the desiccant box and the subphase surface due to subphase evaporation during the measurement set (see Supporting Information of Publication IV for details).

## 4.3 MOLECULAR DYNAMICS SIMULATIONS

Molecular dynamics (MD) simulations were used in Publication III in combination with the experimental methods described in the previous section. The simulation models used in this work were classical atomistic models, where each atom in the simulated system in characterized by a single particle. The forces between the particles are determined by the force field, which describes the bonded and non-bonded interactions between the particles. Bonded interactions include bond-stretching, angle-bending, and dihedral-twisting. Non-bonded interactions include Lennard-Jones interactions, depicting steric repulsion and van der Waals dispersion, and long-range electrostatics according to Coulomb's law.

In this work, all the simulations were performed using the GROMACS simulation package.[237] The general workflow of MD simulations starts with generating an initial configuration of molecules, followed by energy minimization using general optimization algorithms to reach a configuration, which is close to equilibrium and does not produce excessive forces. The system dynamics are then modeled by numerically integrating Newton's second equation of motion $\boldsymbol{a} = \boldsymbol{F}/m$, where $\boldsymbol{F}$ is the sum of all forces acting on particle with mass $m$, causing acceleration $\boldsymbol{a}$. Based on this equation, the velocity and position of each particle can be described over time. The methodology of MD simulations has been discussed in great detail in the literature,[238,239] and is therefore not covered in this thesis. Here, we instead

discuss the aspects and details that are specifically related to and particularly important to the present thesis project.

### 4.3.1 FORCE FIELD SELECTION AND VALIDATION

Most lipid MD simulations are focused on simulating cell membranes, and therefore most of the developed force fields contain parameters for common polar lipids that make up the cell membranes. However, since the TFLL is largely composed of special lipid classes, such as WEs, diesters, and OAHFAs that are not abundant in other tissues, the applicable force fields for simulating these lipids are limited. Therefore, an all-atom model was developed in Publication III to simulate tear film WEs. The choice of force field was guided by earlier studies, which have shown that bulk properties, such as melting points, are important in determining the organization of WEs on the aqueous interface.[99] We therefore used melting points and solid phase structure to initially screen applicable force fields. In the initial force field selection phase, several force fields, including CHARMM,[240] OPLS,[241] L-OPLS,[242,243] and the MacRog force field developed by Maciejewski et al.[244] were considered. The original OPLS force field has been reported to perform poorly when simulating hydrocarbons exceeding six carbon atoms in length,[242,245] and was therefore not considered suitable for TFLL lipids, which are characterized by very long hydrocarbon chains.

For the other force fields, preliminary melting point simulations were performed by generating an initial configuration consisting of 200 palmityl palmitate molecules, where approximately half of the molecules were in a crystalline lattice and the other half were in a disordered conformation. During the simulations, the system evolved either to a completely liquid state or a completely crystalline state depending on the temperature, and equilibrated systems could be used to obtain simulated melting points and densities. The MacRog model was found to produce a kinked ester conformation in the solid phase in these preliminary simulations, in contrast to the linear conformation found in experiments,[88,89] and was not considered further. The models that were compared further were CHARMM, L-OPLS, and a combination of OPLS and L-OPLS (L-OPLS/OPLS), where only L-OPLS hydrocarbon parameters were used, and other atoms were characterized using OPLS parameters. The densities obtained from the melting point simulations showed that the L-OPLS/OPLS force field provided good agreement with experimental properties (Figure 8). The melting points of other wax esters (palmityl laurate and behenyl oleate) were further simulated with the L-OPLS/OPLS force field in Publication III and good agreement was found with experimentally determined melting points. The L-OPLS/OPLS force field was therefore used in the production simulations of this work, to describe the studied WEs.

In addition to the lipid force field, a water model is required to simulate tear film lipids at the aqueous tear film surface. In order to correctly

reproduce the properties of the air-water interface, the water model employed needs to have a good depiction of surface tension. Therefore, the 4-point "optimal point charge" (OPC) water model[246] was used in this work, since it reproduces the experimental surface tension of water better than all the other commonly used water models.[247]

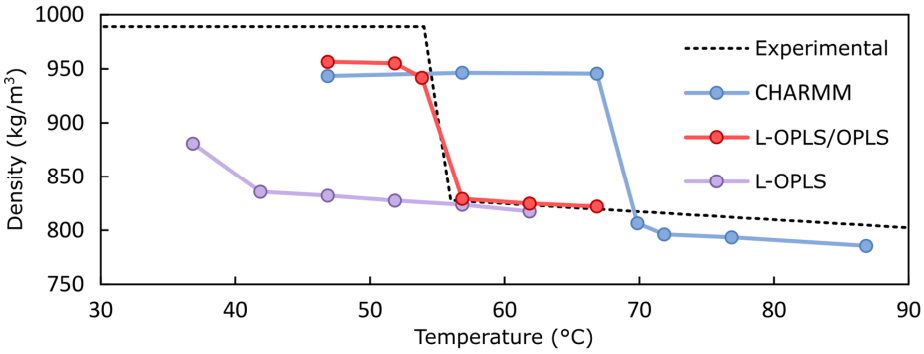


**Figure 8** Comparison of force fields for wax ester simulations. Density of palmityl palmitate obtained from melting/crystallization simulations is shown as a function of temperature. Experimental density shown is based on experimental melting point,[98] and densities at 20 °C and 50 °C.[248] Density in the liquid phase was extrapolated based on the temperature dependence of alkane density.[249]

### 4.3.2 MONOLAYER SIMULATIONS

Molecular dynamics simulations were used to simulate monolayers of BO as a model of tear film wax esters. In monolayer simulations, a symmetric configuration consisting of a water slab with two monolayers of 100–200 BO molecules on both sides of the water slab. The two sides of the water slab were separated by a sufficiently large vacuum to prevent the two monolayers from interacting with each other due to the periodic boundary conditions. 30% of the BO molecules were initially placed with their polar ester groups facing the water surface, whereas the rest of the BO molecules were placed in a tightly packed initial conformation, based on the reported crystal structure of saturated wax esters.[88-90] This kind of initial configuration was used to facilitate the formation of solid monolayer phase, since the presence of an initial crystal nucleus makes the formation of a solid monolayer phase possible within the time scale accessible by all-atom MD simulations. However, the initial crystal configuration will also have an impact on the structure of the formed solid phase. The monolayer simulations were run until the total energy of the system had converged, after which the configuration of the BO monolayer was analyzed.

### 4.3.3 SIMULATING EVAPORATION RESISTANCE

Further simulations were performed to study the permeation of water through BO films using the inhomogeneous solubility-diffusion model.[250,251] Using this model, the evaporation resistance $R$ caused by the lipid film can be obtained by integrating the local permeation resistance over the monolayer along the monolayer normal $z$ according to

$$R = \int_{z_1}^{z_2} \frac{\exp\left(\frac{\Delta A(z)}{N_A kT}\right)}{D(z)} dz, \tag{11}$$

where $\Delta A$ is the Helmholtz free energy difference between the position $z_1$ and $z$, $N_A$ is the Avogadro constant, $k$ is the Boltzmann constant, and $D$ is the local diffusion coefficient within the film.

The Helmholtz free energy profile was approximated by the potential of mean force (PMF) obtained by using Umbrella sampling[252] along the path from the liquid water to the overlying vacuum through the lipid film. In Umbrella sampling, the position of a single water molecule was restrained in different positions along the interface normal using a bias potential. The biased probability distribution obtained was unbiased using the weighted histogram analysis method to obtain the PMF.[253] The position-dependent diffusion coefficient along the lipid film was estimated based on the mean squared displacement of a water molecule along the interface plane restrained at different positions along the interface normal. Using these parameters that were readily obtained from the simulations, the evaporation resistance of the simulated lipid film can be calculated.

# 5 RESULTS AND DISCUSSION

## 5.1 CHEMICAL STABILITY OF TEAR FILM LIPIDS

In many cases, nonpolar tear film lipids, such as WEs, CEs, or diesters did not form a stable monolayer on the aqueous interface. Even when a monolayer was formed, the surface pressure isotherms were often found not to be repeatable upon repeated expansion and compression. In previous studies, this has been interpreted to mean that the film was not properly equilibrated and therefore multiple compression-expansion cycles have typically been performed until no further change occurred in the isotherms.[99,109,112,129,130,254,255] In Publication II, we investigated this issue in detail using BO as a representative model of tear film WEs. BO films spread on water also appeared to be unstable over time, and the film initially expanded, followed by a contraction that was characterized by appearance of solid monolayer domains (Figure 9). Such a two-step process would not be expected if the film was simply equilibrating, and interestingly, the time scale of this process was found to depend on the level of ambient ground-level ozone in the outside air during the measurements. Further, this effect was eliminated when an ozone-free environment was maintained within the box where the measurements were performed. Therefore, it appeared evident that a chemical reaction involving ozone was occurring in the film. To characterize this reaction, lipids were collected from the aging film at different time points and the lipids were analyzed using thin-layer chromatography and LC-MS.

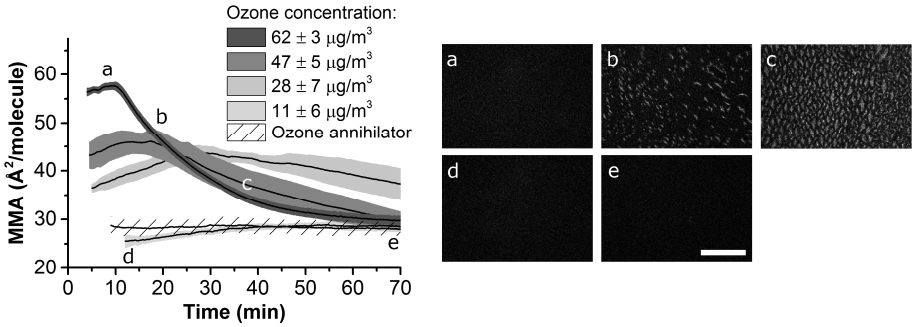


**Figure 9** Oxidation of behenyl oleate (BO) monolayers in ambient laboratory conditions. The monolayers were maintained at constant surface pressure of 0.5 mN/m at 36 ± 1 °C. Mean molecular area (MMA) of the film is shown as a function of time with the corresponding Brewster angle microscopy (BAM) images. Shaded areas in the graphs represent standard error of the mean. BAM images a–c were captured at the highest ozone concentration and d-e with the lowest concentration. Scale bar is 500 μm. Adapted with permission from Paananen et al.[256] Copyright 2015 The Association for Research in Vision and Ophthalmology, Inc.

These results confirmed that BO was degrading due to direct attack by ambient ozone on the double bond in BO. This resulted in formation of characteristic ozonolysis products either in the form of an ozonide with a 1,2,4-trioxolane ring (BOoz) or an aldehyde product (Boxno) (Figure 10A). The formation of polar intermediate products, namely Criegee intermediates (CI) and hydroxyhydroperoxides (HHP), as well as volatile short-chain compounds in the reaction explained the initial expansion of the film. The following contraction resulted when the final long-chained ozonolysis products were formed (Figure 10B). In total, these results demonstrated that monounsaturated WEs are vulnerable to degradation by ozone even in ambient laboratory conditions, and within the time scales required to conduct typical monolayer experiments (~1 h). The oxidation mechanism was consistent with previous studies on autoxidation of oleic acid, methyl oleate, and unsaturated phospholipid monolayers.[257-261]

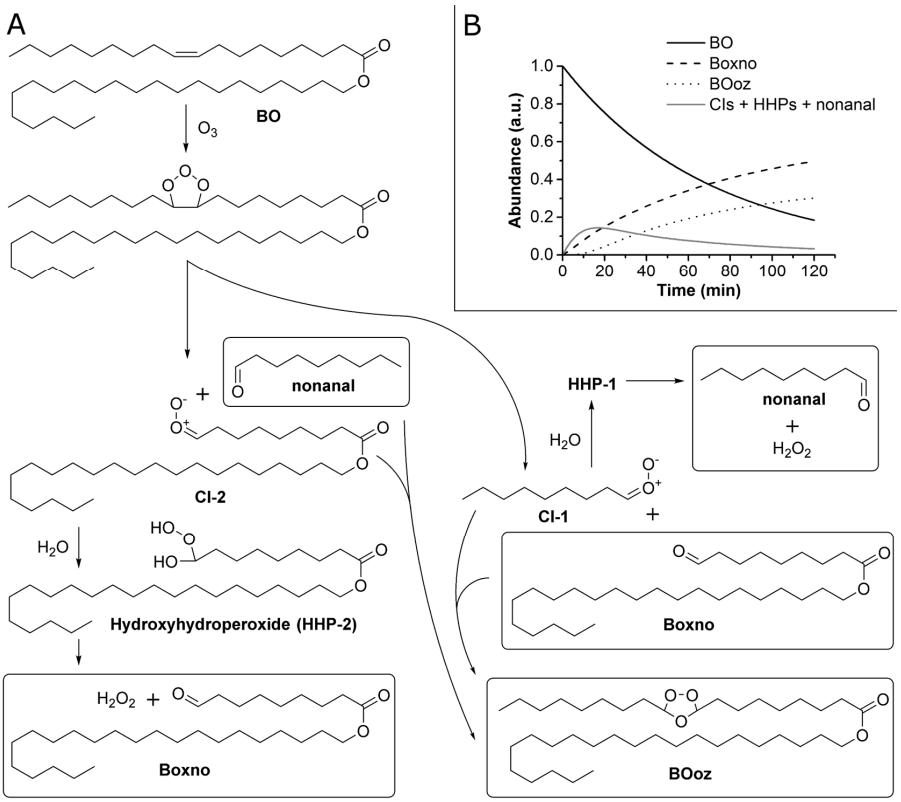


**Figure 10** Ozonolysis of behenyl oleate (BO) the air-water interface. **A)** Reaction scheme for the ozonolysis of BO. CI: Criegee intermediate, HHP: Hydroxyhydroperoxide. Reaction end products are highlighted. **B)** A model of the reaction kinetics of BO oxidation and the abundance of various oxidation products at the air-water interface. Reprinted with permission from Paananen et al.[256] Copyright 2015 The Association for Research in Vision and Ophthalmology, Inc.

Therefore, this mechanism is not limited to only WEs, but also other tear film lipids that contain double bonds are likely susceptible to degradation by ozone during the experiments.

This prompted us to study the possibility of TFLL ozonolysis *in vivo* by investigating the lipid composition of pooled tear fluid samples from healthy subjects (N = 5) using LC-MS. No lipids corresponding to the ozonolysis products identified here were detected, suggesting that similar oxidation processes are not likely to significantly affect TFLL function.

However, when TFLL lipids are studied in Langmuir monolayers, the experimental atmosphere should be controlled in order to prevent ozonolysis during the experiments. Because this has not been the case in earlier studies, many of the earlier results obtained for unsaturated tear film lipids without controlling for oxidation need to be interpreted with caution, especially in cases where multiple compression-expansion cycles over an extended period of time have been performed. In most of the work (Publications III–V) described in the following subsections, ozonolysis during the experiments was prevented by maintaining a low-ozone atmosphere in the enclosure, where the experiments were performed.

## 5.2 ORGANIZATION OF TEAR FILM LIPIDS

This section provides an overview of the phase behavior and organization of the tear film lipid classes studied in this work including WEs, Type II diesters, OAHFAs, and CEs on the aqueous interface.

### 5.2.1 WAX ESTERS

Wax esters were the only TFLL lipid class that exhibited clear evaporation resistant properties in previous studies.[99,108] Interestingly, the evaporation resistance of monolayers formed by various WEs was limited to a temperature range slightly below their melting point and was speculated to be related to formation of a specific condensed phase.[99] In this thesis (Publications I and III), the relationship between the WE film structure and evaporation resistance was investigated in more detail. In this work, BO and BP were used as models of TFLL wax esters, since their structure corresponds to the WEs naturally occurring in the tear film.

Three different behaviours were identified for wax ester films on the aqueous interface depending on the temperature. First, at temperatures well below the melting point of each WEs, no spreading occurred, as indicated by the lack of surface pressure (Figure 11A,a). In this state, the WE formed solid aggregates on the aqueous surface. This is typical for highly nonpolar lipids, as described in subsection 2.3.3, and results from the fact that the intermolecular cohesion between WEs is strong compared to the attraction between the polar ester groups and water.

Second, when the temperature was increased close to the WE melting point (Figure 11A,b–d), a liquid monolayer was observed to spread around the solid aggregates, until the aqueous surface was completely covered by either a liquid monolayer or solid domains of WE. This was accompanied by an increase in surface pressure. Such coexistence of a monolayer with solid aggregates a few degrees (~4 °C for BP) below the melting point of the WE can be explained by pre-melting induced by the aqueous interface.[262] At the bulk melting point, the free energies in the bulk solid and liquid phases are equal. However, the free energy in a liquid monolayer state is even lower than in the bulk liquid state, due to the attractive interactions between the polar ester groups and water. Therefore, melting into the monolayer state occurs before the bulk melting point, as long as there is free aqueous interface available. After the whole interface is covered by the monolayer, melting no longer proceeds. If the available area of the aqueous interface is decreased by compressing the film in this temperature range, a transition from the monolayer phase back to the solid phase is observed and solid domains can be seen to grow on the interface (Figure 11B,ii–iv). It should be emphasized that the solid domains formed in this manner are not part of a monolayer phase, but instead the molecular organization in this phase is determined by the intramolecular interactions between WEs, like in a bulk solid phase.

Third, when the temperature was increased above the melting point of the WE, the solid aggregates melted, and a liquid monolayer coexisting with liquid droplets was formed (Figure 11A,e).

The molecular orientation in the wax ester films was studied in more detail using surface potential measurements and molecular dynamics simulations in BO films.

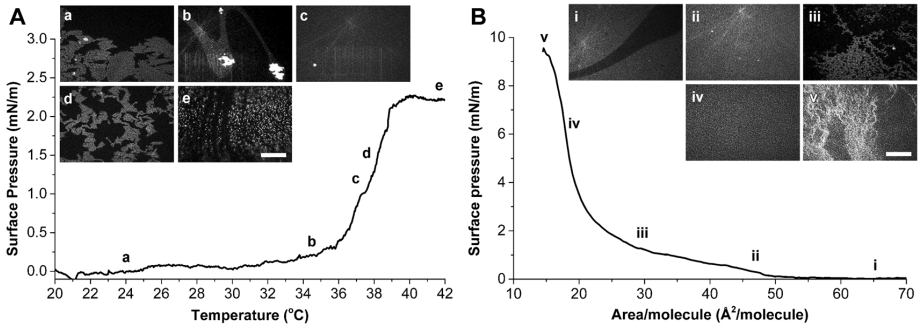


**Figure 11** Phase behaviour of behenyl palmitoleate (BP) at the air-water interface. Surface pressure generated by the film and corresponding Brewster angle microscopy (BAM) images are shown. **A)** BP isochor measured at a mean molecular area of 30 Å$^2$. **B)** Compression isotherm of BP measured at constant 36 °C temperature. Note that the exposure time is longer in BAM images b, c, i, and ii than in images a, d, e, and iii–v. Scale bars depict 500 µm. Adapted with permission from Paananen et al.[263] Copyright 2014 American Chemical Society.

These results revealed that in the monolayer phase, the wax esters adopted a V-shaped configuration on average, with the ester group facing the water and hydrocarbons oriented towards the air with a 80-90° angle between the acyl and alkoxy chains (kink angle) on average (Figure 12B,E). However, the configuration was highly disordered with a wide distribution of kink angles, and only 50% of the ester groups facing the water surface (Figure 12D). Such a disordered configuration resulted in an average molecular dipole moment of approximately 400–500 mD perpendicular to the aqueous interface in these films (Figure 12C), similar to what has been observed in other long-chained esters.[107,111] These results are consistent with other studies that have suggested a V-shaped conformation for expanded WE monolayers.[106,111,112] However, the weak attachment of the ester groups to the aqueous layer suggests that the organization within the expanded lipid film is not strictly monolayer-like, but some of the WEs exhibit bulk-like organization.

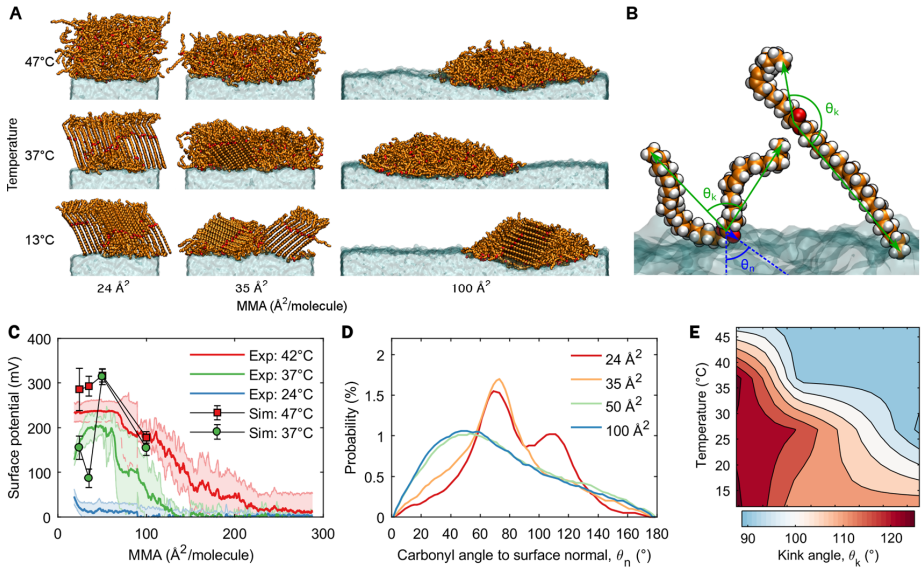


**Figure 12** Structure of behenyl oleate (BO) films based on molecular dynamics simulations and experiments. **A)** Simulation snapshots of BO films at different temperatures. BO carbons are depicted in orange, and oxygens in red, whereas water is shown in blue. Hydrogens are not shown for clarity. **B)** Examples of the V-shaped monolayer conformation and the extended solid conformation of BO on the aqueous surface. Kink angle ($\theta_k$) and carbonyl angle to surface normal ($\theta_n$) are also shown. Hydrogens are shown in white. **C)** Surface potential of BO films. Solid lines: experimentally determined surface potential, where shaded regions depict standard deviation. Markers and lines: surface potential from MD simulations, with error estimated using block averaging. **D)** Simulated distribution of the angles between the BO carbonyl bond and surface normal ($\theta_n$) at 37 °C. **E)** Mean kink angle ($\theta_k$) calculated from simulated BO films. Adapted with permission from Paananen et al.[264] (https://pubs.acs.org/doi/10.1021/acs.jpclett.9b01187). Copyright 2019 American Chemical Society.

The MD simulations also provided insight into the solid phase formed by WEs. In the BO film simulations, solid domains were formed on the aqueous surface when a crystal nucleus was included in the initial simulation setup (Figure 12A). In the solid domains, the molecules adopted an extended upright conformation (Figure 12B) analogous to the bulk crystal structure of saturated WEs. Interestingly, despite the bulk-like molecular conformation that lacks any interaction between the polar ester groups and water, a uniform solid layer of monomolecular thickness was formed by WEs on the aqueous surface (Figure 11B,iv). The thickness of such a solid layer formed by BP was determined based on BAM image intensity to be 42 ± 6 Å, which is in good agreement with the extended upright molecular conformation observed in the simulations. This extended conformation is in contrast with the "hairpin" conformation suggested in early studies by Langmuir and Adam.[106,110] However, Langmuir noted that his results appeared to indicate an extended conformation, but discarded this possibility, since it was not expected to lead to monolayer formation.[110] However, as described above, the solid domains do not actually consist of a monolayer phase, but a monomolecular layer of WE with structure corresponding to bulk material.

However, some uncertainty still exists regarding the extended solid phase conformation described above. Since no experimental data on the crystal structure of WEs occurring in the TFLL has been reported, the structure of the initial crystal nucleus in the BO simulations presented here was based on the crystal structure reported for saturated WEs,[88-91] which was described in section 2.3.2. Since the initial crystal nucleus affects the structure of the solid domains formed in the simulations, these results must be interpreted with caution. However, the formation of these solid domains resulted in a decrease in simulated surface potential corresponding to the surface potential observed experimentally (Figure 12C), which suggests that the simulated crystal structure is likely correct.

In conclusion, these results showed that the evaporation resistance of WE films could be attributed to the formation of solid WE domains of monomolecular thickness on the aqueous the interface. However, these solid domains did not spread on the interface, and therefore a high coverage of the interface by the solid film only occurred in conditions, where a liquid WE monolayer coexisted with the solid phase. In these conditions, the molecules can diffuse along the water surface between solid WE domains, which enables the growth of the crystal domains on the surface to obtain a high coverage. Interestingly, the melting point of the model WEs that most closely resemble TFLL WEs (BO and BP) is 37–38 °C,[96,99] and therefore it is plausible that a similar mechanism could be at work in the TFLL at physiological ocular surface temperature (32–36 °C).[120-123] If this is the case, WEs may form a part of the polar sublayer of the TFLL, which would be consistent with the X-ray diffraction studies performed with meibum.[134]

### 5.2.2 TYPE 2 DIESTERS

Type II diesters (see Figure 2) resemble WEs in structure, consisting of only linear hydrocarbon chains connected by two ester groups. They are a relatively minor component of the Meibomian gland secretions,[27,62,77] and no data is currently available on their physical properties. However, decreased levels of Type II diesters have been associated with DED in a pilot study,[227] suggesting that they may be needed for proper TFLL function. In Publication IV, we attempted to characterize their biophysical properties on the aqueous interface in order to understand their role in the TFLL. Since the ultra-long-chained diesters found in the TFLL are not readily available and their chemical synthesis is complicated, four shorter diester analogues (Figure 7) were studied as model compounds.

The shorter diesters with melting points below room temperature (8-DiE, 12-DiE, and 15-DiE) readily formed a disordered monolayer on the aqueous surface at 35 °C, similar to WEs (Figure 13). Based on the larger area occupied by the diesters in the monolayer at surface pressure lift-off (113–125 Å$^2$/molecule) and approximately two times larger molecular dipole moment (800–1000 mD) compared to WEs, the diesters appeared to lie relatively flat on the water surface with both the ester groups facing the water (Figure 13i). Upon compression, diester monolayers collapsed at low surface pressures (< 10 mN/m) to form liquid droplets (Figure 13iii), similar to WEs. The collapse surface pressure decreased with increasing chain length, reflecting the increasing strength of intermolecular cohesion compared to the attraction between the ester groups and water.

The longest diester that was studied here (20-DiE) had a melting point of 41 °C, and therefore it remained as solid aggregates at 35 °C and did not show any surface activity. When the measurements were conducted above the melting point at 43 °C, a small increase in surface pressure was observed upon compression (Figure 13), but the BAM images revealed that the film was partially collapsed directly after spreading. This is line with the observed decrease in surface activity with increasing chain length. The lack of monolayer formation also prevents the spreading of the solid crystal on the aqueous surface by 20-DiE below the melting point, as was observed in the case of WEs.

Due to the presence of two ester moieties, diesters have an intermediate polarity compared to polar OAHFAs and nonpolar WEs and CEs.[74] Because of this they have been suggested to reside in between the polar OAHFAs and nonpolar WEs and CEs and connect the polar and nonpolar sublayers of the TFLL together.[74] However, these results suggests that this is not likely to be the case. Type II diesters occurring in the tear film mostly contain 64–68 carbons in total,[62] whereas the longest diester studied here (20-DiE) contained only 56 carbons. Considering that even 20-DiE did not spread to form a monolayer, whereas WEs such as BO and BP did, the diesters occurring in the TFLL should rather be characterized as less polar than WEs in the context of TFLL organization. Therefore, it appears more likely that

the diesters would partition into the nonpolar TFLL sublayer rather than to the polar sublayer or the aqueous interface. However, it is possible that some specific interactions between DiEs and polar lipids such as OAHFAs could cause such an effect.

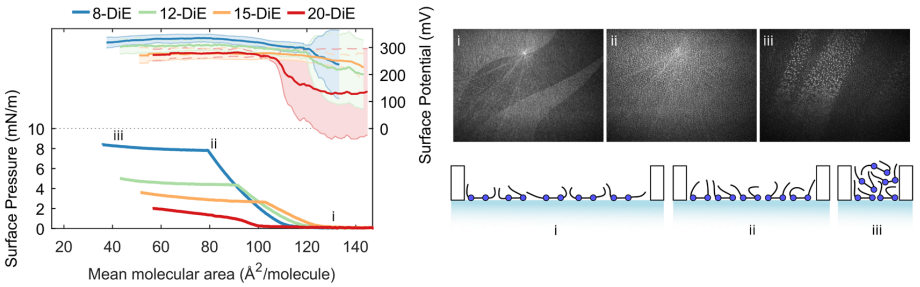


**Figure 13** Organization of Type II diesters on the aqueous interface. Surface pressure and surface potential (mean ± standard deviation) measured during compression are shown. 8-DiE, 12-DiE, and 15-DiE were measured at 35 °C, whereas 20-DiE was measured at 43 °C. Representative Brewster angle microscopy images from 8-DiE (i-iii) are shown with a scheme describing the molecular arrangement in each situation. Blue circles represent ester groups and lines represent hydrocarbon chains. Adapted with permission from Bland et al.[232] (https://pubs.acs.org/doi/10.1021/acs.langmuir.8b04182). Copyright 2019 American Chemical Society.

### 5.2.3 (O-ACYL)-ω-HYDROXY FATTY ACIDS

(O-acyl)-ω-hydroxy fatty acids contain a terminal carboxylic acid group, which makes them distinctly more polar than other major TFLL lipids (see Figure 2). Due to their polarity, they have been suggested to have a central role in connecting the nonpolar TFLL lipids to the aqueous tear film and in stabilization of TFLL structure.[74,112,265] In this work, a set of three OAHFAs with varying chain lengths (Figure 7) was studied to gain insight into their surface organization and how it is affected by chain length.

All the studied OAHFAs readily formed a monolayer on the PBS surface at 35 °C, which could be compressed to a high (> 30 mN/m) surface pressure before collapse occurred, in contrast to the nonpolar lipids studied in this work. At low surface pressures, all the OAHFAs formed a disordered monolayer with a large mean molecular area at surface pressure lift-off (100–120 Å²/molecule) and homogenous film appearance in BAM images (Figure 14i,iv). The likely conformation in this expanded monolayer phase consists of OAHFAs lying flat on the aqueous interface, with both the ester and carboxylic acid groups facing the water, as suggested previously.[112,265]

The behaviour at higher surface pressures was dramatically different depending on the OAHFA chain length. The shortest 12-OAHFA remained in a disordered monolayer phase until collapse, and no phase transition was observed (Figure 14ii–iii).

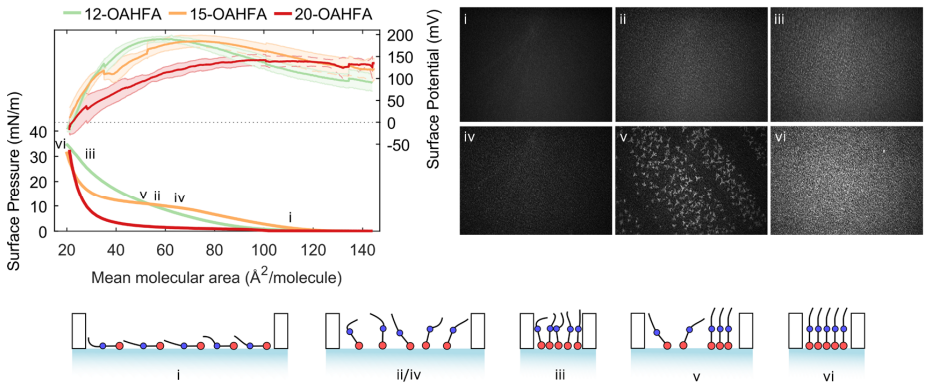


**Figure 14** OAHFA phase behaviour on the aqueous interface. Surface pressure and surface potential (mean ± standard deviation), with representative Brewster angle microscopy images from 12-OAHFA (i-iii) and 15-OAHFA (iv-vi) are shown with schemes describing the molecular arrangement in each case. Blue circles represent ester groups, red circles represent carboxylic acid groups and lines represent hydrocarbon chains. All measurements were performed at 35°C. Adapted with permission from Bland et al.[232] (https://pubs.acs.org/doi/10.1021/acs.langmuir.8b04182). Copyright 2019 American Chemical Society.

However, a major reorganization of the molecules occurred upon compression to 20 Å²/molecule, indicated by the decrease in molecular dipole moment from approximately 600 mD to 50 mD, observed as a decrease in surface potential (Figure 14). This likely reflects 12-OAHFA adopting a vertical extended configuration, where the ester groups reorient away from the aqueous interface (Figure 14ii–iii).

In contrast, upon compression of the longer 15-OAHFA and 20-OAHFA, a liquid-solid monolayer phase transition occurred, indicated by the plateaus in the surface pressure isotherms, as well as formation and growth of crystalline high-intensity domains in BAM images (Figure 14iv–vi). A change in the molecular dipole moment similar to 12-OAHFA was also observed, indicating that the solid monolayer phase consisted of OAHFAs in a similar vertical configuration (Figure 14vi). The formation of a solid monolayer phase was favoured by increasing the OAHFA chain length, likely driven by the increased intermolecular van der Waals interactions. A surface pressure plateau similar to 15-OAHFA was also observed in a previous study on (O-oleyl)-ω-hydroxy palmitic acid, but it was not identified as a liquid-solid phase transition.[112]

Although the OAHFAs studied here were shorter compared to naturally occurring OAHFAs, these results can be used to infer how naturally occurring OAHFAs behave at the aqueous interface. As shown in Table 2, the most abundant OAHFAs are 10–14 carbons longer than the longest OAHFA studied here (20-OAHFA). Such a large increase in chain length likely would further drive the organization towards a solid monolayer phase and may lead to slow spreading on the aqueous surface, as observed for long alkanols and

alkoxy ethanols.[266] However, the most abundant naturally occurring OAHFAs contain an unsaturated hydroxy fatty acid chain (Table 2), in contrast to the model OAHFAs studied here. The disordering effect caused by the presence of an additional double bond in the hydroxy fatty acid chain likely counteracts the increased chain length to some degree and may facilitate the rapid spreading observed here.

### 5.2.4 CHOLESTERYL ESTERS

Most abundant tear film cholesteryl esters contain very long (24–26 carbons) fatty acid moieties, most of which contain either a methyl-branch or a double bond. In Publication V, cholesteryl nervonate, the most abundant unsaturated CE in meibum was used to represent these CEs. Such a long CE did not spread on an aqueous interface 35 °C, and therefore it was mixed with polar phospholipid POPC to facilitate the formation of a lipid film. When mixed with POPC, a small amount of CN (up to 30%) initially formed a mixed monolayer with POPC on the aqueous surface (Figure 15i). However, compression of the monolayer or addition of a more CN caused an additional multilayer of CN to form over the POPC monolayer, observed as fluid, high intensity regions in BAM and FM images (Figure 15ii–iv). At higher surface pressures, CN was completely transferred from the monolayer to the overlying multilayers. This two-layered film structure resembled the "double layer" formed by shorter unsaturated CEs as described in subsection 2.3.3.

When the ratio of POPC and CN in the film was 1:9, CN formed a uniform layer that completely covered the underlying polar monolayer (Figure 15iv), but addition of more CN to the film led to formation of additional multilayer lamellae (Figure 15vi). These additional multilayers did not spread uniformly on the surface, but more layers were formed locally in some areas. Based on the BAM intensity, the thickness of the CN lamellae was estimated to be approximately 4.2 nm, corresponding to the lamellar thickness observed for CN liquid crystal phase.[116] Based on surface pressure isotherms and quantitative analysis of the corresponding BAM and FM images, the area per molecule in the overlying CN layer ($a'_{multi}$, see Figure 16) could be estimated to be 30 ± 1 Å$^2$. This is slightly larger than the area occupied by CN in the solid state (28.5 Å$^2$),[267] further suggesting that the lamellae formed by CN on the surface of the polar lipid monolayer were in a liquid crystalline state with an antiparallel arrangement of cholesteryl esters (Figure 16). This is in contrast with a previous estimate of approximately 38 Å$^2$ for the mean molecular area in CE double layers, which suggested parallel packing limited by the size of the cholesteryl moiety.[114] Such parallel packing is not typical for cholesteryl esters, whereas the antiparallel orientation suggested by our results is characteristic of the smectic liquid crystal phase exhibited by CN.[100]

As mixed films containing POPC and CN were compressed to surface pressures above 12 mN/m, an interesting phenomenon was observed, in which holes started forming in the CN multilayer (Figure 15v).

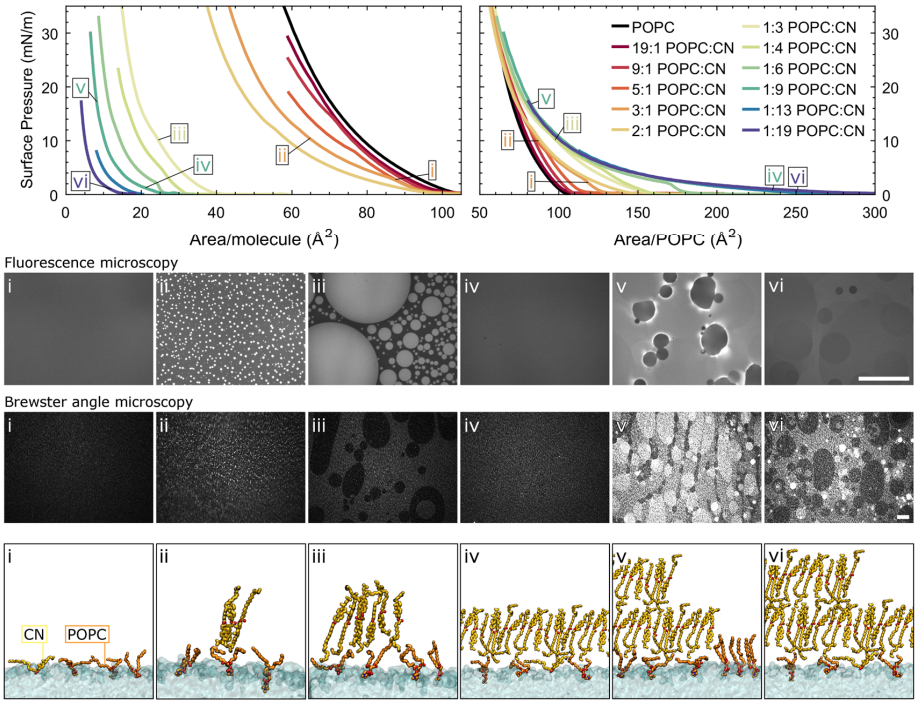


**Figure 15** Structure of mixed films of 1-palmitoyl-2-oleoyl-sn-glycero-3-phosphocholine (POPC) and cholesteryl nervonate (CN). Surface pressure isotherms of POPC:CN mixtures relative to the total number of molecules (left) and to the number of POPC molecules (right) are shown. Corresponding fluorescence and Brewster angle microscopy images, as well as schematic representations of the film structure are shown in (i–vi). Scale bars represent 300 μm. Reprinted from Paananen et al.[268]

It was clear that although mixing polar POPC with CN initially allowed the formation of a multi-layered film, the spreading of the CN multilayer was inhibited when the surface concentration of POPC was increased sufficiently. This can be explained by considering that spreading of a CN multilayer on a polar lipid monolayer is driven by the interdigitation of CN acyl chains from the multilayer and the acyl chains of the monolayer lipids. When the surface concentration of polar lipids is sufficiently low, acyl chains from the overlying CN molecules can penetrate into the monolayer (Figure 16i). This is also consistent with the increased area occupied by the film in the presence of a CN multilayer compared to a monolayer without an overlying CN lamella (Figure 15). However, as the surface concentration of polar lipids increases, the acyl chains of the monolayer lipids begin to pack more closely, expelling the interdigitated acyl chains (Figure 16ii), which leads to loss of spreading. In the absence of a spreading force, the cohesion between CN molecules and air-lipid surface tension then leads to CN aggregation.

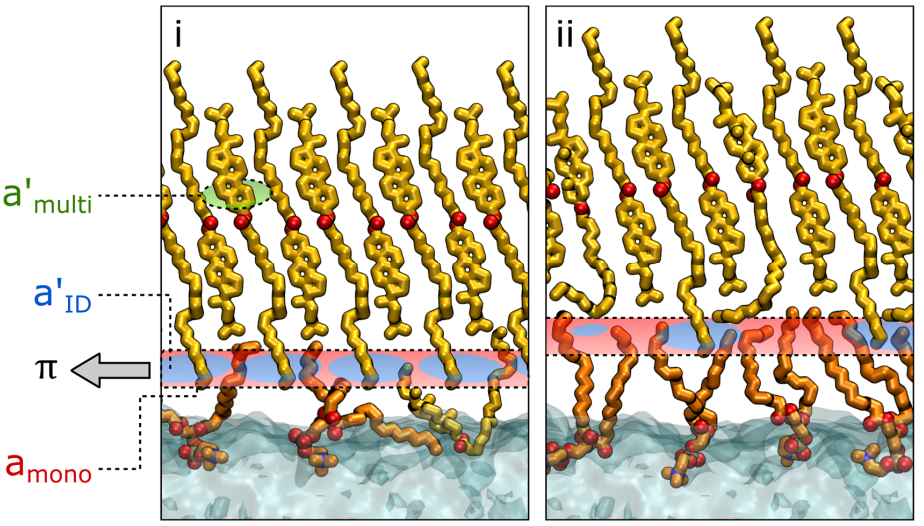


**Figure 16** Interdigitation of acyl chains in multilayers containing 1-palmitoyl-2-oleoyl-sn-glycero-3-phosphocholine (POPC) and cholesteryl nervonate (CN). The plane depicts the region where entropic repulsion of acyl chain occurs, resulting in surface pressure ($\pi$). $a'_{multi}$ represents area per molecule in the CN multilayer, whereas area occupied by multilayer acyl chains in the underlying monolayer is represented by $a'_{ID}$. The area occupied by the monolayer molecules is represented by $a_{mono}$. **i)** At low surface pressures the monolayer is significantly expanded by interdigitation of CN acyl chain into the monolayer. **ii)** At high surface pressures, CN acyl chains are excluded from the monolayer. Reprinted from Paananen et al.[268]

This also explains why only the first CN multilayer lamella spreads uniformly over the polar monolayer, whereas further lamellae do not, since the interdigitation only affects the CN lamella directly adjacent to the polar monolayer. In this respect, the interdigitation-driven multilayer model proposed here directly contrasts the double layer model by Smaby & Brockman, which suggested that significant interdigitation of acyl chains does not occur between the polar monolayer and the overlying non-polar lamella.[114] As a result, their model was not able to explain the instability of the CE multilayer observed at high surface concentrations of polar lipids.

### 5.2.5 MIXED FILMS OF CHOLESTERYL ESTERS AND OAHFAS

Although the results described in the previous subsection generally describe the multilamellar ordering of cholesteryl ester in the presence of polar lipids, they are likely not directly relevant for the TFLL, since only small amounts of phospholipids are expected to exist in the TFLL, as described in subsection 2.3.1. More relevant results were obtained in Publication V from studies with mixed films of 20-OAHFA and CN. These films organized in a similar multilayer structure as described in the previous subsection, with a

monolayer of mostly 20-OAHFA at the aqueous interface and an overlying multilayer of CN. However, a liquid-solid monolayer transition occurred in the underlying 20-OAHFA monolayer even in films containing 90% of CN, similar to pure 20-OAHFA (Figure 14). The formation of a solid monolayer was observed as dark crystalline domains in FM images (Figure 17i–iii,vi). The multilayer lamella of CN that formed over the monolayer, seen as bright regions in the BAM images, did not spread over the condensed domains in the monolayer, resulting in complex multilayer domain shapes (Figure 17iii). This reflects the fact that the tightly packed condensed monolayer phase of 20-OAHFA did not induce the spreading of CN due to the lack of interdigitation between the monolayer and CN, as was described for POPC in the previous subsection. These findings are important because they demonstrate that OAHFAs can form a solid monolayer in the presence of excess non-polar lipids, which would correspond to the TFLL conditions. This can likely be attributed to the strong surface activity of OAHFAs, evidenced by their high collapse surface pressures (Figure 14). The formation of a condensed monolayer phase is central for the evaporation resistance of the lipid films studied here, as discussed in the following section.

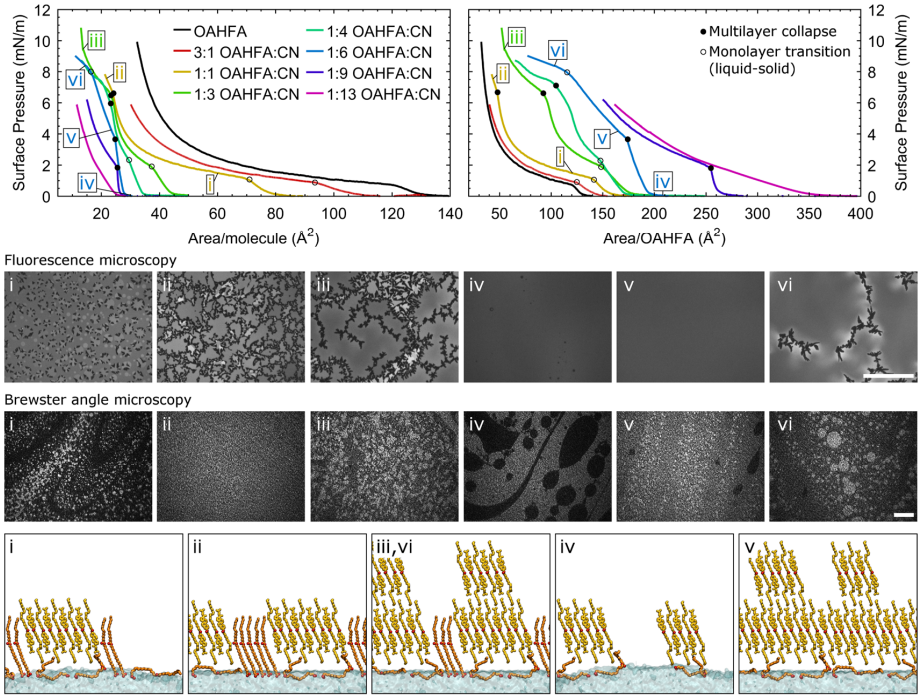


**Figure 17** Structure of mixed films of 20-OAHFA and cholesteryl nervonate (CN). Surface pressure isotherms are shown relative to the total number of molecules (left) and to the number of 20-OAHFA molecules (right). Corresponding fluorescence and Brewster angle microscopy images, as well as schematic representations of the film structure are shown in (i–vi). Scale bars represent 300 μm. Reprinted from Paananen et al.[268]

## 5.3 EVAPORATION RESISTANCE OF TEAR FILM LIPID SPECIES

Evaporation resistance of the tear film lipid layer has been estimated to be 9–13 s/cm *in vivo*,[151,156] as described in subsection 2.3.7. However, it was not clear, which lipid classes or structural features of the TFLL are linked to the evaporation resistance of the TFLL. To provide insight into the role of WEs, CEs, Type II diesters, and OAHFAs in TFLL function, the evaporation resistance of model lipids from all these lipid classes was evaluated in this work.

In the case of WEs, we focused on BO and BP, both of which have been previously shown to form films that slow down evaporation of water in physiological conditions.[99] As described in the previous section, these WEs spread on the aqueous surface as disordered monolayers. Experimentally, no evaporation resistance of was detected for the disordered monolayer but using molecular dynamics simulations the evaporation resistance of disordered WE films could be estimated. The simulations showed that a disordered layer of BO could be characterized by an approximately constant diffusion coefficient and solubility throughout the film, with no interfacial resistance to evaporation (Figure 18). The local permeation resistance of a disordered BO film was $(1.9 \pm 1.2) \times 10^5$ s/cm², which would result in negligible evaporation resistance for a film with monomolecular thickness, in agreement with experimental results. To provide appreciable (> 1 s/cm) evaporation resistance, duplex films of WEs would need to be at least 50 nm thick, in line with results previously reported for duplex films of lipids or oils.[162]

In contrast, simulations of crystalline BO films showed very high permeation resistance of up to $10^{17}$ s/cm² at the interface between the water and the film (Figure 18D). This would result in evaporation resistance of $10^9$ s/cm, many orders of magnitude higher than ever reported in experiments for lipid monolayers. In this work, evaporation resistance of approximately 3 s/cm was observed experimentally when the aqueous surface was completely covered by solid domains formed by BP at 37 °C, and the evaporation resistance rapidly declined when the surface was not completely covered by solid domains.

Taken together, these results suggest that water does not evaporate through solid domains of BO, but instead through domain boundaries. This effect could also be demonstrated in the evaporation simulations by assessing the resistance to permeation through a domain boundary between two crystalline domains with different alignments. In this case, the evaporation resistance was 20 s/cm, which is of the same order of magnitude as experimentally reported evaporation resistances for condensed monolayers.[172] These results agree with the most recent theories on monolayer evaporation resistance described in subsection 2.3.6, which also propose that evaporation mainly proceeds through domain boundaries.[171,175]

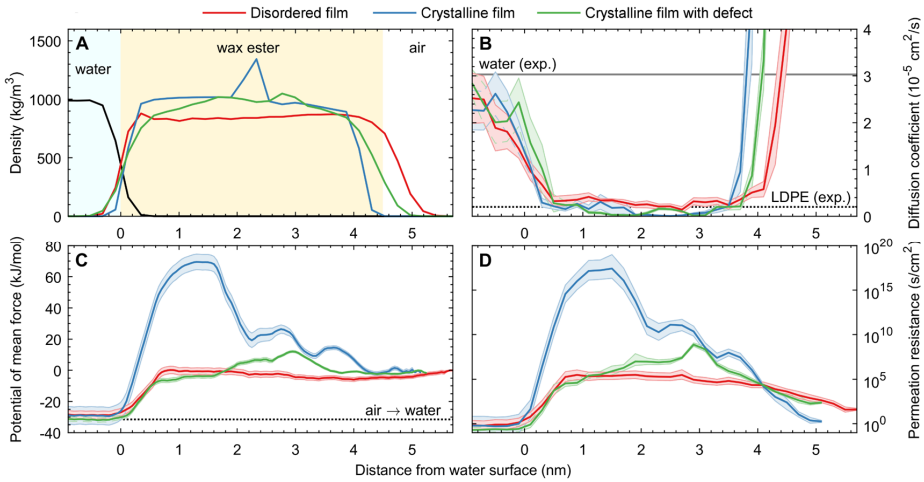


**Figure 18** Simulated permeation of water through behenyl oleate (BO) films. Permeation through a disordered film (red), a crystalline film (blue), and a crystalline film with a domain boundary (green) were studied. All the simulations were performed at mean molecular area of 24Å$^2$/molecule. Shaded regions depict error estimates. **A)** Density profiles of the BO films at the water interface. Water density is shown in black. **B)** Local diffusion coefficient throughout the films. Diffusion coefficients in water[269] and amorphous low-density polyethylene (LDPE)[270] are shown for comparison. **C)** Potential of mean force along the surface normal. Hydration free energy calculated from free-energy perturbation simulations is shown for reference (dotted line). **D)** Permeation resistance profiles. Note the logarithmic y-axis. Adapted with permission from Paananen et al.[264] (https://pubs.acs.org/doi/10.1021/acs.jpclett.9b01187). Copyright 2019 American Chemical Society.

In conclusion, these findings elaborate the effectiveness of thin solid WE films in resisting water evaporation, but also highlight the importance of uniform spreading of the film to cover the aqueous interface. Although the solid WE domains spread to cover the surface in a narrow temperature range below the WE melting point, the spreading rate of the solid domains appears to be low, and microscopic defects in the solid film were observed to persist for tens of minutes. Evaporation through such defect of domain boundaries likely limits the effectiveness of WEs in resisting evaporation in practice and explains the relatively low evaporation resistance observed experimentally.

In contrast to WEs, Type II diesters studied in this work did not exhibit evaporation resistance in physiological conditions. In the case of the shorter diesters (8-DiE, 12-DiE, and 15-DiE), the lack of evaporation resistance can be explained by their disordered organization in the monolayer phase (Figure 13). 20-DiE formed solid aggregates at 35 °C but did not spread as a monolayer. In the absence of monolayer formation, the solid domains did not cover the aqueous interface, which explains the lack of evaporation resistance.

Polar OAHFAs readily spread as monolayers in physiological conditions and were found to form evaporation resistant films. Evaporation resistance

of OAHFAs was found to increase with chain length, as predicted by the energy barrier theory,[165,169] and in line with previous results with other evaporation resistant polar lipid classes.[171] The shortest 12-OAHFA exhibited no detectable evaporation resistance, whereas 15-OAHFA and 20-OAHFA had evaporation resistances of 2 s/cm and 5 s/cm, respectively (Figure 19). Similar to WEs, the evaporation resistance was linked to the formation of a solid structure on the aqueous surface, which was observed for 15-OAHFA and 20-OAHFA (Figure 14). The shortest 12-OAHFA, which did not resist evaporation, only exhibited a liquid monolayer phase. Further, 15-OAHFA and 20-OAHFA initially formed a liquid monolayer at low surface concentrations, which likely increases the rate at which they spread to cover the aqueous interface. This was not studied directly in this work, but this effect can be seen indirectly when comparing 15-OAHFA and 20-OAHFA with their alcohol analogues, 15-OAHFAL and 20-OAHFAL. Both 15-OAHFA and 15-OAHFAL exhibit a liquid monolayer phase and have very similar evaporation resistance. In contrast, 20-OAHFAL only exhibits a condensed monolayer phase and has a markedly lower evaporation resistance than 20-OAHFA (Figure 19).

Based on these results, it is possible to speculate why the special lipid class of ultra-long OAHFAs is found in the TFLL. The ultra-long chain length is likely connected to evaporation resistance, since evaporation resistance increases with chain length for OAHFAs, as shown here. However, as the chain length increases and the films become increasingly condensed, also the spreading rate of lipid monolayers tends to decrease.[172]

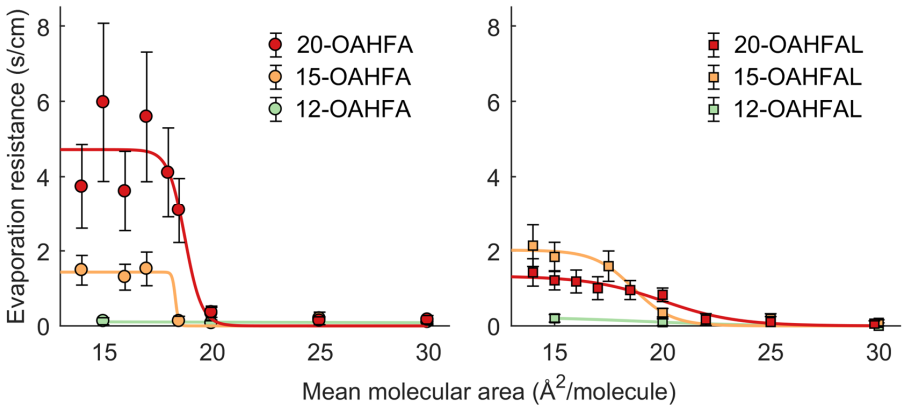


**Figure 19** Evaporation resistance of O-acyl-ω-hydroxy fatty acid (12-OAHFA, 15-OAHFA, and 20-OAHFA) and their alcohol analogues (12-OAHFAL, 15-OAHFAL, and 20-OAHFAL) as a function of mean molecular area at 35 °C. Reprinted with permission from Bland et al.[232] (https://pubs.acs.org/doi/10.1021/acs.langmuir.8b04182). Copyright 2019 American Chemical Society.

This limits the practical reduction in evaporation that can be achieved, as has been previously reported for a number of lipid classes.[172] The special structure of tear film OAHFAs with a polar ester group in the middle of the molecule and double bonds in the acyl and hydroxy fatty acid chains may work to facilitate spreading as a liquid monolayer, as was observed here for 15-OAHFA and 20-OAHFA, despite the ultra-long chain length. Such a combination of ultra-long chain length and efficient spreading would be expected to provide an effective barrier to evaporation, but this needs to be confirmed by studying the naturally occurring OAHFA species.

In addition to the condensed interfacial films formed by WEs and OAHFAs, the bulk of the nonpolar sublayer of the TFLL has also been suggested to play a significant role in the evaporation resistance of the TFLL.[11-14] Since nonpolar CN formed a second layer on top of polar monolayers when mixed with POPC or 20-OAHFA, it presents a good model system to investigate whether an additional layer of non-polar lipids overlying a polar monolayer can provide additional evaporation resistance. To address this, we measured the evaporation resistance of a film composed of 1:9 ratio of POPC and CN, where the CN lamella covered the whole surface (Figure 15iv). However, the overlying CN lamella was not found to provide detectable evaporation resistance. In addition, the evaporation resistance of a mixed film of 20-OAHFA and CN was identical to pure 20-OAHFA. This lack of evaporation resistance is likely due to the liquid crystalline structure of the CN lamella, which is not condensed enough to significantly hinder the permeation of water. This indicates that in order to provide evaporation resistance, the nonpolar sublayer of the TFLL likely needs to contain condensed lamellae, as suggested by King-Smith et al.[12] On the other hand, the overlying CN lamellae also did not appear to hinder the evaporation resistance of the 20-OAHFA monolayer at the interface. This suggests that an evaporation resistant layer may form in the polar sublayer of the TFLL despite the presence of large amounts of nonpolar lipids at the tear film surface.

# 6 SUMMARY AND CONCLUSIONS

## 6.1 TEAR FILM LIPID LAYER STRUCTURE AND FUNCTION

The first aim of this thesis was to investigate how different TFLL lipid classes organize at the aqueous interface, which was accomplished by studying pure tear film lipid model compounds, as described in section 5.2. Although the model lipids used do not perfectly match the most abundant lipid species in the TFLL, the results presented provide a solid basis for understanding TFLL organization at the molecular level. Based on the results of this work, CEs and Type II diesters are not expected to be present in significant amounts in the polar sublayer of the TFLL, but rather form droplets or aggregates on top of the polar sublayer. Out of the studied lipids, CE was the only lipid class that formed multilamellar layers above the aqueous interface, suggesting that CEs or Type I-St diesters promote multilamellar organization of the nonpolar TFLL sublayer. In contrast, OAHFAs and WEs were shown to spread at the aqueous interface, suggesting that they are likely the main components of the polar sublayer. Further, OAHFAs and WEs formed solid monomolecular structures that are central for evaporation resistance.

While this work focused on single-component and two-component films, the TFLL is a complex mixture and its cooperative organization may differ from the simplified films studied here. Therefore, it is of interest to compare the results obtained here with studies of natural meibum. Interestingly, the findings of this work are consistent with the grazing incidence X-ray diffraction results of human meibum, which suggested that Meibomian lipids form an ordered monolayer with lattice spacings that indicate it may consist of OAHFAs and/or WEs.[134] These results suggest that the polar sublayer of the TFLL likely has a condensed structure similar to the structures described in this work for OAHFAs and WEs.

The second aim of the thesis was to provide insight into the evaporation resistance mechanism of the TFLL. In this work, we found that solid films formed by pure WEs and OAHFAs at the aqueous interface had evaporation resistant properties. However, since the surface activity of WEs is very low, they would be readily replaced from the aqueous interface by more polar lipids. If these polar lipids do not resist evaporation, like phospholipids, the evaporation resistance is lost. This has been demonstrated in earlier work showing that evaporation resistance of WE films diminished when phospholipids were added to the film.[108] Therefore, the evaporation resistance of an interfacial film mostly composed of WEs would be very sensitive to the presence of polar lipids. Because of this, an interfacial layer formed by WEs has been suggested not to be effective in resisting evaporation in a complex lipid mixture such as the TFLL.[8] OAHFAs, on the

other hand, have a high surface activity and the monolayers formed by OAHFAs are stable until high surface pressures, as shown in Publication IV. Therefore, they are expected to form a stable monolayer at the aqueous tear film surface. Since the monolayers formed by OAHFAs were also shown to have significant evaporation resistance, OAHFAs are likely to have a central role in the evaporation resistant function of the TFLL. However, it should be noted that currently all the data on the properties of OAHFAs are based on model compounds with shorter chain lengths than the ultra-long OAHFAs that naturally occur in the TFLL. However, since a longer chain length is related to higher evaporation resistance in OAHFAs and other amphiphiles, this conclusion is likely to be accurate for the natural OAHFAs as well.

The third aim of this thesis was to investigate the role of polar and nonpolar lipids in TFLL function. Taken together, the findings presented in this thesis challenge the conventional view of TFLL structure and function, which states that polar lipids act as spreaders that allow formation of a uniform duplex film by nonpolar lipids on the tear film surface.[11-14,119] This layer of nonpolar lipids, which makes up most of the TFLL, is considered to provide a stabilizing function by retarding evaporation of water.[11-14] As described in subsection 2.3.6, the evaporation resistance of such duplex film could theoretically be up to 5 s/cm, but experimentally achieved evaporation resistances have been one order of magnitude less than this.[162] In contrast, evaporation resistance of OAHFA monolayers was found to be up to 5 s/cm in this work. To consider its clinical relevance, this would correspond to a 50-80% decrease in evaporation rate in typical conditions corresponding to the ocular surface.

Further, the results presented in this work and previous studies[171,175] show that evaporation resistance of lipid monolayers is highly sensitive to local defects in the monolayer structure. Analogously, the evaporation resistance of the TFLL would also be sensitive to local variations in TFLL thickness, if the evaporation resistance was mainly due to the resistance of the non-polar duplex film. Since *in vivo* studies have shown that the TFLL thickness is highly nonuniform,[131,132] a high evaporation resistance would not be expected by such a mechanism.

An alternative model, which is favoured by the results of this work, suggests that the evaporation resistance of the TFLL originates from the polar sublayer itself. This is supported by the fact that OAHFAs and WEs can form condensed evaporation resistant monolayers in conditions corresponding to the natural tear film, and the monolayers formed by OAHFAs are not disturbed by the presence of non-polar lipids. Further, the results presented here show that the high surface concentration of polar lipids necessary for evaporation resistance is not compatible with the suggested spreading function of polar TFLL lipids. At high surface concentrations, the polar lipids studied here did not have a spreading effect on nonpolar CEs. In fact, this lack of nonpolar lipid spreading would be

consistent with the uneven thickness distribution of the TFLL observed *in vivo*.[131,132]

According to this model, the functional significance of the nonpolar layer of the TFLL is reduced. Nonpolar lipids would likely mostly act as a medium to transport the evaporation resistant lipids from the Meibomian glands to the ocular surface, and serve as a reservoir, from which evaporation resistant lipids spread to the ocular surface as the eye is opened after the blink. The spreading rate of the evaporation resistant lipids is likely also faster when they are dissolved in this lipid reservoir compared to spreading from solid bulk crystals. This would be an important factor in TFLL function, since the TFLL needs to rapidly spread to cover the tear film as the eye is opened to reduce evaporation during the interblink period. Slow spreading from solid bulk is known to limit the practical evaporation reduction by long chained amphiphiles,[172] but the spreading rate can be increased by mixing them with non-polar oil.[271] This model would also explain the lack of correlation between TFLL thickness and evaporation rate,[1,153,154,198] since as long as the lipid reservoir is sufficient, the thickness of the nonpolar lipid layer would not be related to evaporation resistance.

## 6.2 FUTURE DIRECTIONS

The main strength of the studies presented here is that lipid films studied had a well-defined composition containing high purity lipids. This enabled detailed characterization of the film structure, which is often very difficult when complex lipid mixtures such as meibum are studied directly. Unfortunately, currently many of the abundant lipids in the TFLL such as branched WEs and CEs, or ultra-long OAHFAs and diesters are not readily available for studies similar to the work presented here. Chemical synthesis of these lipids would provide an essential tool for further work aiming to identify the structures that form within the TFLL.

In addition, a wider utilization of surface analysis methods that can provide details into the structure of TFLL lipids at the molecular level, such as neutron or X-ray scattering techniques, could provide significant advances in understanding TFLL structure, especially if combined with use of synthetically produced standard lipids.

Further, well-controlled measurement of evaporation resistance by Meibomian lipids *in vitro* and development of methods to determine evaporation resistance of the TFLL *in vivo* could help to reconcile the controversy around TFLL evaporation resistance. These steps could further advance the work undergone in this thesis and elucidate the role of the TFLL in health and disease. This could potentially lead to new diagnosis and treatment opportunities related to tear film function.

# ACKNOWLEDGEMENTS

This thesis project started out in 2013 at the Helsinki Eye Lab in the Department of Ophthalmology, University of Helsinki under the supervision of the late Professor Juha Holopainen. Juha's endless enthusiasm and fun approach to doing science really sparked my interest in research and pushed me to finish this work after his passing. I will forever be grateful for the time I got to spend with him, and all the guidance and inspiration over the years.

After Juha's passing, Professor Ilpo Vattulainen and Adjunct Professor Jukka Moilanen were kind enough to take over the supervision of my thesis project, and I am greatly thankful of all their support and advice. I also wish to thank Adjunct Professor Anu Jalanko and Professor Tero Kivelä for providing research facilities for this work. In addition, the funding provided by the Biomedicum Helsinki Foundation, the Mary and Georg C. Ehrnrooth Foundation, the Evald and Hilda Nissi Foundation, the Orion Research Foundation, the Eye and Tissue Bank Foundation, the Finnish Eye Foundation, and the Jenny and Antti Wihuri Foundation to support this work is gratefully acknowledged.

I also wish to thank the reviewers of this thesis, Professors Emma Sparr and Kari Laasonen for their time and valuable comments to improve this thesis.

Over the course of this work, I have been fortunate to be able to work with many great colleagues and collaborators, and I want to thank Jevgeni Parshintsev, Helena Bland, Jan-Erik Raitanen, Agnieszka Olżyńska, Lukasz Cwiklik, and Tuomo Viitaja for their expertise and contributions to this work. Special thanks go to Matti Javanainen for introducing me to the world of molecular dynamics simulations and for all his support over the years. This work could not have been possible without Filip Ekholm, whose support during the final years of this project has been invaluable and has really helped to push this work to the next level. I also want to thank original Helsinki Eye Lab team, Pipsa Kulovesi, Antti Rantamäki, and Alexandra Robciuc for their advice and all the great times we shared both inside and outside the lab.

Finally, I want to thank my family for all their support and encouragement over the years. Most importantly, I wish to thank my partner Katriina for all her love and understanding, and for always being there for me, and my daughter Aino for all the fun, meaning, and perspective you have brought to my life.

# REFERENCES

1. King-Smith PE, Hinel EA, Nichols JJ. Application of a novel interferometric method to investigate the relation between lipid layer thickness and tear film thinning. *Invest Ophthalmol Vis Sci*. 2010;51(5):2418–2423.

2. Kimball SH, King-Smith PE, Nichols JJ. Evidence for the major contribution of evaporation to tear film thinning between blinks. *Invest Ophthalmol Vis Sci*. 2010;51(12):6294–6297.

3. Nichols JJ, King-Smith PE, Hinel EA, Thangavelu M, Nichols KK. The use of fluorescent quenching in studying the contribution of evaporation to tear thinning. *Invest Ophthalmol Vis Sci*. 2012;53(9):5426–5432.

4. Nichols JJ, Mitchell GL, King-Smith PE. Thinning rate of the precorneal and prelens tear films. *Invest Ophthalmol Vis Sci*. 2005;46(7):2353–2361.

5. Palakuru JR, Wang J, Aquavella JV. Effect of blinking on tear dynamics. *Invest Ophthalmol Vis Sci*. 2007;48(7):3032–3037.

6. Tiffany JM. The lipid secretion of the meibomian glands. *Adv Lipid Res*. 1987;22:1–62.

7. Bron AJ, Tiffany JM, Gouveia SM, Yokoi N, Voon LW. Functional aspects of the tear film lipid layer. *Exp Eye Res*. 2004;78(3):347–360.

8. Millar TJ, Schuett BS. The real reason for having a meibomian lipid layer covering the outer surface of the tear film–A review. *Exp Eye Res*. 2015;137:125–138.

9. Georgiev GA, Eftimov P, Yokoi N. Structure-function relationship of tear film lipid layer: A contemporary perspective. *Exp Eye Res*. 2017;163:17–28.

10. Butovich IA. Tear film lipids. *Exp Eye Res*. 2013;117:4–27.

11. McCulley JP, Shine W. A compositional based model for the tear film lipid layer. *Trans Am Ophthalmol Soc*. 1997;95:79–93.

12. King-Smith PE, Bailey MD, Braun RJ. Four characteristics and a model of an effective tear film lipid layer (TFLL). *Ocul Surf*. 2013;11(4):236–245.

13. Rosenfeld L, Cerretani C, Leiske DL, Toney MF, Radke CJ, Fuller GG. Structural and rheological properties of meibomian lipid. *Invest Ophthalmol Vis Sci*. 2013;54(4):2720–2732.

14. Svitova TF, Lin MC. Dynamic interfacial properties of human tear-lipid films and their interactions with model-tear proteins in vitro. *Adv Colloid Interface Sci.* 2016;233:4–24.

15. Willcox MDP, Argüeso P, Georgiev GA, Holopainen JM, Laurie GW, Millar TJ, Papas EB, Rolland JP, Schmidt TA, Stahl U, Suarez T, Subbaraman LN, Uçakhan OÖ, Jones L. TFOS DEWS II tear film report. *Ocul Surf.* 2017;15(3):366–403.

16. Craig JP, Nichols KK, Akpek EK, Caffery B, Dua HS, Joo C, Liu Z, Nelson JD, Nichols JJ, Tsubota K, Stapleton F. TFOS DEWS II definition and classification report. *Ocul Surf.* 2017;15(3):276–283.

17. Stapleton F, Alves M, Bunya VY, Jalbert I, Lekhanont K, Malet F, Na K, Schaumberg D, Uchino M, Vehof J, Viso E, Vitale S, Jones L. TFOS DEWS II epidemiology report. *Ocul Surf.* 2017;15(3):334–365.

18. Forrester JV, Dick AD, McMenamin PG, Roberts F, Pearlman E. Chapter 5 - physiology of vision and the visual system. In: Forrester JV, Dick AD, McMenamin PG, Roberts F, Pearlman E, eds. *The eye (fourth edition).* W.B. Saunders; 2016:269–337.e2.

19. Meek KM, Knupp C. Corneal structure and transparency. *Prog Retin Eye Res.* 2015;49:1–16.

20. Nichols B, Dawson CR, Togni B. Surface features of the conjunctiva and cornea. *Invest Ophthalmol Vis Sci.* 1983;24(5):570–576.

21. Uchino Y. The ocular surface glycocalyx and its alteration in dry eye disease: A review. *Invest Ophthalmol Vis Sci.* 2018;59(14):DES157–DES162.

22. Ablamowicz AF, Nichols JJ. Ocular surface membrane-associated mucins. *Ocul Surf.* 2016;14(3):331–341.

23. Dartt DA. Neural regulation of lacrimal gland secretory processes: Relevance in dry eye diseases. *Prog Retin Eye Res.* 2009;28(3):155–177.

24. Sirigu P, Shen RL, Pinto da Silva P. Human meibomian glands: The ultrastructure of acinar cells as viewed by thin section and freeze-fracture transmission electron microscopies. *Invest Ophthalmol Vis Sci.* 1992;33(7):2284–2292.

25. Olami Y, Zajicek G, Cogan M, Gnessin H, Pe'er J. Turnover and migration of meibomian gland cells in rats' eyelids. *Ophthalmic Res.* 2001;33(3):170–175.

26. Knop E, Knop N, Millar T, Obata H, Sullivan DA. The international workshop on meibomian gland dysfunction: Report of the subcommittee

on anatomy, physiology, and pathophysiology of the meibomian gland. *Invest Ophthalmol Vis Sci.* 2011;52(4):1938–1978.

27. Nicolaides N, Kaitaranta JK, Rawdah TN, Macy JI, Boswell FM, Smith RE. Meibomian gland studies: Comparison of steer and human lipids. *Invest Ophthalmol Vis Sci.* 1981;20(4):522–536.

28. King-Smith E, Fink B, Hill R, Koelling K, Tiffany J. The thickness of the tear film. *Curr Eye Res*. 2004;29(4–5):357–368.

29. Bai Y, Nichols JJ. Advances in thickness measurements and dynamic visualization of the tear film using non-invasive optical approaches. *Prog Retin Eye Res.* 2017;58:28–44.

30. Hilkens J, Ligtenberg MJL, Vos HL, Litvinov SV. Cell membrane-associated mucins and their adhesion-modulating property. *Trends Biochem Sci.* 1992;17(9):359–363.

31. Berman ER. *Biochemistry of the eye.* New York: Plenum Press; 1991.

32. Gachon AM, Richard J, Dastugue B. Human tears: Normal protein pattern and individual protein determinations in adults. *Curr Eye Res.* 1983;2(5):301–308.

33. Fullard RJ, Snyder C. Protein levels in nonstimulated and stimulated tears of normal human subjects. *Invest Ophthalmol Vis Sci.* 1990;31(6):1119–1126.

34. Green-Church KB, Nichols KK, Kleinholz NM, Zhang L, Nichols JJ. Investigation of the human tear film proteome using multiple proteomic approaches. *Mol Vis*. 2008;14:456–470.

35. Baier G, Wollensak G, Mur E, Redl B, Stöffler G, Göttinger W. Analysis of human tear proteins by different high-performance liquid chromatographic techniques. *J Chromatogr*. 1990;525(2):319–328.

36. Ragland SA, Criss AK. From bacterial killing to immune modulation: Recent insights into the functions of lysozyme. *PLOS Pathogens.* 2017;13(9):e1006512.

37. Ward PP, Paz E, Conneely OM. Multifunctional roles of lactoferrin: A critical overview. *Cell Mol Life Sci*. 2005;62(22):2540–2548.

38. Flanagan JL, Willcox MDP. Role of lactoferrin in the tear film. *Biochimie*. 2009;91(1):35–43.

39. Corthésy B. Multi-faceted functions of secretory IgA at mucosal surfaces. *Front Immunol*. 2013;4:185.

40. Dartt DA. Tear lipocalin: Structure and function. *Ocul Surf*. 2011;9(3):126–138.

41. Gipson IK. Goblet cells of the conjunctiva: A review of recent findings. *Prog Retin Eye Res*. 2016;54:49–63.

42. Hori Y. Secreted mucins on the ocular surface. *Invest Ophthalmol Vis Sci*. 2018;59(14):DES151–DES156.

43. McKenzie RW, Jumblatt JE, Jumblatt MM. Quantification of MUC2 and MUC5AC transcripts in human conjunctiva. *Invest Ophthalmol Vis Sci*. 2000;41(3):703–708.

44. Spurr-Michaud S, Argüeso P, Gipson I. Assay of mucins in human tear fluid. *Exp Eye Res*. 2007;84(5):939–950.

45. Yu DF, Chen Y, Han JM, Zhang H, Chen XP, Zou WJ, Liang LY, Xu CC, Liu ZG. MUC19 expression in human ocular surface and lacrimal gland and its alteration in Sjögren syndrome patients. *Exp Eye Res*. 2008;86(2):403–411.

46. Hsu SM. Boundary lubrication: Current understanding. *Tribology Letters*. 1997;3(1):1–11.

47. Baudouin C, Rolando M, Benitez Del Castillo, Jose M., Messmer EM, Figueiredo FC, Irkec M, Van Setten G, Labetoulle M. Reconsidering the central role of mucins in dry eye and ocular surface diseases. *Prog Retin Eye Res*. 2019;71:68–87.

48. Braun RJ. Dynamics of the tear film. *Annu Rev Fluid Mech*. 2012;44:267–297.

49. Braun RJ, King-Smith PE, Begley CG, Li L, Gewecke NR. Dynamics and function of the tear film in relation to the blink cycle. *Prog Retin Eye Res*. 2015;45:132–164.

50. Meng ID, Kurose M. The role of corneal afferent neurons in regulating tears under normal and dry eye conditions. *Exp Eye Res*. 2013;117:79–87.

51. Nichols JJ, Nichols KK, Puent B, Saracino M, Mitchell GL. Evaluation of tear film interference patterns and measures of tear break-up time. *Optom Vis Sci*. 2002;79(6):363–369.

52. Tian L, Qu J, Zhang X, Sun X. Repeatability and reproducibility of noninvasive keratograph 5M measurements in patients with dry eye disease. *Journal of Ophthalmology*. 2016;2016:e8013621.

53. Tsubota K. Tear dynamics and dry eye. *Prog Retin Eye Res*. 1998;17(4):565–596.

54. Cho B, Jee DH, Kim WJ, Shin MC, Kim EC, Kim MS, Hwang HS. Direct visualization of continuous meibum secretion from the orifices of meibomian glands to the tear film. *Cornea*. 2019;38(10):1245–1252.

55. Yokoi N, Yamada H, Mizukusa Y, Bron AJ, Tiffany JM, Kato T, Kinoshita S. Rheology of tear film lipid layer spread in normal and aqueous tear-deficient dry eyes. *Invest Ophthalmol Vis Sci*. 2008;49(12):5319–5324.

56. King-Smith PE, Fink BA, Nichols JJ, Nichols KK, Braun RJ, McFadden GB. The contribution of lipid layer movement to tear film thinning and breakup. *Invest Ophthalmol Vis Sci*. 2009;50(6):2747–2756.

57. Khanal S, Millar TJ. Nanoscale phase dynamics of the normal tear film. *Nanomedicine*. 2010;6(6):707–713.

58. Tomlinson A, Khanal S. Assessment of tear film dynamics: Quantification approach. *Ocul Surf*. 2005;3(2):81–95.

59. Mochizuki H, Yamada M, Hatou S, Tsubota K. Turnover rate of tear-film lipid layer determined by fluorophotometry. *Br J Ophthalmol*. 2009;93(11):1535–1538.

60. Brown SH, Kunnen CM, Duchoslav E, Dolla NK, Kelso MJ, Papas EB, Lazon de la Jara, P, Willcox MD, Blanksby SJ, Mitchell TW. A comparison of patient matched meibum and tear lipidomes. *Invest Ophthalmol Vis Sci*. 2013;54(12):7417–7424.

61. Lam SM, Tong L, Duan X, Petznick A, Wenk MR, Shui G. Extensive characterization of human tear fluid collected using different techniques unravels the presence of novel lipid amphiphiles. *J Lipid Res*. 2014;55(2):289–298.

62. Chen J, Green KB, Nichols KK. Quantitative profiling of major neutral lipid classes in human meibum by direct infusion electrospray ionization mass spectrometry. *Invest Ophthalmol Vis Sci*. 2013;54(8):5730–5753.

63. Kunnen CME, Brown SHJ, Lazon de la Jara, Percy, Holden BA, Blanksby SJ, Mitchell TW, Papas EB. Influence of meibomian gland expression methods on human lipid analysis results. *Ocul Surf*. 2016;14(1):49–55.

64. Saville JT, Zhao Z, Willcox MDP, Ariyavidana MA, Blanksby SJ, Mitchell TW. Identification of phospholipids in human meibum by nano-electrospray ionisation tandem mass spectrometry. *Exp Eye Res*. 2011;92(3):238–240.

65. Tsai PS, Evans JE, Green KM, Sullivan RM, Schaumberg DA, Richards SM, Dana MR, Sullivan DA. Proteomic analysis of human meibomian gland secretions. *Br J Ophthalmol*. 2006;90(3):372–377.

66. Butovich IA, Lu H, McMahon A, Ketelson H, Senchyna M, Meadows D, Campbell E, Molai M, Linsenbardt E. Biophysical and morphological evaluation of human normal and dry eye meibum using hot stage polarized light microscopy. *Invest Ophthalmol Vis Sci*. 2014;55(1):87–101.

67. Ong B, Hodson SA, Wigham T, Miller F, Larke JR. Evidence for keratin proteins in normal and abnormal human meibomian fluids. *Curr Eye Res*. 1991;10(12):1113–1119.

68. Chen J, Green KB, Nichols KK. Compositional analysis of wax esters in human meibomian gland secretions by direct infusion electrospray ionization mass spectrometry. *Lipids*. 2016;51(11):1269–1287.

69. Hancock SE, Ailuri R, Marshall DL, Brown SHJ, Saville JT, Narreddula VR, Boase NR, Poad BLJ, Trevitt AJ, Willcox MDP, Kelso MJ, Mitchell TW, Blanksby SJ. Mass spectrometry-directed structure elucidation and total synthesis of ultra-long chain (O-acyl)-ω-hydroxy fatty acids. *J Lipid Res*. 2018;59(8):1510–1518.

70. Lam SM, Tong L, Yong SS, Li B, Chaurasia SS, Shui G, Wenk MR. Meibum lipid composition in asians with dry eye disease. *PLoS One*. 2011;6(10):e24339.

71. Butovich IA. Meibomian glands, meibum, and meibogenesis. *Exp Eye Res*. 2017;163:2–16.

72. Butovich IA, McMahon A, Wojtowicz JC, Lin F, Mancini R, Itani K. Dissecting lipid metabolism in meibomian glands of humans and mice: An integrative study reveals a network of metabolic reactions not duplicated in other tissues. *Biochim Biophys Acta*. 2016;1861(6):538–553.

73. Butovich IA, Wilkerson A, Bhat N, McMahon A, Yuksel S. On the pivotal role of Elovl3/ELOVL3 in meibogenesis and ocular physiology of mice. *FASEB J*. 2019;33(9):10034–10048.

74. Miyamoto M, Sassa T, Sawai M, Kihara A. Lipid polarity gradient formed by ω-hydroxy lipids in tear film prevents dry eye disease. *eLife*. 2020;9:e53582.

75. Lam SM, Tong L, Duan X, Acharya UR, Tan JH, Petznick A, Wenk MR, Shui G. Longitudinal changes in tear fluid lipidome brought about by eyelid-warming treatment in a cohort of meibomian gland dysfunction. *J Lipid Res*. 2014;55(9):1959–1969.

76. Lam SM, Tong L, Reux B, Duan X, Petznick A, Yong SS, Khee CBS, Lear MJ, Wenk MR, Shui G. Lipidomic analysis of human tear fluid reveals structure-specific lipid alterations in dry eye syndrome. *J Lipid Res*. 2014;55(2):299.

77. Chen J, Nichols KK. Composition of diesters in human meibum. *Invest Ophthalmol Vis Sci*. 2016;57(12):4818.

78. Butovich IA, Uchiyama E, McCulley JP. Lipids of human meibum: Mass-spectrometric analysis and structural elucidation. *J Lipid Res*. 2007;48(10):2220–2235.

79. Butovich IA, Uchiyama E, Di Pascuale MA, McCulley JP. Liquid chromatography-mass spectrometric analysis of lipids present in human meibomian gland secretions. *Lipids*. 2007;42(8):765–776.

80. Brown SHJ, Kunnen CME, Papas EB, Lazon de la Jara, P., Willcox MDP, Blanksby SJ, Mitchell TW. Intersubject and interday variability in human tear and meibum lipidomes: A pilot study. *Ocul Surf*. 2016;14(1):43–48.

81. Wojtowicz JC, McMahon A, Butovich IA. Human tear film lipid variability – A year-long assessment. *Invest Ophthalmol Vis Sci*. 2017;58(8):4382–4382.

82. Ngo W, Chen J, Panthi S, Nichols KK, Nichols JJ. Comparison of collection methods for the measure of human meibum and tear film-derived lipids using mass spectrometry. *Curr Eye Res*. 2018;43(10):1244–1252.

83. Chen J, Nichols KK, Wilson L, Barnes S, Nichols JJ. Untargeted lipidomic analysis of human tears: A new approach for quantification of O-acyl-omega hydroxy fatty acids. *Ocul Surf*. 2019;17(2):347–355.

84. Rohit A, Stapleton F, Brown SHJ, Mitchell TW, Willcox MDP. Comparison of tear lipid profile among basal, reflex, and flush tear samples. *Optom Vis Sci*. 2014;91(12):1391–1395.

85. Dean AW, Glasgow BJ. Mass spectrometric identification of phospholipids in human tears and tear lipocalin. *Invest Ophthalmol Vis Sci*. 2012;53(4):1773–1782.

86. Rantamäki AH, Seppänen-Laakso T, Oresic M, Jauhiainen M, Holopainen JM. Human tear fluid lipidome: From composition to function. *PLOS ONE*. 2011;6(5):e19553.

87. Stafford RE, Dennis EA. Lysophospholipids as biosurfactants. *Colloids and Surfaces*. 1987;30(1):47–64.

88. Kohlhaas R. Röntgenographische untersuchung von definierten einkristallen des palmitinsäure-cetylesters. *Z Kristallogr Cryst Mater*. 1938;98(1–6):418–438.

89. Dorset DL. Electronographic crystal-structure analysis of cetyl palmitate. *Bioorg. Khim*. 1976;2(6):781–788.

90. Lutz DA, Eddy CR, Hunter JJ. X-ray diffraction study of some normal alkyl esters of long-chain acids. *Lipids*. 1967;2(3):204–207.

91. Aleby S, Fischmeister I, Iyengar BTR. The infrared spectra and polymorphism of long chain esters: IV. some esters from tetradecanol, hexadecanol, octadecanol, eicosanol, docosanol and dodecanoic, tetradecanoic, hexadecanoic, octadecanoic and eicosanoic acid. *Lipids*. 1971;6(6):421–425.

92. Heyding RD, Russell KE, Varty TL, St-Cyr D. The normal paraffins revisited. *Powder Diffraction*. 1990;5(2):93–100.

93. Bouzidi L, Li S, Di Biase S, Rizvi SQ, Narine SS. Lubricating and waxy esters, I. synthesis, crystallization, and melt behavior of linear monoesters. *Chem Phys Lipids*. 2012;165(1):38–50.

94. Dorset DL. Rectangular and oblique layer packings of alkane chains and the eutectic solid formed by their interaction. *J Polym Sci B Polym Phys*. 1989;27(5):1161–1171.

95. Cholakova D, Denkov N. Rotator phases in alkane systems: In bulk, surface layers and micro/nano-confinements. *Adv Colloid Interface Sci*. 2019;269:7–42.

96. Lu H, Wojtowicz JC, Butovich IA. Differential scanning calorimetric evaluation of human meibomian gland secretions and model lipid mixtures: Transition temperatures and cooperativity of melting. *Chem Phys Lipids*. 2013;170:55–64.

97. Patel S, Nelson DR, Gibbs AG. Chemical and physical analyses of wax ester properties. *J Insect Sci*. 2001;1:4.

98. Iyengar B, Schlenk H. Melting points of synthetic wax esters. *Lipids*. 1969;4(1):28–30.

99. Rantamäki AH, Wiedmer SK, Holopainen JM. Melting points--the key to the anti-evaporative effect of the tear film wax esters. *Invest Ophthalmol Vis Sci*. 2013;54(8):5211–5217.

100. Ginsburg GS, Atkinson D, Small DM. Physical properties of cholesteryl esters. *Prog Lipid Res*. 1984;23(3):135–167.

101. Dorset DL. *Crystallography of the polymethylene chain: An inquiry into the structure of waxes*. New York: Oxford University Press; 2005:232.

102. Israelachvili JN. 20 - soft and biological structures. *Intermolecular and Surface Forces (Third Edition)*. 2011:535–576.

103. Harkins WD. A general thermodynamic theory of the spreading of liquids to form duplex films and of liquids or solids to form monolayers. *J Chem Phys*. 1941;9(7):552–568.

104. Langmuir I. Oil lenses on water and the nature of monomolecular expanded films. *J Chem Phys*. 1933;1(11):756–776.

105. Rantamäki AH, Telenius J, Koivuniemi A, Vattulainen I, Holopainen JM. Lessons from the biophysics of interfaces: Lung surfactant and tear fluid. *Prog Retin Eye Res*. 2011;30(3):204–215.

106. Adam NK. The structure of surface films. Part XIV. Some esters of fatty acids. Evidence of flexibility in the long chains. *Proceedings of the Royal Society of London.Series A, Containing Papers of a Mathematical and Physical Character*. 1930:366–372.

107. Alexander AE, Schulman JH. Orientation in films of long-chain esters. *Proc R Soc A*. 1937;161(904):115–127.

108. Rantamäki AH, Javanainen M, Vattulainen I, Holopainen JM. Do lipids retard the evaporation of the tear fluid? *Invest Ophthalmol Vis Sci*. 2012;53(10):6442–6447.

109. Schuett BS, Millar TJ. Lipid component contributions to the surface activity of meibomian lipids. *Invest Ophthalmol Vis Sci*. 2012;53(11):7208–7219.

110. Langmuir I. The constitution and fundamental properties of solids and liquids. II. liquids. *J Am Chem Soc*. 1917;39(9):1848–1906.

111. Caruso B, Martini MF, Pickholz M, Perillo MA. V-shaped molecular configuration of wax esters of jojoba oil in a Langmuir film model. *Langmuir*. 2018;34(26):7887–7898.

112. Schuett BS, Millar TJ. An investigation of the likely role of (O-acyl) ω-hydroxy fatty acids in meibomian lipid films using (O-oleyl) ω-hydroxy palmitic acid as a model. *Exp Eye Res*. 2013;115:57–64.

113. Sarkar A, Suresh KA. Self-assembly and molecular packing in cholesteryl esters at interfaces. *J Chem Phys*. 2017;146(21):214702.

114. Smaby JM, Brockman HL. Novel surface phase containing cholesteryl esters. 1. Structural characteristics determined from surface pressure--area measurements. *Biochemistry*. 1981;20(4):718–723.

115. Smaby JM, Brockman HL. Novel surface phase containing cholesteryl esters. 2. Nonequivalence of cholesteryl arachidonate and those with 18-carbon, cis-unsaturated acyl groups. *Biochemistry*. 1981;20(4):724–730.

116. Millar TJ, King-Smith PE. Analysis of comparison of human meibomian lipid films and mixtures with cholesteryl esters in vitro films using high resolution color microscopy. *Invest Ophthalmol Vis Sci*. 2012;53(8):4710–4719.

117. Holly FJ. Formation and rupture of the tear film. *Exp Eye Res*. 1973;15(5):515–525.

118. Kaganer VM, Möhwald H, Dutta P. Structure and phase transitions in Langmuir monolayers. *Rev Mod Phys*. 1999;71(3):779.

119. Cwiklik L. Tear film lipid layer: A molecular level view. *Biochim Biophys Acta, Biomembr*. 2016;1858(10):2421–2430.

120. Purslow C, Wolffsohn JS. Ocular surface temperature: A review. *Eye Contact Lens*. 2005;31(3):117–123.

121. Terada O, Chiba K, Senoo T, Obara Y. Ocular surface temperature of meibomia gland dysfunction patients and the melting point of meibomian gland secretions. *Nippon Ganka Gakkai Zasshi*. 2004;108(11):690–693.

122. Efron N, Young G, Brennan NA. Ocular surface temperature. *Curr Eye Res*. 1989;8(9):901–906.

123. Klamann MK, Maier AB, Gonnermann J, Klein JP, Pleyer U. Measurement of dynamic ocular surface temperature in healthy subjects using a new thermography device. *Curr Eye Res*. 2012;37(8):678–683.

124. Borchman D, Foulks GN, Yappert MC, Kakar S, Podoll N, Rychwalski P, Schwietz E. Physical changes in human meibum with age as measured by infrared spectroscopy. *Ophthalmic Res*. 2010;44(1):34–42.

125. Leiske DL, Leiske CI, Leiske DR, Toney MF, Senchyna M, Ketelson HA, Meadows DL, Fuller GG. Temperature-induced transitions in the structure and interfacial rheology of human meibum. *Biophys J*. 2012;102(2):369–376.

126. Leiske DL, Raju SR, Ketelson HA, Millar TJ, Fuller GG. The interfacial viscoelastic properties and structures of human and animal meibomian lipids. *Exp Eye Res*. 2010;90(5):598–604.

127. Kaercher T, Hönig D, Möbius D. Brewster angle microscopy. A new method of visualizing the spreading of meibomian lipids. *Int Ophthalmol*. 1994;17(6):341–348.

128. Arciniega JC, Uchiyama E, Butovich IA. Disruption and destabilization of meibomian lipid films caused by increasing amounts of ceramides and cholesterol. *Invest Ophthalmol Vis Sci*. 2013;54(2):1352–1360.

129. Georgiev GA, Yokoi N, Ivanova S, Tonchev V, Nencheva Y, Krastev R. Surface relaxations as a tool to distinguish the dynamic interfacial properties of films formed by normal and diseased meibomian lipids. *Soft matter*. 2014;10(30):5579–5588.

130. Yoshida M, Yamaguchi M, Sato A, Tabuchi N, Kon R, Iimura K. Role of endogenous ingredients in meibum and film structures on stability of the tear film lipid layer against lateral compression. *Langmuir*. 2019;35(25):8445–8451.

131. King-Smith PE, Nichols JJ, Braun RJ, Nichols KK. High resolution microscopy of the lipid layer of the tear film. *Ocul Surf*. 2011;9(4):197–211.

132. Bai Y, Ngo W, Nichols JJ. Characterization of the thickness of the tear film lipid layer using high resolution microscopy. *Ocul Surf*. 2019;17(2):356–359.

133. Petrov PG, Thompson JM, Rahman IBA, Ellis RE, Green EM, Miano F, Winlove CP. Two-dimensional order in mammalian pre-ocular tear film. *Exp Eye Res*. 2007;84(6):1140–1146.

134. Leiske DL, Miller CE, Rosenfeld L, Cerretani C, Ayzner A, Lin B, Meron M, Senchyna M, Ketelson HA, Meadows D. Molecular structure of interfacial human meibum films. *Langmuir*. 2012;28(32):11858–11865.

135. Georgiev GA, Eftimov P, Yokoi N. Contribution of mucins towards the physical properties of the tear film: A modern update. *Int J Mol Sci*. 2019;20(24):6132.

136. Millar TJ, Tragoulias ST, Anderton PJ, Ball MS, Miano F, Dennis GR, Mudgil P. The surface activity of purified ocular mucin at the air-liquid interface and interactions with meibomian lipids. *Cornea*. 2006;25(1):91–100.

137. Pandit JC, Nagyová B, Bron AJ, Tiffany JM. Physical properties of stimulated and unstimulated tears. *Exp Eye Res*. 1999;68(2):247–253.

138. Millar TJ, Mudgil P, Butovich IA, Palaniappan CK. Adsorption of human tear lipocalin to human meibomian lipid films. *Invest Ophthalmol Vis Sci*. 2009;50(1):140–151.

139. Mudgil P, Millar TJ. Adsorption of apo- and holo-tear lipocalin to a bovine meibomian lipid film. *Exp Eye Res*. 2008;86(4):622–628.

140. Glasgow BJ, Abduragimov AR. Interaction of ceramides and tear lipocalin. *Biochim Biophys Acta Mol Cell Biol Lipids*. 2018;1863(4):399–408.

141. Miano F, Calcara M, Millar TJ, Enea V. Insertion of tear proteins into a meibomian lipids film. *Colloids Surf B Biointerfaces*. 2005;44(1):49–55.

142. Mudgil P, Torres M, Millar TJ. Adsorption of lysozyme to phospholipid and meibomian lipid monolayer films. *Colloids Surf B Biointerfaces*. 2006;48(2):128–137.

143. Tiffany JM. Measurement of wettability of the corneal epithelium. II. contact angle method. *Acta Ophthalmologica*. 1990;68(2):182–187.

144. Tiffany JM. Measurement of wettability of the corneal epithelium. I. particle attachment method. *Acta Ophthalmologica*. 1990;68(2):175–181.

145. Lin SP, Brenner H. Tear film rupture. *J Colloid Interface Sci*. 1982;89(1):226–231.

146. Peng C, Cerretani C, Braun RJ, Radke CJ. Evaporation-driven instability of the precorneal tear film. *Adv Colloid Interface Sci*. 2014;206:250–264.

147. Bhamla MS, Chai C, Rabiah NI, Frostad JM, Fuller GG. Instability and breakup of model tear films. *Invest Ophthalmol Vis Sci*. 2016;57(3):949–958.

148. Rosenfeld L, Fuller GG. Consequences of interfacial viscoelasticity on thin film stability. *Langmuir*. 2012;28(40):14238–14244.

149. Rideal EK. On the influence of thin surface films on the evaporation of water. *J Phys Chem*. 1925;29(12):1585–1588.

150. Mishima S, Maurice DM. The oily layer of the tear film and evaporation from the corneal surface. *Exp Eye Res*. 1961;1:39–45.

151. Iwata S, Lemp MA, Holly FJ, Dohlman CH. Evaporation rate of water from the precorneal tear film and cornea in the rabbit. *Invest Ophthalmol*. 1969;8(6):613–619.

152. Sassa T, Tadaki M, Kiyonari H, Kihara A. Very long-chain tear film lipids produced by fatty acid elongase ELOVL1 prevent dry eye disease in mice. *FASEB J*. 2018;32(6):2966–2978.

153. Craig JP, Tomlinson A. Importance of the lipid layer in human tear film stability and evaporation. *Optom Vis Sci*. 1997;74(1):8–13.

154. King-Smith PE, Reuter KS, Braun RJ, Nichols JJ, Nichols KK. Tear film breakup and structure studied by simultaneous video recording of fluorescence and tear film lipid layer images. *Invest Ophthalmol Vis Sci*. 2013;54(7):4900–4909.

155. Dursch TJ, Li W, Taraz B, Lin MC, Radke CJ. Tear-film evaporation rate from simultaneous ocular-surface temperature and tear-breakup area. *Optom Vis Sci*. 2018;95(1):5.

156. Peng C, Cerretani C, Li Y, Bowers S, Shahsavarani S, Lin MC, Radke CJ. Flow evaporimeter to assess evaporative resistance of human tear-film lipid layer. *Ind Eng Chem Res*. 2014;53(47):18130–18139.

157. Brown SI, Dervichian DG. The oils of the meibomian glands. physical and surface characteristics. *Arch Ophthalmol*. 1969;82(4):537–540.

158. Herok GH, Mudgil P, Millar TJ. The effect of meibomian lipids and tear proteins on evaporation rate under controlled in vitro conditions. *Curr Eye Res*. 2009;34(7):589–597.

159. Borchman D, Foulks GN, Yappert MC, Mathews J, Leake K, Bell J. Factors affecting evaporation rates of tear film components measured in vitro. *Eye Contact Lens*. 2009;35(1):32–37.

160. Borchman D, Yappert MC, Milliner SE, Duran D, Cox GW, Smith RJ, Bhola R. 13C and 1H NMR ester region resonance assignments and the composition of human infant and child meibum. *Exp Eye Res*. 2013;112:151–159.

161. Sledge SM, Khimji H, Borchman D, Oliver AL, Michael H, Dennis EK, Gerlach D, Bhola R, Stephen E. Evaporation and hydrocarbon chain conformation of surface lipid films. *Ocul Surf*. 2016;14(4):447–459.

162. Cerretani CF, Ho NH, Radke CJ. Water-evaporation reduction by duplex films: Application to the human tear film. *Adv Colloid Interface Sci*. 2013;197–198:33–57.

163. Hertz H. Ueber den druck des gesättigten quecksilberdampfes. *Annalen der Physik*. 1882;253(10):193–200.

164. Knudsen M. Die maximale verdampfungsgeschwindigkeit des quecksilbers. *Annalen der Physik*. 1915;352(13):697–708.

165. Langmuir I, Schaefer VJ. Rates of evaporation of water through compressed monolayers on water. *J Franklin Inst*. 1943;235(2):119–162.

166. Archer RJ, La Mer VK. The effect of monolayers on the rate of evaporation of water. *Ann N Y Acad Sci*. 1954;58(6):807–829.

167. Sebba F, Briscoe HVA. 21. The evaporation of water through unimolecular films. *J Chem Soc*. 1940:106–114.

168. Rusdi M, Moroi Y. Study on water evaporation through 1-alkanol monolayers by the thermogravimetry method. *J Colloid Interface Sci*. 2004;272(2):472–479.

169. Archer RJ, La Mer VK. The rate of evaporation of water through fatty acid monolayers. *J Phys Chem*. 1955;59(3):200–208.

170. La Mer VK, Healy TW, Aylmore LAG. The transport of water through monolayers of long-chain n-paraffinic alcohols. *J Colloid Sci*. 1964;19(8):673–684.

171. Barnes GT. Permeation through monolayers. *Colloids Surf Physicochem Eng Aspects*. 1997;126(2):149–158.

172. Barnes GT. The potential for monolayers to reduce the evaporation of water from large water storages. *Agric Water Manage*. 2008;95(4):339–353.

173. Blank M. An approach to a theory of monolayer permeation by gases. *J Phys Chem*. 1964;68(10):2793–2800.

174. Barnes GT, Quickenden TI, Saylor JE. A statistical calculation of monolayer permeation by water. *J Colloid Interface Sci*. 1970;33(2):236–243.

175. Pu G, Longo ML, Borden MA. Effect of microstructure on molecular oxygen permeation through condensed phospholipid monolayers. *J Am Chem Soc*. 2005;127(18):6524–6525.

176. Schatzberg P. Diffusion of water through hydrocarbon liquids. *J Polym Sci, Part C: Polym Symp*. 1965;10(1):87–92.

177. Miano F, Calcara M, Giuliano F, Millar TJ, Enea V. Effect of meibomian lipid layer on evaporation of tears. *J Phys Condens Matter*. 2004;16(26):S2461.

178. Li W, Graham AD, Selvin S, Lin MC. Ocular surface cooling corresponds to tear film thinning and breakup. *Optom Vis Sci*. 2015;92(9):e248–e256.

179. Su T, Chang S, Yang C, Chiang HK. Direct observation and validation of fluorescein tear film break-up patterns by using a dual thermal-fluorescent imaging system. *Biomed Opt Express*. 2014;5(8):2614–2619.

180. Wolffsohn JS, Arita R, Chalmers R, Djalilian A, Dogru M, Dumbleton K, Gupta PK, Karpecki P, Lazreg S, Pult H, Sullivan BD, Tomlinson A, Tong L, Villani E, Yoon KC, Jones L, Craig JP. TFOS DEWS II diagnostic methodology report. *Ocul Surf*. 2017;15(3):539–574.

181. Bron AJ, de Paiva CS, Chauhan SK, Bonini S, Gabison EE, Jain S, Knop E, Markoulli M, Ogawa Y, Perez V, Uchino Y, Yokoi N, Zoukhri D, Sullivan DA. TFOS DEWS II pathophysiology report. *Ocul Surf*. 2017;15(3):438–510.

182. Bourcier T, Acosta MC, Borderie V, Borrás F, Gallar J, Bury T, Laroche L, Belmonte C. Decreased corneal sensitivity in patients with dry eye. *Invest Ophthalmol Vis Sci*. 2005;46(7):2341–2345.

183. Xu K, Yagi Y, Toda I, Tsubota K. Tear function index: A new measure of dry eye. *Arch Ophthalmol*. 1995;113(1):84–88.

184. Shimazaki J, Goto E, Ono M, Shimmura S, Tsubota K. Meibomian gland dysfunction in patients with sjögren syndrome. *Ophthalmology*. 1998;105(8):1485–1488.

185. Lemp MA, Crews LA, Bron AJ, Foulks GN, Sullivan BD. Distribution of aqueous-deficient and evaporative dry eye in a clinic-based patient cohort: A retrospective study. *Cornea*. 2012;31(5):472–478.

186. Viso E, Gude F, Rodríguez-Ares MT. The association of meibomian gland dysfunction and other common ocular diseases with dry eye: A population-based study in spain. *Cornea*. 2011;30(1):1–6.

187. Tong L, Chaurasia SS, Mehta JS, Beuerman RW. Screening for meibomian gland disease: Its relation to dry eye subtypes and symptoms in a tertiary referral clinic in Singapore. *Invest Ophthalmol Vis Sci*. 2010;51(7):3449–3454.

188. Rabensteiner DF, Aminfar H, Boldin I, Schwantzer G, Horwath-Winter J. The prevalence of meibomian gland dysfunction, tear film and ocular surface parameters in an austrian dry eye clinic population. *Acta Ophthalmol*. 2018;96(6):e707–e711.

189. Nelson JD, Shimazaki J, Benitez-del-Castillo JM, Craig JP, McCulley JP, Den S, Foulks GN. The international workshop on meibomian gland dysfunction: Report of the definition and classification subcommittee. *Invest Ophthalmol Vis Sci*. 2011;52(4):1930–1937.

190. Tomlinson A, Bron AJ, Korb DR, Amano S, Paugh JR, Pearce EI, Yee R, Yokoi N, Arita R, Dogru M. The international workshop on meibomian gland dysfunction: Report of the diagnosis subcommittee. *Invest Ophthalmol Vis Sci*. 2011;52(4):2006–2049.

191. Guillon JP, Guillon M. Tear film examination of the contact lens patient. *Optician*. 1993;206:21–29.

192. Yokoi N, Takehisa Y, Kinoshita S. Correlation of tear lipid layer interference patterns with the diagnosis and severity of dry eye. *Am J Ophthalmol*. 1996;122(6):818–824.

193. Goto E, Dogru M, Kojima T, Tsubota K. Computer-synthesis of an interference color chart of human tear lipid layer, by a colorimetric approach. *Invest Ophthalmol Vis Sci*. 2003;44(11):4693–4697.

194. Korb DR, Baron DF, Herman JP, Finnemore VM, Exford JM, Hermosa JL, Leahy CD, Glonek T, Greiner JV. Tear film lipid layer thickness as a function of blinking. *Cornea*. 1994;13(4):354–359.

195. Blackie CA, Solomon JD, Scaffidi RC, Greiner JV, Lemp MA, Korb DR. The relationship between dry eye symptoms and lipid layer thickness. *Cornea*. 2009;28(7):789–794.

196. King-Smith PE, Braun RJ. Author response: More to stable tears than thickness of the lipid layer. *Invest Ophthalmol Vis Sci*. 2015;56(3):1602.

197. Ji Y, Lee J, Lee H, Seo K, Kim E, Kim T. Automated measurement of tear film dynamics and lipid layer thickness for assessment of non-Sjögren dry eye syndrome with meibomian gland dysfunction. *Cornea*. 2017;36(2):176–182.

198. Fenner BJ, Tong L. More to stable tears than thickness of the tear film lipid layer. *Invest Ophthalmol Vis Sci*. 2015;56(3):1601.

199. Goto E, Tseng SCG. Differentiation of lipid tear deficiency dry eye by kinetic analysis of tear interference images. *Arch Ophthalmol*. 2003;121(2):173–180.

200. Cohen Y, Trokel S, Arieli Y, Epshtien S, Gefen R, Harris A. Mapping the lipid layer of the human tear film. *Cornea*. 2020;39(1):132–135.

201. Wong S, Murphy PJ, Jones L. Tear evaporation rates: What does the literature tell us? *Cont Lens Anterior Eye*. 2018;41(3):297–306.

202. Yamada M, Tsubota K. Measurement of tear evaporation from ocular surface. *Nippon Ganka Gakkai Zasshi*. 1990;94(11):1061–1070.

203. Tsubota K, Yamada M. Tear evaporation from the ocular surface. *Invest Ophthalmol Vis Sci*. 1992;33(10):2942–2950.

204. Uchiyama E, Aronowicz JD, Butovich IA, McCulley JP. Increased evaporative rates in laboratory testing conditions simulating airplane

cabin relative humidity: An important factor for dry eye syndrome. *Eye Contact Lens*. 2007;33(4):174–176.

205. McCulley JP, Uchiyama E, Aronowicz JD, Butovich IA. Impact of evaporation on aqueous tear loss. *Trans Am Ophthalmol Soc*. 2006;104:121–128.

206. McCulley JP, Shine WE, Aronowicz J, Oral D, Vargas J. Presumed hyposecretory/hyperevaporative KCS: Tear characteristics. *Trans Am Ophthalmol Soc*. 2003;101:141–154.

207. McCulley JP, Aronowicz JD, Uchiyama E, Shine WE, Butovich IA. Correlations in a change in aqueous tear evaporation with a change in relative humidity and the impact. *Am J Ophthalmol*. 2006;141(4):758–760.

208. Arciniega JC, Wojtowicz JC, Mohamed EM, McCulley JP. Changes in the evaporation rate of tear film after digital expression of meibomian glands in patients with and without dry eye. *Cornea*. 2011;30(8):843–847.

209. Goto E, Endo K, Suzuki A, Fujikura Y, Matsumoto Y, Tsubota K. Tear evaporation dynamics in normal subjects and subjects with obstructive meibomian gland dysfunction. *Invest Ophthalmol Vis Sci*. 2003;44(2):533–539.

210. Wang Y, Ogawa Y, Dogru M, Tatematsu Y, Uchino M, Kamoi M, Okada N, Okamoto S, Tsubota K. Baseline profiles of ocular surface and tear dynamics after allogeneic hematopoietic stem cell transplantation in patients with or without chronic GVHD-related dry eye. *Bone Marrow Transplant*. 2010;45(6):1077–1083.

211. Ibrahim OMA, Matsumoto Y, Dogru M, Adan ES, Wakamatsu TH, Shimazaki J, Fujishima H, Tsubota K. In vivo confocal microscopy evaluation of meibomian gland dysfunction in atopic-keratoconjunctivitis patients. *Ophthalmology*. 2012;119(10):1961–1968.

212. Matsumoto Y, Sato EA, Ibrahim OMA, Dogru M, Tsubota K. The application of in vivo laser confocal microscopy to the diagnosis and evaluation of meibomian gland dysfunction. *Mol Vis*. 2008;14:1263–1271.

213. Tomlinson A, Madden LC, Simmons PA. Effectiveness of dry eye therapy under conditions of environmental stress. *Curr Eye Res*. 2013;38(2):229–236.

214. Butovich IA, Bhat N, Wojtowicz JC. Comparative transcriptomic and lipidomic analyses of human male and female meibomian glands reveal

common signature genes of meibogenesis. *Int J Mol Sci*. 2019;20(18):4539.

215. Butovich IA, Lu H, McMahon A, Eule JC. Toward an animal model of the human tear film: Biochemical comparison of the mouse, canine, rabbit, and human meibomian lipidomes. *Invest Ophthalmol Vis Sci*. 2012;53(11):6881–6896.

216. Chen J, Panthi S. Lipidomic analysis of meibomian gland secretions from the tree shrew: Identification of candidate tear lipids critical for reducing evaporation. *Chem Phys Lipids*. 2019;220:36–48.

217. Dougherty JM, Osgood JK, McCulley JP. The role of wax and sterol ester fatty acids in chronic blepharitis. *Invest Ophthalmol Vis Sci*. 1991;32(6):1932–1937.

218. Osgood JK, Dougherty JM, McCulley JP. The role of wax and sterol esters of meibomian secretions in chronic blepharitis. *Invest Ophthalmol Vis Sci*. 1989;30(9):1958–1961.

219. Shine WE, McCulley JP. The role of cholesterol in chronic blepharitis. *Invest Ophthalmol Vis Sci*. 1991;32(8):2272–2280.

220. Dougherty JM, McCulley JP. Analysis of the free fatty acid component of meibomian secretions in chronic blepharitis. *Invest Ophthalmol Vis Sci*. 1986;27(1):52–56.

221. Shine WE, McCulley JP. Role of wax ester fatty alcohols in chronic blepharitis. *Invest Ophthalmol Vis Sci*. 1993;34(13):3515–3521.

222. Shine WE, McCulley JP. Meibomian gland triglyceride fatty acid differences in chronic blepharitis patients. *Cornea*. 1996;15(4):340–346.

223. Shine WE, McCulley JP. Association of meibum oleic acid with meibomian seborrhea. *Cornea*. 2000;19(1):72–74.

224. Shine WE, McCulley JP. Keratoconjunctivitis sicca associated with meibomian secretion polar lipid abnormality. *Arch Ophthalmol*. 1998;116(7):849–852.

225. Shine WE, McCulley JP. Polar lipids in human meibomian gland secretions. *Curr Eye Res*. 2003;26(2):89–94.

226. Joffre C, Souchier M, Grégoire S, Viau S, Bretillon L, Acar N, Bron AM, Creuzot-Garcher C. Differences in meibomian fatty acid composition in patients with meibomian gland dysfunction and aqueous-deficient dry eye. *Br J Ophthalmol*. 2008;92(1):116–119.

227. Chen J, Keirsey JK, Green KB, Nichols KK. Expression profiling of nonpolar lipids in meibum from patients with dry eye: A pilot study. *Invest Ophthalmol Vis Sci.* 2017;58(4):2266–2274.

228. Borchman D, Ramasubramanian A, Foulks GN. Human meibum cholesteryl and wax ester variability with age, sex, and meibomian gland dysfunction. *Invest Ophthalmol Vis Sci.* 2019;60(6):2286–2293.

229. Hetman ZA, Borchman D. Concentration dependent cholesteryl-ester and wax-ester structural relationships and meibomian gland dysfunction. *Biochem Biophys Rep*. 2020;21:100732.

230. Borchman D, Ramakrishnan V, Henry C, Ramasubramanian A. Differences in meibum and tear lipid composition and conformation. *Cornea.* 2020;39(1):122–128.

231. Borchman D, Foulks GN, Yappert MC, Bell J, Wells E, Neravetla S, Greenstone V. Human meibum lipid conformation and thermodynamic changes with meibomian-gland dysfunction. *Invest Ophthalmol Vis Sci*. 2011;52(6):3805–3817.

232. Bland HC, Moilanen JA, Ekholm FS, Paananen RO. Investigating the role of specific tear film lipids connected to dry eye syndrome: A study on O-acyl-ω-hydroxy fatty acids and diesters. *Langmuir*. 2019;35(9):3545–3552.

233. Taylor DM, De Oliveira ON, Morgan H. Models for interpreting surface potential measurements and their application to phospholipid monolayers. *J Colloid Interface Sci*. 1990;139(2):508–518.

234. de Mul M, Mann JA. Determination of the thickness and optical properties of a langmuir film from the domain morphology by Brewster angle microscopy. *Langmuir*. 1998;14(9):2455–2466.

235. Otsu N. A threshold selection method from gray-level histograms. *IEEE Transactions on Systems, Man, and Cybernetics*. 1979;9(1):62–66.

236. Schneider CA, Rasband WS, Eliceiri KW. NIH image to ImageJ: 25 years of image analysis. *Nat Methods*. 2012;9(7):671–675.

237. Abraham MJ, Murtola T, Schulz R, Páll S, Smith JC, Hess B, Lindahl E. GROMACS: High performance molecular simulations through multi-level parallelism from laptops to supercomputers. *SoftwareX*. 2015;1:19-25.

238. Frenkel D, Smit B. *Understanding molecular simulation: From algorithms to applications*. 2nd ed. Elsevier; 2002:1–638.

239. Tieleman DP, Marrink SJ, Berendsen HJ. A computer perspective of membranes: Molecular dynamics studies of lipid bilayer systems. *Biochim Biophys Acta*. 1997;1331(3):235–270.

240. Klauda JB, Venable RM, Freites JA, O'Connor JW, Tobias DJ, Mondragon-Ramirez C, Vorobyov I, MacKerell AD, Pastor RW. Update of the CHARMM all-atom additive force field for lipids: Validation on six lipid types. *J Phys Chem B*. 2010;114(23):7830–7843.

241. Jorgensen WL, Maxwell DS, Tirado-Rives J. Development and testing of the OPLS all-atom force field on conformational energetics and properties of organic liquids. *J Am Chem Soc*. 1996;118(45):11225–11236.

242. Siu SW, Pluhackova K, Böckmann RA. Optimization of the OPLS-AA force field for long hydrocarbons. *J Chem Theory Comput*. 2012;8(4):1459–1470.

243. Pluhackova K, Morhenn H, Lautner L, Lohstroh W, Nemkovski KS, Unruh T, Böckmann RA. Extension of the LOPLS-AA force field for alcohols, esters, and monoolein bilayers and its validation by neutron scattering experiments. *J Phys Chem B*. 2015;119(49):15287–15299.

244. Maciejewski A, Pasenkiewicz-Gierula M, Cramariuc O, Vattulainen I, Rog T. Refined OPLS all-atom force field for saturated phosphatidylcholine bilayers at full hydration. *J Phys Chem B*. 2014;118(17):4571–4581.

245. Thomas LL, Christakis TJ, Jorgensen WL. Conformation of alkanes in the gas phase and pure liquids. *J Phys Chem B*. 2006;110(42):21198–21204.

246. Izadi S, Anandakrishnan R, Onufriev AV. Building water models: A different approach. *J Phys Chem Lett*. 2014;5(21):3863–3871.

247. Vega C, de Miguel E. Surface tension of the most popular models of water by using the test-area simulation method. *J Chem Phys*. 2007;126(15):154707.

248. Rumble JR, ed. *CRC handbook of chemistry and physics*. 100th ed. Boca Raton: CRC Press/Taylor & Francis.

249. Caudwell DR, Trusler JPM, Vesovic V, Wakeham WA. The viscosity and density of n-dodecane and n-octadecane at pressures up to 200 MPa and temperatures up to 473 K. *Int J Thermophys*. 2004;25(5):1339–1352.

250. Diamond JM, Katz Y. Interpretation of nonelectrolyte partition coefficients between dimyristoyl lecithin and water. *J Membr Biol.* 1974;17(1):121–154.

251. Marrink S, Berendsen HJ. Simulation of water transport through a lipid membrane. *J Phys Chem*. 1994;98(15):4155–4168.

252. Torrie GM, Valleau JP. Nonphysical sampling distributions in Monte Carlo free-energy estimation: Umbrella sampling. *J Comput Phys*. 1977;23(2):187–199.

253. Hub JS, de Groot BL, van der Spoel D. g_wham — A free weighted histogram analysis implementation including robust error and autocorrelation estimates. *J Chem Theory Comput*. 2010;6(12):3713–3720.

254. Kulovesi P, Rantamäki AH, Holopainen JM. Surface properties of artificial tear film lipid layers: Effects of wax esters. *Invest Ophthalmol Vis Sci*. 2014;55(7):4448–4454.

255. Butovich IA, Arciniega JC, Wojtowicz JC. Meibomian lipid films and the impact of temperature. *Invest Ophthalmol Vis Sci*. 2010;51(11):5508–5518.

256. Paananen RO, Rantamäki AH, Parshintsev J, Holopainen JM. The effect of ambient ozone on unsaturated tear film wax esters. *Invest Ophthalmol Vis Sci*. 2015;56(13):8054–8062.

257. Voss LF, Bazerbashi MF, Beekman CP, Hadad CM, Allen HC. Oxidation of oleic acid at air/liquid interfaces. *J Geophys Res Atmos*. 2007;112(D6).

258. King MD, Rennie AR, Thompson KC, Fisher FN, Dong CC, Thomas RK, Pfrang C, Hughes AV. Oxidation of oleic acid at the air–water interface and its potential effects on cloud critical supersaturations. *Phys Chem Chem Phys*. 2009;11(35):7699–7707.

259. Pfrang C, Sebastiani F, Lucas CO, King MD, Hoare ID, Chang D, Campbell RA. Ozonolysis of methyl oleate monolayers at the air–water interface: Oxidation kinetics, reaction products and atmospheric implications. *Phys Chem Chem Phys*. 2014;16(26):13220–13228.

260. Lai CC, Yang SH, Finlayson-Pitts BJ. Interactions of monolayers of unsaturated phosphocholines with ozone at the air-water interface. *Langmuir*. 1994;10(12):4637–4644.

261. Liljeblad JFD, Bulone V, Tyrode E, Rutland MW, Johnson CM. Phospholipid monolayers probed by vibrational sum frequency spectroscopy: Instability of unsaturated phospholipids. *Biophys J*. 2010;98(10):L50–L52.

262. Riegler H, Köhler R. How pre-melting on surrounding interfaces broadens solid–liquid phase transitions. *Nature physics*. 2007;3(12):890–894.

263. Paananen RO, Rantamäki AH, Holopainen JM. Antievaporative mechanism of wax esters: Implications for the function of tear fluid. *Langmuir*. 2014;30(20):5897–5902.

264. Paananen RO, Javanainen M, Holopainen JM, Vattulainen I. Crystalline wax esters regulate the evaporation resistance of tear film lipid layers associated with dry eye syndrome. *J Phys Chem Lett*. 2019;10(14):3893–3898.

265. Butovich IA. Lipidomics of human meibomian gland secretions: Chemistry, biophysics, and physiological role of meibomian lipids. *Prog Lipid Res*. 2011;50(3):278–301.

266. Deo AV, Kulkarni SB, Gharpurey MK, Biswas AB. On the rate of spreading of long chain n-alcohols and n-alkoxy ethanols from solid into monolayer on water. *J Colloid Sci*. 1964;19(9):820–830.

267. Sawzik P, Craven BM. Conformation and packing of unsaturated chains in crystals of cholesteryl nervonate at 123 K. *J Lipid Res*. 1984;25(8):851–856.

268. Paananen RO, Viitaja T, Olżyńska A, Ekholm FS, Moilanen J, Cwiklik L. Interactions of polar lipids with cholesteryl ester multilayers elucidate tear film lipid layer structure. *Ocular Surf*. 2020;18(4):545–553.

269. Mills R. Self-diffusion in normal and heavy water in the range 1-45. deg. *J Phys Chem*. 1973;77(5):685–688.

270. Börjesson A, Erdtman E, Ahlström P, Berlin M, Andersson T, Bolton K. Molecular modelling of oxygen and water permeation in polyethylene. *Polymer*. 2013;54(12):2988–2998.

271. Miller IR, Bavly-Luz A, eds. *Some physical properties of monolayers and their relation to evaporation retardation*. New York: Academic Press; 1962. La Mer V. K., ed. Retardation of Evaporation by Monolayers: Transport Processes.

# ORIGINAL PUBLICATIONS